Errata

Page	Paragraph	Comment
15	-	For "Distance of plane from neutral axis"read "Distance from neutral axis".
18	-	For "intergral" read "integral".
21	3	The high-pressure pumps come into action before the nitrogen gas in the accumulators.
37	2	For "The channel blockage achieved in these experiments is shown in figure 8" read "The channel blockage was averaged over successively smaller parts of the centre of the same bundle. The results are compared in figure 8".
68	1	For "figures 22-24" read "figures 25-28".
68	2	For "figures 25-28" read "figures 22-24".
68	2	The symbol "x" represents the angular position of the surface, relative to the line of centres of the rod bundle.
68	2	The symbol "h" represents the average heat flux divided by the average temperature difference between the cladding and the coolant.
70	2	For "Uraniumdioxide" read "Uranium Dioxide".
75	3	For "in the present work" read "in calculations 1 to 5".
77	3	For "shown in figure 34" read "is shown in figure 34".
114	-	"Haque 1982" refers to ; "The Prediction of Forced Convection in a Cusp-shaped Channel." Haque MA, Hassan AKA, Turner JT and Barrow H, 7th Int. Heat Transfer Conference, Munich (1982).
143	2	For "Crossections" read "Cross-sections".

Prediction of PWR Fuel Cladding Failure Strain in a Loss-of-coolant Accident

by

John Rhys Jones

BSc (Eng), ACGI

April 1986

A Thesis Submitted for the degree of
Doctor of Philosophy
In the Faculty of Engineering
University of London.

Nuclear Power Section
Department of Mechanical Engineering
Imperial College of Science and Technology
London SW7 2BX.

Summary

The ADVICE computer program has been constructed to predict the failure strain of PWR fuel cladding during a Loss of Coolant Accident. The code calculates the temperature profile in a transverse section of the fuel pin and uses it to determine the cladding deformation.

The variation in surface-heat-transfer coefficient around the cladding circumference is found using a correlation and the eccentricity of the pellet stack is determined using a simple model of clad bowing.

The code has been used to model the NRU MT3 experiment. Predicted cladding temperatures were in close agreement with those obtained using the MABEL code. Deformation calculations led to failure strains within the range of those observed.

Calculation of the effect of cladding thickness variation showed that this could be the cause of the wide range of failure strains observed under nominally identical conditions.

The bowing calculations were found to be sensitive to the radiation transport model used in the pellet-clad gap.

This study demonstrates the feasibility of constructing a model of bowing and shows that it can be used to improve understanding of cladding failure behaviour.

Dedicated to
my Parents.

Acknowledgements

The author would like to express his appreciation to Dr. S J Peerless of the Mechanical Engineering Department, Imperial College for his invaluable help and encouragement. Our discussions were always enjoyable and boosted my confidence and enthusiasm. Thanks are also due to the Nuclear Installations Inspectorate for their financial support of this programme of work, but it should be pointed out that the views expressed in this thesis are those of the author and do not necessarily reflect those of the Inspectorate. In addition, thanks are due to Dr. C W Rapley of the Mechanical Engineering Department, Sunderland Polytechnic for carrying out the calculations of rod bundle heat-transfer coefficient profiles, upon which the correlations used in ADVICE are based, and to Miss M de Roeck for her assistance preparing this document.

"There is no absolute knowledge ...
all information is imperfect.
We have to treat it with humility."

Jacob Bronowski (1975)

Contents

Chapter 1

Contents

Chapter 2

Contents **Page**

Chapter 3

Contents **Page**

Chapter 4

Contents **Page**

Chapter 5

Contents **Page**

List of Figures

Nomenclature

A	Zirconium creep structure constant
A_1	Area of sector 1
C_p	Specific heat capacity
D	Cladding diameter
d	Cladding thickness
E	Young's modulus
F	Anisotropy coefficient (Hill 1950)
f	Radiation configuration factor
G	Anisotropy coefficient (Hill 1950)
H	Anisotropy coefficient (Hill 1950)
h	Heat-transfer coefficient
k	Thermal conductivity
l	Length
n	Stress-sensitivity exponent
P	Rod bundle pitch
Q	Activation energy
q	Heat flux
R	Gas constant
R	Radius of curvature of rod
r	Radial coordinate
T	Temperature
S	Volumetric heat generation rate
t	Time
V	Volume fraction of phase
y	Distance of plane from neutral axis of cladding
Z	Axial coordinate

Greek Symbols

α	Alpha phase
β	Beta phase
δ	Oxidation thickness
∂	Partial differential operator
Δ	Incremental operator
$\dot{\varepsilon}$	Strain rate (1/l . dl/dt)
E	Emissivity
ρ	Density
σ	Stress
θ	Tangential coordinate
Σ	Stephan-Boltzmann constant

Subscripts

0	original value
1	surface number
2	surface number
α	Alpha phase
b	defined in figure 17
c	defined in figure 17
β	Beta phase
eff	effective
eq	equlibrium value
ox	oxide
p	Primary creep
θ	Tangential coordinate
r	Radial coordinate
s	super-plastic
Z	Axial coordinate

Glossary

ADVICE:	Computer model of clad ballooning developed as part of this work.
CEGB:	Central Electricity Generating Board
Creep Rate:	Rate at which a structure undergoes thermally induced strain
Copla nar Deformation:	Deformation at the same axial position in the rod bundle
Ductility:	Local strain of a material at its failure site
Engineering Strain:	Elongation of an object under load normalized by its original length ie. $(\Delta l)/l_0$
LOCA :	Loss of coolant accident.
MABEL:	UKAEA Clad Ballooning Code (Appendix 1)
NRC:	Nuclear Regulatory Commission

ORNL: Oak Ridge National Laboratory

RELAP: Transient two-phase flow model of the primary circuit behaviour in a LOCA. (Brittain 1982)

True Strain: The intergal of the extension an object under load normalized by its current length. $\int_{L_0}^{L} dl/l$

UKAEA: United Kingdom Atomic Energy Authority.

Chapter 1

Contents **Page**

Introduction

In order to ensure that nuclear power plants are acceptably safe the effects of conceivable accidents are studied. One such accident is the loss of coolant from the core of the reactor resulting from damage to piping in the primary cooling circuit. This accident is often called a LOCA and is the subject of considerable study as part of the safety assessment of the pressurized water reactor.

This thesis contributes to the study of the behaviour of nuclear fuel during a large loss-of-coolant accident in a pressurized water reactor. The reactor is designed with emergency core cooling systems capable of coping with pipe breaks up to, and including, the loss of one of the main pipes supplying the coolant to the pressure vessel. This accident is often regarded as the most serious loss-of-coolant that the plant could conceivably sustain. If it happened, some damage to the cladding of the hottest fuel could occur. This work studies the extent to which deformation of the fuel cladding reduces the space available for coolant flow.

Before going on to consider the details of fuel behaviour under high temperature transient conditions, some background description of the pressurized water reactor and relevant accident scenarios is required. This is presented in the following sections on the pressurized water reactor and the loss-of-coolant accident.

1.1 The Pressurized Water Reactor

The construction of a commercial pressurized water reactor (PWR) is remarkably simple. The PWR core consists of a large number of long, thin, heating elements called fuel pins (typically 50 000 (NNC1982)) in a steel pressure vessel, through which water is pumped. The water is not only the primary coolant, but also slows down the neutrons generated by the nuclear fission process and keeps enough of them in the reactor to burn the fuel. Steam is less dense than water and neither cools the fuel, nor slows down neutrons to the same extent, so the water in the core is kept under pressure to prevent it boiling. The pressure chosen is a compromise between the high temperatures required to generate electricity and the need for low stresses in structural materials. A typical value is 150 atmospheres.

The core is cooled by a number of independent circuits. Water from the cold leg of these circuits is pumped into an annular space between the pressure vessel wall and the fuel assemblies. (figure 2). The coolant flows down into a lower plenum then turns and passes up through the gaps between the fuel pins. Finally it leaves the core through an upper plenum and passes through the hot-leg piping to the steam generators where it gives up its energy to the secondary cooling circuit.

Should the core pressure decrease rapidly, cold water is forced into each of these circuits from four pairs of storage vessels, by the action of nitrogen gas. When the core pressure permits it, a number of different pumps take over from the accumulators to circulate cold water and remove any residual heat.

1.2 The Cold Leg Break Loss-of-coolant Accident

The design of the emergency cooling system is based upon a postulated maximum credible accident involving the double-ended guillotine break of one of the main coolant pipes which supplies cold water to the pressure vessel. If such a pipe fracture were to occur, much of the water injected into the intact cooling circuits would leave the pressure vessel through the broken pipe, by-passing the core. This accident could result in clad temperatures high enough to cause fuel-cladding deformation and it is the subject of the work reported here.

The processes taking place in the primary system, during this LOCA, are often described by dividing the scenario into three phases; blow down, refill and reflood.

1.2.1. Blow Down

Subsequent to the break, a pressure wave propagates through the primary system and the water in the pipes is accelerated until sonic velocities are reached. Within a tenth of a second the pressure in the core drops below the saturation pressure and rapid boiling takes place. Once boiling starts, the compressibility of the two-phase mixture of water and steam present in the core is increased and the sonic velocity is reduced. Consequently the core pressure decreases less rapidly. The rate of depressurisation depends upon the size of the break. In the case of a double ended break of a main pipe, the core pressure drops to only a few atmospheres in approximately thirty seconds. The reduction in core moderation results in termination of the fission reaction within two seconds (Routledge 1982).

As the pressure drops, the water stored in the high pressure coolant injection system enters the cold legs of the primary coolant circuit and flows into the top of the annular down-flow channel which surrounds the core. If the break is in the cold leg of the primary circuit, steam flowing up the down-comer prevents the water from flowing down to enter the core. Instead the water leaves the down-comer annulus through the broken pipe, by-passing the core.

During the blowdown phase of the accident the cladding receives heat generated by the decay of fission products (approximately 6 percent of operating power) and energy stored in the fuel pellets redistributes itself. The core progresses rapidly through a number of cooling regimes in this period. Single phase convection rapidly gives way to nucleate boiling as the pressure in the upper part of the core drops to the saturation value. The rate at which the pressure drops is linked to the rate of vaporisation. As the amount of water in the core decreases, the fuel rods dry out and their temperatures start to rise. Film boiling conditions give way to single phase convective cooling as the froth level in the core drops and the core is filled with superheated steam.

1.2.2. Refill

After about 30 seconds the pressure in the core has dropped sufficiently to permit water to flow down the down-comer annulus and start to fill the lower plenum. This process takes about 10 seconds, during which time there is little flow in the core and cooling takes place mainly by single phase convection to superheated steam. In the absence of significant cooling, the cladding temperature rises rapidly and can reach temperatures where the strength of the cladding is reduced sufficiently for creep deformation to start.

1.2.3. Reflood

As the water level in the down-comer rises, the hydrostatic pressure at the base of the core increases and water enters the core. When it makes contact with hot structural material and fuel it boils rapidly and the pressure rises locally, slowing down, or in some cases, reversing the flow. The increase in pressure increases steam flow rates through the core and the steam generators until a balance is obtained between the pressure drop of the steam flow through the primary system and the static head provided by the water in the downcomers. As more water enters the core the wetting front rises progressively up the fuel rods, cooling more of the core by nucleate boiling, until eventually the core completely fills with water and single phase liquid cooling is re-established.

The limitation on reflooding resulting from the system back pressure is sometimes referred to as "steam binding" and is largely responsible for the fact that reflooding is the longest part of the transient, lasting for several minutes.

The cooling of the fuel improves progressively during this period resulting in first a slowing down, then a reversing of the temperature rise of the cladding, followed by rapid quenching of the cladding at the water level. During reflooding, sufficient cooling can take place to slow down localised deformation at hot spots on the clad surface and axially extended balloons may be possible.

1.3 Deformation of Zirconium

Zirconium is used for the fuel cladding because it combines an extremely low neutron absorption cross-section with excellent corrosion resistance. It does suffer from a relatively low creep resistance, but this is not a serious problem at normal temperatures.

During normal operation the external pressure of the coolant on the cladding of zirconium clad fuel is sufficient to cause the cladding to creep inwards towards the fuel pellets. Subsequent rapid temperature changes during plant start-up, cause hoop stresses in the cladding. It has therefore become common practice to fill the fuel element with inert gas to limit the cross-cladding pressure difference and improve fuel reliability. (This practice also aids heat transmission). Unfortunately during a large loss of coolant accident the pressure in the core drops below the pressure in the fuel pin and the cladding tends to expand outwards like a balloon. The deformation is mainly by various creep mechanisms and the rate at which it occurs depends very strongly upon the cladding temperature. Above 750^0C deformation can be sufficiently rapid to cause failure in the few minutes that the core is likely to be uncovered. The failure strain of the cladding is of interest because clad ballooning reduces the size of the coolant channels in the core and may affect the rate of reflooding and the cladding temperature.

In order to predict channel blockage, the deformation of zirconium needs to be studied.

1.3.1 The metallurgy of Zirconium

Zirconium exists in two allotropes. A hexagonal close –packed alpha phase is present at temperatures below 820^0C and a body-centered-cubic beta phase exists above 980^0C. At intermediate temperatures a mixture of the two phases exists. For the purposes of deformation in a LOCA, further distinctions can be made. Below 750^0C creep is relatively slow, but superplasticity can be observed. This becomes less important above 750^0C because grain growth occurs and also dislocation creep becomes more rapid. Above 820^0C the existence of phase boundaries allows superplastic creep to occur again, but the deformation becomes more temperature sensitive because the beta phase is much less creep resistant. Above 900^0C the oxidation of the clad surface makes it brittle.

Large LOCA would normally result in temperatures below 820^0C, so the alpha phase properties are most important.

Alpha phase zirconium is not a perfect close-packed hexagonal prism and it is unable to undergo slip on the basal planes of the prism. The only major slip systems are perpendicular to this, in the prismal planes $(10\bar{1}0)$. As deformation proceeds these slip planes become progressively aligned, so cold-worked zirconium does not resist deformation in an isotropic manner.

Zirconium exhibits exceptional ductility over a large range of temperatures and, under certain conditions, can achieve strains of several hundred percent.

1.4 The Interaction of Thermohydraulics and Deformation

The thermal behaviour of a fuel pin affects its deformation rate very strongly, so deformation models need accurate predictions about cladding temperature distributions, but the temperature distributions are also influenced by the deformation.

Although the ductility of zirconium is very high, the temperature and stress sensitivity are also high and these factors dominate the behaviour of ballooning cladding. The deformation rate approximately doubles for every 20^0C temperature rise and is proportional to stress to an exponent of about 5 in the alpha phase (Donaldson 1983). The mechanism of cladding failure proceeds as follows; the deformation rate at the hottest point on the cladding surface exceeds that of the surrounding material and it starts to thin locally; the resulting increase in stress accelerates the process and the local ductility is exceeded, despite relatively low strains in the rest of the cladding. Temperature gradients are therefore beneficial because they result in unstable deformation which causes localised strain and early cladding failure, before the majority of the cladding has undergone much deformation. This limits the diametral strains that can be achieved, and hence the coolant channel blockage that can occur.

Temperature gradients exist in both the axial and the tangential directions.

1.4.1 Axial Temperature Distribution

The axial temperature profile in the cladding is determined by variation in heat flux from the cladding surface and axial temperature gradient in coolant, resulting from convective heat transfer. The effect of axial temperature variation on the deformation profile is limited by the cooling of the cladding which occurs when it lifts off the fuel pellet stack. Provided that the steam flow is sufficient to produce significant convective cooling of the cladding, the cladding temperature is determined by the thermal resistance of the pellet-clad gap and the heat flux across it. If one part of the cladding becomes hotter than the rest and deforms more rapidly, a larger pellet-clad gap will result and the thermal resistance of the gap will go up. This causes a temporary reduction in the gap heat flux, and the rate of temperature drop at this point is more rapid than that of the rest of the rod. Consequently the rate of deformation slows down and the axial deformation profile is stabilized.

1.4.2 Azimuthal Temperature Gradients

In addition to axial temperature gradients, variation in cladding surface heat flux also causes azimuthal temperature gradients. These result from two phenomena:

1 Pellet-cladding Offset

Variations in the pellet-clad gap, resulting from relative offset between the pellet and the cladding, can cause large azimuthal temperature gradients. This relative offset is not easy to predict, but there is some evidence that even highly fractured pellet stacks remain largely intact (Garlick 1982). If the pellet stack is assumed to remain central while the cladding deforms, some relative offset will result from the bowing of the cladding caused by non-uniform deformation.

2 Variation in Surface Heat-transfer Coefficient

The surface heat-transfer coefficient is fairly uniform around the circumference of undeformed cladding, but as the cladding deforms the coolant passage which surrounds it becomes increasingly cusp-shaped. Turbulent heat transfer in the corners of the cusp eventually decreases and the cladding temperature rises locally.

These sources of azimuthal temperature gradients result in a significant reduction in the diametral strain at failure that cladding is capable of achieving under ideal conditions.

1.5 Purpose of this Work

Computer codes capable of predicting cladding failure strain are under constant development, but current codes are deficient in two ways; firstly they do not take account of variation of surface heat-transfer coefficient resulting from the surrounding coolant passage shape and secondly the relative offset of the pellet and the cladding is set by the user, yet it is not determined independently of the code being used. Parametric studies are carried out and the offset value which best agrees with known experimental results is used in subsequent calculations.

This work attempts to demonstrate the feasibility of constructing a mechanistic description of the clad bowing, which allows physically-based determination of the relative offset of the pellet and the cladding.

A surface heat-transfer coefficient correlation has been developed and a two-dimensional model of the fuel-pin behaviour has been constructed to describe clad bowing.

Chapter 2

Contents **Page**

Literature Review

Clad-ballooning causes lower coolant flow rates during reflooding than would otherwise occur and, consequently, higher cladding temperatures. In order to ensure that the cooling system can prevent the fuel temperature exceeding the permitted maximum value, work is being carried out in two areas, thermo-hydraulics and fuel rod deformation modelling. The former attempts to predict the effect of channel blockage upon fuel temperatures, while the latter attempts to predict the extent of coolant channel blockage resulting from clad-ballooning. This review limits itself to reporting on fuel deformation modelling.

Reviews of experimental work on this subject have already been carried out (Mann 1982), (Hindle 1979). This chapter describes the modelling used in existing clad-ballooning computer programs and relates the development of these models to experimental results. A brief description of the major ballooning computer codes is found in appendix 1.

2.1 Clad Ballooning Code Construction

The object of constructing a clad ballooning computer code is to predict the axial variation of cladding diametral strain as a function of time. The following processes need to be modelled to achieve this:-

1. Transient heat transfer in the fuel.

This can be modelled using the finite difference or finite element method.

2. Expansion of the gas in the pin and hence the internal pressure.

The release of fission products from the fuel during the accident is small (Karb 1981), so pressure can be calculated using the gas laws.

3. Convective heat transfer from the fuel pin surface.

In the absence of good three-dimensional models of two-phase convection, the fuel-pin surface-heat-transfer coefficient is calculated using one-dimensional, empirical correlations. The specification of these correlations is one of the main goals of thermo-hydraulic studies.

4. Deformation of the cladding.

Until cladding failure approaches, the deformation rate is sufficiently uniform to be predicted adequately by one dimensional models which calculate diametral hoop strain from a nominally uniform hoop stress. Models of this type include LOCTA (Routledge 1982) and SYSST (Gulden 1982). They can provide a reasonable estimate of the strain rate, but they cannot predict the cladding failure strain because the final deformation is limited to part of the cladding circumference. Recent work in the deformation field has attempted to predict the circumferential variation in strain and hence the diametral strain at failure.

2.2 Cladding Strain at Failure

Tests on nuclear fuel in reactors are expensive and inconvenient, so only a limited number of nuclear-heated tests have been made. Instead, electrical heaters have been developed which simulate the heating provided by a stack of uranium dioxide fuel pellets.

A large number of experiments have been carried out on single fuel rod simulators to investigate cladding behaviour. The rod is usually surrounded by a larger tube which is used as a shroud, and coolant is passed through the annular space between the cladding and the shroud. By controlling the coolant flow and/or the rod power, LOCA conditions are approximated and the cladding is forced to balloon and fail. The construction of one such rod simulator is shown in figure 3.

The results of this type of experiment have been used to provide bounding curves of cladding failure strain against temperature (figure 4). Unfortunately these results are often specific to the conditions found in the tests. Results of experiments with cladding surrounded by a cold shroud are compared with those obtained using a heated shroud and with multi-rod tests in figure 5. The use of unheated shrouds in single rod experiments gives misleading results, so experiments need to reflect reactor conditions as closely as possible if their results are to be used directly.

The importance of thermal conditions was shown experimentally at KfK. (Borgwaldt 1983). Tests using instrumented fuel rod simulators demonstrated that, for temperatures below the phase change of the cladding material, the diametral strain at failure is principally a function of the azimuthal temperature range at the failure location (figure 6). This conclusion has been supported by a number of theoretical studies (Healey 1985). The strain at failure in the presence of an azimuthal temperature range of 80^0C has been shown to be virtually independent of the material ductility, but dependent upon the sensitivity of the strain rate to temperature (Barlow 1983).

The connection between azimuthal temperature range and diametral failure strain is shown diagrammatically in figure 7 (Mann 1982). The temperature sensitivity of the creep leads to unstable deformation and failure occurs at lower strain in non-uniform temperature fields.

The discovery of this relationship has lead to a change in modelling emphasis away from correlations of experimental data, which can be shown to mislead (Burman 1981), and towards the modelling of thermal asymmetry. Two-dimensional R-θ routines, such as TAPSWEL and AZI (appendix 1), have been developed to calculate the azimuthal deformation variation at a chosen axial position and to predict the diametral strain at which the local strain exceeds a prescribed failure criterion.

While two-dimensional calculations provide more detailed models of the physical processes, they are still not completely comprehensive descriptions of the fuel behaviour. Most codes model only one fuel rod, so that the effect of variation in thermal conditions external to that rod is neglected and the main source of azimuthal temperature gradients is assumed to be the variation in the pellet-clad gap, resulting from the offset between the pellet and the cladding. Furthermore codes usually require the specification of a parameter called the pellet eccentricity. This is defined as the offset of the pellet axis (relative to that of the cladding) divided by the mean gap between the pellet and the cladding.

Not enough direct evidence about the behaviour of the fuel yet exists to allow this parameter to be specified independently of the code used to predict the failure strain.

The approach used by Healey (1982) has been to carry out an experiment with a limited number of nuclear heated rods and to measure the failure strain for each rod. Calculations were then performed with the TAPSWEL computer code to find the value of the pellet eccentricity ratio that would allow the code to predict the failure strain of each rod correctly. Having completed the calculation of pellet eccentricity ratio for all of the rods, an average offset ratio was obtained which was used in subsequent calculations. This approach is basically empirical, with pellet eccentricity being used as a calibrating parameter for the code. Instead of extrapolating experimental results using empirical functions, the changes in dependent variables are described using physically based modelling, but the accuracy of the result depends on the extent to which the reference experiment is a true representation of reactor conditions, and on the completeness of the physical model used in the extrapolation.

The relative offset values used by Healey were obtained from analysis of the NRU MT3 experiment (Gibson 1982). In this experiment ballooning occurred during the reflooding phase of the simulated LOCA. Nevertheless, the values obtained proved satisfactory in predicting the failure strain achieved, under completely different conditions, in the MT4 experiment. In the MT4 experiment clad failure occurred during the refill part of the accident when azimuthal temperature gradients were low (Routledge 1982). The use of single pin models seems, therefore, to permit the description of experiments reasonably well. Extrapolation to a reactor may, however, introduce errors of scaling.

2.3 Effect of Rod-Bundle Size

Clad-ballooning experiments carried out at Halden on a bundle of five rods surrounded by cold structures resulted in engineering failure strains of 20-40% (Healey 1985), while the MT3 experiment, which used 12 pressurized rods with, 12 unpressurized rods as thermal shields, obtained engineering strains ranging from 30% to 53%.

The effect of bundle size has been investigated experimentally at ORNL (Chapman 1984). Electrically heated fuel rods were tested in both 4x4 and 8x8 bundles under nearly identical conditions. The coolant channel blockage achieved in these experiments is shown in figure 8. The centre of the 8x8 bundle obtained higher strains than the 4x4 bundle and the amount of coolant channel blockage in the center of the 8x8 bundle was significantly greater than that of the bundle as a whole. Temperature measurement demonstrated that the central 16 rods of the bundle were significantly hotter than the rest. The temperature variation across the bundle was probably due to the influence of the shroud on adjacent rods and, since shrouds are not present in reactors, actual flow blockages could be more severe than those observed in experiments.

Chapman recommended that, if the effect of bundle size was to be eliminated from tests in which large balloons were expected, at least two rows of deforming rods should surround the rods under investigation. His study was carried out in slowly flowing steam, under conditions which are not expected to arise in an accident in a modern PWR, so the effect may be exaggerated, but nuclear heated reflooding tests have not used bundles of this size, so available experimental results may not be free from the effects of bundle size.

Since codes like TAPSWEL do not include the effect of surrounding rods, temperature gradients resulting from external conditions can be wrongly attributed to pellet offset. The influence of surrounding rods has been studied using the MABEL code (Haste 1984). The MABEL code models one rod in detail, but the effect of surrounding rods is allowed for both by radiation calculations and by solving the flow field in four subchannels surrounding the subject rod.

Haste investigated the effect of the constraint provided by the surrounding rods after contact. The constraint on deformation in the MT3 experiment was different from that found in a reactor core. Assuming that coplanar blockage occurs in the core, rods start to flatten after they make contact at a strain of 29% (33% engineering strain). The curvature of unsupported arcs of cladding increases and the stress is reduced, stabilizing the deformation. In the MT3 experiment only 12 rods were pressurized (figure 9), so that when they made contact, instead of flattening, they moved apart until the unpressurized guard rods were contacted. Haste calculated that the effect of this difference in constraint could result in an increase in engineering failure strain from 43% in the test to 45% in a reactor, (assuming a relative offset of 0.35).

Investigation of the effect of shrouds or control rod guides is limited if the MABEL computer code is used, because the code models only one rod in detail and requires the specification of surrounding rod temperatures relative to the subject rod. This difficulty is overcome in the FRETA-B code which models as many rods as desired . However this code calculates only radiative transfer across the bundle; convective heat transfer is assumed uniform in the transverse direction.

The FRETA-B code has been used to model both nuclear and electrically heated bundles; it predicted qualitatively similar patterns of temperature and strains to those observed (Uchida 1983). Temperature gradients were however under-predicted because of the omission of a three-dimensional flow field solution.

2.4 Coplanar Deformation

Quantitative knowledge about the interaction of balloons in a rod bundle is limited. Experiments have shown that axial deformation profiles vary between rods, and the locations of the positions of peak strain may be sufficiently different to reduce coolant channel blockage considerably. The MT3 experiment resulted in a 50 percent reduction in flow area, but if the deformation had been coplanar the blockage would have been 90 percent.

Since computer codes do not generally model more than one rod, they generally assume coplanar deformation, but (Healey 1982) attempted to calculate the likely variation in deformation by summing the variances of parameters like pellet enrichment and pellet eccentricity. Pellet eccentricity was the most important parameter and, since this was not a physically measured quantity, its use is difficult to justify, nevertheless the extent of the variation in strain was under-predicted.

The tendency for non-coplanar deformation to occur has been attributed to the cooling of neighbouring rods resulting from perturbations in the flow field (Mann 1982). The argument proceeds as follows; if one rod deforms more rapidly than its neighbours the coolant flow around it is reduced and the diverted flow enters neighbouring subchannels, cooling surrounding rods more. If the flow distribution is the main cause of non-coplanar deformation, the effect on neighbouring rods will be greater in small bundles where a larger proportion of the diverted flow passes through neighbouring channels. The deformation may, therefore, be more coplanar in the core than in test bundles.

The temperature of surrounding rods may also be important if contact is achieved. If the neighbouring rod is cooler than the deforming rod, the rate of deformation at the hot spot will be reduced and axially extended balloons could result. If on the other hand, the neighbouring rods are hotter than the deforming rod, the deformation will be destabilized, leading to early failure (figure 10).

In the absence of a large number of realistic, nuclear heated ballooning tests, the effect of experimental scale could be investigated by constructing a computer code similar to the CANSIM code (Sills 1983) which is being developed for CANDU LOCA analysis. The code would need to model part of a bundle in three dimensions and include the effects of flow redistribution, but even if such a code were constructed, the correct prediction of scaling effects could not be guaranteed if the current approach to prescribing pellet offset were adopted. It is likely that even fairly small external temperature gradients could lead to changes in the pellet offset behaviour. Bowing of the cladding is an auto-catalytic process, so the size of the initial temperature perturbation which results

in uneven deformation may be important in determining the final offset of the cladding and hence the temperature field. A mechanistic model of pellet eccentricity is required.

To construct such a model some assumptions need to be made about the behaviour of the pellet stack.

2.5 Pellet Relocation

The stack of used nuclear fuel pellets is often highly fragmented, so the possibility of it crumbling needs to be considered. If this occurred it would cause relocation of the fragments in such a way that they might remain in contact with the cladding surface over a large proportion of the circumference. This could lead to more even heating than would be obtained by the intact fuel pellet assumed in most computer calculations. Alternatively, axial relocation could cause more fuel to collect at a particular axial location, resulting in more heat generation at this point and localized deformation leading to failure.

Indirect evidence against pellet stack break-up or pellet relocation comes from a number of sources:

I. Post-Experimental Examination

The behaviour of the pellet stack is being investigated by the UKAEA. Ballooning experiments have been carried out by direct electrical heating of the cladding of irradiated fuel and large strains were obtained. Then when the deformation was over, the fuel rods were filled with resin. X-ray photographs revealed little break-up of the fuel stack in the region of the failure. (Garlick 1982).

2. Temperature Measurement

Single rod ballooning tests were performed in the reactor at Kfk (Karb 1981). Rods were instrumented with thermocouples at the very top of the pellet stack to detect relocation of the fuel. Relocation was not found to occur until the cladding failed (figure 11).

3. Observation of Failure Strain Profiles

The thickness profile observed in post-experimental examination provides evidence of the way in which the deformation destabilized. The deformation shape observed in the MT3 experiment agrees well with MABEL calculations assuming an intact pellet stack (Haste 1984). Furthermore, the single neck found in cladding which failed in the alpha phase temperature region is not duplicated in failures occurring in the beta phase region (figure 12). This suggests that eccentricity is determined by the cladding behaviour rather than that of the pellet stack.

4. Comparison Between New and Old Fuel Behaviour

Karb (1981) also carried out comparison between new fuel, old fuel and ceramic fuel rod simulators. The circumferential strain at failure is shown for each of those types of rod in Figure 13. No observable difference in the pattern of failure strain is apparent.

The relative offset between the pellet and the cladding of a fractured pellet stack must therefore be similar to that of a largely unfractured pellet stack or a solid rod.

On the basis of this evidence it would appear that the pellet stack remains intact and retains a rod-like geometry. The next problem to resolve is whether the relative offset is a result of the movement of the pellet stack or the cladding.

2.6 Pellet Stack Movement

It is conceivable that, even if the pellet stack remained intact, it should move in such a way as to maintain contact with the cladding and thus obtain support. Should this happen, the pellet eccentricity would take its maximum value of I and low failure strain would result. Both MABEL (Haste I983) and TAPSWEL (Healey I982) have been used to demonstrate that this assumption would lead to lower failure strains than observed in the MT3 experiment and must therefore, be invalid.

If the pellet stack is to remain intact and is not supported by the cladding, it is likely that the relative offset of the pellet and the cladding results from bowing of the cladding.

2.7 Cladding Bowing

In the presence of azimuthal temperature gradients such as those resulting from point contact with the cladding, the deformation rate will not be uniform around the cladding circumference.

Since alpha phase zirconium contracts in the axial direction, the cladding tube will bow towards the heat source as it deforms. Although the bowing may not be fast enough to retain contact between the pellet stack and the cladding, it can be sufficient to maintain a significant relative offset. Since isotropic deformation does not result in shortening of the cladding the amount of bowing will depend upon the anisotropy of the cladding material.

2.8 Anisotropy

A number of sources of anisotropy data exist:

Basal pole orientations have been measured at room temperature and computer programs used to calculate the deformation given the critical resolved shear stress on known slip planes (Franklin 1977).

Deformation tests have also been carried out at both room temperatures and near operating temperature (300^{o}-400^{0}c) and isotropy coefficients are available from these sources (Dresslier 1977) but little data exists about anisotropic behaviour in the high alpha phase temperature region.

Deformation experiments performed over a range of temperatures suggest that the anisotropy increases steadily with temperature until the material starts to change phase (Hindle 1983). Anisotropy then decreases rapidly (figure 14). This is to be expected because, once the phase change has started, deformation takes place mainly by a combination of dislocation creep in the weaker, isotropic, beta phase material and phase boundary sliding (Douglass 1971).

Chapter 3

Contents **Page**

The ADVICE Computer Code

The ADVICE code was constructed to investigate the causes and effects of azimuthal temperature variation in more detail than existing codes. From the start of writing, the interaction between the temperature field in the fuel pin and the azimuthal deformation profile was recognised. The code was therefore constructed to include detailed models of both heat transfer and cladding creep and was designed to permit efficient iterative calculation of the temperature and deformation profiles.

The success of early calculations prompted an attempt to predict clad bowing using the deformation profile. This introduced an additional feed-back into the calculations. Not only is the creep rate affected by the hoop stress and the clad temperature, but also by the axial stress resulting from bending.

Initial convergence difficulties were overcome by second-order iterative techniques and the automatic control of timesteps. ADVICE can now be used without stability problems arising.

3.1 General Description

The ADVICE computer code calculates the deformation of a single rod when it is subjected to a given thermal and pressure history. The rod is assumed to be surrounded by eight others in a square-pitched bundle. All the rods in the bundle are assumed to be at the same temperature and to deform at the same rate, but, while the surrounding rods remain straight, the subject rod is assumed to bow as a result of azimuthal temperature gradients. The extent of the bowing is calculated from the axial strain field. This is used to calculate the offset of the pellet stack relative to the cladding. The pellet stack is assumed to remain straight and intact.

A flow chart of the program is shown in figure 15. Calculations proceed as follows:

1. The geometry existing initially (or at the end of the previous time-step) is used, with the thermal boundary conditions applying to the current time-step, to obtain a first estimate of the temperature field in the fuel.

2. The deformation is calculated using both the old and the new temperature fields and the initial thickness profile.

3. The new thickness profile is obtained and used to improve the deformation calculation.

4. The geometry upon which the thermal calculation is based is updated and the temperature field is recalculated.

5. Temperature and deformation calculations are repeated until consistency is achieved.

The program structure is shown in appendix 2; descriptions of the physical models and their implementation follows:-

3.2 Cladding Deformation

A number of plastic deformation mechanisms operate in zircaloy at different temperatures and deformation rates. At temperatures below 820^0C the material has a hexagonal, close-packed (alpha phase) structure, while above 970^0C it has a body-centered cubic (beta phase) structure. Between these temperatures the material exists as a combination of alpha and beta phase grains. The deformation differs between each of these three regimes.

3.2.1 Alpha phase Deformation

Deformation in the alpha phase can result from a number of mechanisms:

1. Dislocation Creep

This occurs mainly on prism slip plains of the $\{10\bar{1}0\}$ type in the $<11\bar{2}0>$ direction. The process is thermally activated and shows an approximately Arrhenius temperature dependence in the steady state. It is often described by the Norton equation:

$$\dot{\varepsilon} = A\,\sigma^n \exp(-Q/RT) \qquad 3.1$$

where T is the absolute temperature and R is the universal gas constant, σ is the uni-axial equivalent of the applied stresses and A, Q and n are constants.

When the slip process starts the deformation rate is not in equilibrium. The density of dislocations arrested at obstructions is low and slip can occur relatively easily. As slip progresses internal stresses increase and the deformation rate is reduced. Full treatment of the material behaviour requires transient terms to be included in the deformation calculations to take account of changes in temperature and stress. ADVICE uses a simplified model. Isothermal constant-stress creep can be described analytically by factoring the equlibrium creep rate by a term which takes account of the asymptotic approach to the equlibrium deformation rate which occurs during the primary phase of the deformation. The equation used follows:

$$\dot{\varepsilon}_p = \dot{\varepsilon}(1 + \exp(-360\,\varepsilon)) \qquad 3.2$$

Although this simplification does not rigorously apply to varying temperature and stress conditions, it is adequate for LOCA analysis (Donaldson 1983).

2. Grain Boundary Sliding

This process is often called superplastic creep because of the low stress dependence of the deformation rate. Deformation results from diffusion of atoms from one site to another on the grain boundary. It is slow and requires small grains, so it is important at stresses below 20 MPa, but not at stresses found in a large-break LOCA (Ecob 1985). Grain boundary sliding is neglected in alpha phase deformation calculations in ADVICE.

3. Athermal Dislocation Glide

At high stress athermal deformation becomes important and the material is said to yield. This is only likely to happen immediately before cladding failure and is unlikely to have a large effect on the failure time or the diametral strain at failure.

The deformation resulting from athermal dislocation glide can be added in series with that resulting from dislocation creep and this is done in the NORA model of zirconium deformation (Raff S 1982). The correlations used in this model are available in the ADVICE code as an option.

Correlations used in ADVICE

Although prediction of the cladding creep in the ADVICE computer code is based upon mechanistic arguments, numerical parameters need to be determined experimentally before the material behaviour can be predicted quantitatively. The prescription of these parameters is complicated by the large variation in properties between different supplies of cladding and necessitates the adoption of a flexible approach to their specification. The approach used in ADVICE is that of the CANSWEL code (Haste 1982).

Normally the Norton equation is used (equation 3.1), but where material properties have been correlated using Dorn's equation, this option can be selected instead. The Dorn equation follows:

$$\dot{\varepsilon} = A \exp(-Q/RT) \left(\sigma/G\right)^n (\sigma/T) \qquad 3.3$$

Where G is the shear modulus of the material and the other terms have the usual meaning.

The parameters Q, A and n are set by the user from published experimental data. If possible the experiment should be conducted on tube under similar loading conditions to those encountered during ballooning. Furthermore the effect of anisotropy needs to be accounted for. Donaldson (1983) presents his data in the form of hoop stress and hoop strain rate and this must be converted to uni-axial equivalent stress using the proposed anisotropy coefficients.

3.2.2 Anisotropy

The radial orientation of basal poles in alpha phase zirconium makes the material resistant to wall thinning. The anisotropic behaviour prevents the use of the Von Mises equation to describe the three-dimensional nature of the stress field. The relationship can however be modified to obtain a directionally biased equivalent stress as follows (Hill 1950):

$$\sigma_e=\sqrt{(F(\sigma_\theta-\sigma_z)^2 + G(\sigma_z-\sigma_r)^2 + H(\sigma_r-\sigma_\theta)^2)} \quad 3.4$$

where H, F and G are anisotropy coefficients for the material.

The deformation rates in specified directions are then found using the following equations:

$$d\varepsilon_\theta= (d\varepsilon/\sigma) \ (H (\sigma_\theta-\sigma_r) - F (\sigma_z-\sigma_\theta)) \quad 3.5$$

$$d\varepsilon_r= (d\varepsilon/\sigma) \ (G (\sigma_r-\sigma_z) - H (\sigma_\theta-\sigma_r)) \quad 3.6$$

$$d\varepsilon_z= (d\varepsilon/\sigma) \ (F (\sigma_z-\sigma_\theta) - G (\sigma_r-\sigma_z)) \quad 3.7$$

where σ is the stress in the specified direction, which is calculated

assuming the cladding to be a thin shell as follows:

$$\sigma_\theta = (PR/d) \qquad 3.8$$

$$\sigma_z = 0.5(PR/d) \qquad 3.9$$

where P is the differential pressure, R is the cladding mid-wall radius, and d is the cladding thickness.

Little data exists on the temperature dependence of the anisotropy coefficients (Hindle 1983), so the coefficients F, G, H are assumed to remain constant while the material is in the alpha phase, but the material is assumed to obey Von Mises' equation once the transition to the beta phase has started.

3.2.3 Deformation in the Transition Region

The body-centered cubic structure of beta phase zirconium is much softer than the hexagonal close-packed alpha phase. As crystals of beta phase material grow on the boundaries of the alpha phase grains, they affect the deformation in two ways:

Firstly, being much softer, they absorb much of the deformation and secondly they introduce a large number of small grains which are more capable of grain boundary sliding. The deformation model used to describe these processes is similar to that of CANSWEL-2 (Haste 1982).

The way that dislocation creep is shared between the phases is approximated by the following formula:

$$\dot{\varepsilon}_{\alpha\beta} = \dot{\varepsilon}_{\alpha}^{V\alpha} \quad \dot{\varepsilon}_{\beta}^{V\beta} \qquad 3.10$$

where $\dot{\varepsilon}_{\alpha}$ and $\dot{\varepsilon}_{\beta}$ are the deformation rates of the two phases, calculated by assuming the stress to be distributed equally throughout the material. This expression approximates a situation where the deformation, rather than the stress, is equal throughout the two phases.

Deformation due to grain boundary sliding is calculated using the following empirical formula:

$$\dot{\varepsilon}_{s} = \left((K_s \sigma^{n_s}) / T \right) \left(\left(1/(V_{\alpha}^2 + V_{\beta}^2) \right) - 1 \right) \exp(-Q/RT) \qquad 3.11$$

The total deformation is found by a linear addition of the deformation due to dislocation creep and that due to grain boundary sliding.

The strain rate is integrated using an analytical relationship derived from the Norton equation (Haste 1982). Since the actual behaviour of the duplex material is not in accordance with the Norton equation, effective values of the constants used in the Norton equation are calculated. The effective stress exponent n_{eff} and creep activation energy Q_{eff} are calculated using equations of the form:

$$n_{eff} = ((V_\alpha n_\alpha + V_\beta n_\beta) \dot{\varepsilon}_{\alpha\beta} + n_s \dot{\varepsilon}_s) / \dot{\varepsilon}_{total} \qquad 3.12$$

$$Q_{eff} = ((V_\alpha Q_\alpha + V_\beta Q_\beta) \dot{\varepsilon}_{\alpha\beta} + Q_s \dot{\varepsilon}_s) / \dot{\varepsilon}_{total} \qquad 3.13$$

3.2.4 Beta Phase Deformation

It is unlikely that cladding of a modern PWR would reach temperatures above 970^{0}C before clad failure. Should this happen the effect of cladding oxidation on failure strain would be beyond the scope of the oxidation model in the code, but the deformation is modelled using the Norton equation. Again the parameters are supplied by the user. A suitable set of input parameters is given in Table 1.

3.2.5 Phase Change Dynamics

The composition of zirconium in the mixed-phase temperature region is not simply a function of temperature, but depends also on the temperature history of the material. The transformation takes a finite amount of time and even moderate heating can result in material with a composition significantly different from equilibrium at that temperature.

Accurate modelling of the deformation in this temperature region requires a dynamic model of the material composition. Such a model has been developed at Chalk River (Holt 1980). The rate of transformation is given by:-

$$(dV_\alpha/dt) = \text{sign}(T_{eq}-T)\ 130 \exp(-18750/T) \quad |T_{eq}-T|^{2.5} \qquad 3.14$$

where T_{eq} is the temperature at which the present composition would be in equilibrium.

This expression leads to a convoluted integral because the equilibrium temperature at a given instant is a function of the composition at that instant. The expression was integrated numerically using Simpson's rule with increasingly small timesteps. The equilibrium temperature was calculated using the piecewise-linear approximation to the equlibrium composition shown in figure 16.

The phase change calculation takes place at the end of a timestep and the new composition is used in the next timestep without taking account of the changes occurring during that step. The calculation is explicit and could result in errors if too large a timestep is used, but explicit calculation removes the need for iteration in the deformation routines.

3.2.6 Phase Change Energy

The change to beta phase is an endothermic process and affects the cladding temperature. This effect is modelled by incorporating the phase change energy in the calculation of specific heat capacity. The material is, therefore implicitly assumed to be in equilibrium. This approximation permits implicit calculation of the final enthalpy without iterative calculation of the composition.

3.2.7 Cladding Oxidation

When zirconium is surrounded by steam at temperatures above 800^0C significant oxidation of the cladding occurs. This is important for a number of reasons:

1. Heat Generation

The reaction is strongly exothermic and can have a significant effect on the cladding temperature.

The code calculates the rate of reaction and uses the enthalpy of combustion to introduce the heat generation rate into the thermal calculations.

2. Oxidation Hardening

Oxygen is soluble in both alpha and beta phase zirconium. In alpha phase zirconium the oxygen causes solid solution hardening and can strengthen the material by a factor of up to 4, depending on concentration (Burton B 1978). Hardening is not observed in the β phase, but the oxygen causes the retention of the stronger alpha phase at higher temperatures. The ADVICE code calculates the oxide and the alpha phase thickness and assumes the combination of these materials to be stronger than the underlying β phase (or mixed phase) material by a factor of 50 (Haste 1982). When the deformation exceeds 2% the oxide cracks and the cracks extend through both the oxide and the retained alpha phase layer, so that much of the strengthening effect of this layer is lost. ADVICE assumes that the oxide hardening drops to zero at 2% strain.

As strain proceeds, further oxidation occurs at the base of the cracks in the oxide layer and the cracks propagate through the material, eventually causing failure. An embrittlement model is not included in the ADVICE code, so the failure strain of β phase zirconium in steam may not be well predicted if large amounts of oxidation occur.

3. Oxidation Rate Calculations

The oxidation correlation chosen for use in calculating deformation should be different from that used for hydrogen generation calculations. If a conservative calculation of peak clad temperature or hydrogen generation is required, the Baker-Just correlation is used. This correlation provides an upper bound on experimental results (Baker 1962). If, however, an upper-bound calculation is used in deformation calculations, it

over-predicts cladding hardening and azimuthal temperature gradients. This may lead to under-prediction of the failure strain, so best-estimate correlations should be used. The alpha phase and oxide thickness used in ADVICE are calculated as follows:-

$$\delta^2_{\alpha} = 1.523 \exp(-48140/R\ T) \qquad 3.15$$

$$\delta^2_{ox} = 0.0225 \exp(-35890/R\ T) \qquad 3.16$$

(Pawel 1977)

Account is taken of the effect of spatial temperature variation by calculating the oxidation rate at each azimuthal position.

3.3 Effect of Deformation on Fuel-pin Geometry

As the cladding deforms, a number of changes occur in the fuel pin geometry which affect the calculation of the cladding stress and temperature field.

3.3.1 Tangential extension of the cladding

Since the deformation is not uniform around the cladding circumference, the cladding moves in the tangential, as well as the radial direction. If calculations are to represent the deformation by dividing the cladding into sectors, account needs to be taken of the change in angle that these sectors subtend at the cladding center. The simplest way of doing this is to change the tangential spacing of the finite difference mesh to retain

the same amount of cladding in each sector, but this results in progressively poorer mesh refinement near the point of failure. This can be avoided by retaining a tangentially fixed finite difference mesh and modelling the transport of cladding material between one cell of the mesh and the next as the cladding deforms. The procedure used in ADVICE is as follows:

1. Individual strain rates are used to calculate the length of each element of cladding at the end of a time-step.

2. The total length of the cladding is calculated and a new mesh is constructed.

3. The amount of material crossing each mesh boundary is calculated.

4. The new thickness of a mesh element is calculated as a linear combination of the thickness of material that remained in the element and the material entering the element across the boundary.

5. New cladding temperatures for each element are also calculated by linear combination of original values.

This calculation procedure assumes that the cladding properties are uniform within a sector and that step changes occur between sectors.

3.3.2 Fuel Pin Bowing

The modelling of bowing is severely limited by the two-dimensional nature of the ADVICE computer code. In this respect ADVICE cannot be regarded as completely quantitative, but the code demonstrates the feasibility of constructing a more quantitative model and indicates the sort of results which such a model could be expected to provide.

The fuel pin is assumed to consist of two distinct regions of uniform properties; a ballooning region which is assumed to be of uniform curvature and a non-ballooning region which is assumed to behave elastically (figure I7). The lengths of these two regions are set by the user, but they should sum to the spacing between two grids. The direction of bowing is constrained to remain in a plane containing the axes of three adjacent rods. This assumption is based on the fact that anisotropic cladding bows away from its hottest point and, in the symmetrical case, that point is in this plane.

Placing a constraint on the bowing direction reduces the cladding displacement from a vector to a scalar and allows symmetry to be assumed. This permits only half the pin to be modelled. The displacement of the cladding is calculated from the strain field in the following way:

1. The radius of curvature of the cladding at the axial location of interest is found using the following equation:-

$$R_{b=}1/\left(\partial\varepsilon_z / \partial y\right) \qquad 3.17$$

where $\left(\partial\varepsilon_z / \partial y\right)$ is the axial strain gradient in the direction of bowing.

2. The curvature of the unballooned region is calculated by enforcing continuity of strain gradient:

$$R_{c=} R_b \left(L_c / L_b \right) \qquad 3.18$$

3. The curvature of the elastic region is used to determine the axial stress imposed on the balloon by its constraint.

$$\sigma_z = (y\ E)/R_c \qquad 3.19$$

4. The axial stress resulting from the bending calculation is fed back into the deformation calculation and the process is repeated until convergence is obtained.

5. The cladding curvature is then used to calculate the cladding displacement and pellet offset.

The iteration process uses a variant on the trapezoidal method developed for use in ADVICE and contained in a routine called DAMP (appendix 3). This routine is employed whenever iteration is required in ADVICE.

3.4 Thermal Modelling

The temperature field in the fuel pin is solved in the R-θ plane using a finite difference approximation of the following equation:

$$(\partial / \partial r)\,(kr\,\partial T/\partial r)+k(\partial / \partial \theta)\,(\partial T/r\,\partial \theta) + Sr = r\rho C_p(\partial T/\partial t) \quad 3.20$$

Where S is the volumeteric heat generation rate.

The nuclear heat generation per unit length of rod is specified by the user and the code calculates the local heat generation assuming the fuel to be new and the external neutron flux to be uniform. Heat generation by oxidation and plastic deformation is also calculated by the code. Heat transport by radiation is modelled as a source term and is calculated in both the radial and the tangential direction.

3.4.1 Solution of the Energy Equation

The solution of equation 3.20 is formulated in such a way as to reduce computation to a minimum. The full two-dimensional solution of the heat transport equation is preceded by a radial solution using the azimuthal average temperatures and fluid boundary conditions. The modelling of both radiation and temperature-dependence of material properties results in non-linear transport terms, so the equations must be linearised before a direct solution can be obtained. The direct solution must then be repeated until the non-linear terms converge. In order to save computation the variation of thermal properties is calculated only in the radial direction (where the temperature gradients are large). Iterative calculation of the properties is consequently confined to the one-dimensional solution.

In addition to calculation of property values, the one-dimensional solution is employed to provide a first guess for calculation of the two-dimensional temperature field. The one-dimensional solution is not used directly, but the two-dimensional field is changed by the same amount as the one-dimensional field is calculated to change. This approximation retains azimuthal temperature gradients and proves to be an accurate first guess. Convergence often occurs to a tolerance of 0.1^0C in less than 10 iterations.

The finite difference mesh used in these calculations is constructed with uniform spacing in both the pellet and the gas space. This results in parabolic accuracy in discretisation of the temperature gradients. Furthermore account is taken in the discretisation of property variation between cells of the mesh. Satisfactory accuracy can therefore be obtained with a relatively coarse mesh. Further details are given in appendix 4.

3.4.2 Radiative Heat Transfer

Radiative heat transfer occurs at both the inner and the outer surfaces of the cladding. Both of these transfers are modelled.

1. Radiative Heat Transfer from the Cladding Outer Surface

Steam is almost completely transparent to thermal radiation, while water droplets are almost completely opaque. Radiative transfer occurs to neighbouring rods when the steam is dry and to the coolant when the flow is wet. Since the code cannot predict the presence of droplets, the flow is assumed to be transparent and the outer surface is assumed to radiate to a surface at the average temperature of the subject rod. Little net radiative transfer from the rod is calculated to occur, but this model results in cooling of hot spots in the cladding.

2. Radiative Heat Transfer Between the Pellet and the Cladding

As the gap between the pellet and the cladding increases the importance of radiation transfer across the gap increases.

Initially the gap is small and both the thermal resistance and the pellet-cladding temperature differences are low, but as the gap increases, so does the resistance to conductive heat transfer. Heat transfer by conduction is a linear function of temperature difference, while radiation depends upon the cube of the temperature difference. As temperature differences increase, a higher proportion of the heat is transfered by radiation until eventually the cladding temperature difference rises sufficiently for radiative heat transfer to be as important as conduction. A detailed model of radiative heat transfer is therefore required.

Accurate calculation of radiative transfer between surfaces which are not at uniform temperatures is computationally expensive, so this work limits itself to improving upon the "thin gap" approximation used in other codes.

The thin gap approximation assumes that all radiation leaving the pellet surface travels radially to the cladding. In reality some radiation is emitted at an angle to the surface normal and will result in tangential heat transfer.

If the pin is considered to be made up of a number of segments, the radiative heat transfer can be modelled by calculating the radiation view factor for transfer from a segment of the pellet to a sector of the cladding. In this study the view factor for radiation transfer within a segment is calculated using the "crossed string" method (Mc Adams 1954) and the remaining radiation is assumed to be divided equally between the two adjacent sectors. Radiation transfer beyond the adjacent sectors is neglected.

In the limit, as sector size tends to zero, this approximation tends to the thin gap approximation, but for practical mesh sizes it provides a means of taking some account of azimuthal radiation transfer which can reduce azimuthal temperature gradients.

The surfaces of the cladding and pellet are assumed to be grey and diffusely reflecting. The heat transfer is calculated by the following formula:-

$$q_{12} = \Sigma \, (T^4_1 - T^4_2) \, / \, ((1/E_1 - 1) + 1/f_{12} + (1/E_2 - 1) A_1 / A_2) \quad 3.21$$

3.4.3 Coolant Flow Between Rods

General Comments

The cooling of fuel rods during a LOCA is essentially a two-phase phenomenon and even during early reflooding, much of the fuel rods is cooled by film boiling. Fortunately ballooning of the fuel cladding can only occur in poor cooling conditions where the coolant is steam well above the saturation temperature, so the flow past ballooning cladding can be

treated as single-phase (Yadigaroglu 1980). Even in the region of highest cladding temperatures there are some water droplets in the flow, but the rate of cooling is not sensitive to them provided that the number of droplets is low (Fairbairn 1984). Note that the concept of flow quality is not relevant to the mixture of super-heated steam and water droplets found during reflooding because the assumption of thermodynamic equlibrium cannot be made in these rather extreme flow conditions.

This work treats the flow through the rod bundle as fully-developed, single-phase and turbulent. The correlations developed to predict the circumferential variation of surface heat-transfer coefficient are derived from calculations of steady flow in long uniform rod bundles. In fact balloons can only be considered uniform over a length of ten diameters at best, but analysis of the essentially three-dimensional flow which exists in reality, is only just within the capabilities of current techniques and is too complicated to be considered here in detail. Perturbations in the geometry of the rod bundle will result in cross-flow between subchannels. The flow through the gap between balloons will be affected by the reduction of turbulence resulting from acceleration. Axial vortices in the flow will be stretched, increasing their angular velocity, and the structure of the turbulence will not have enough time to reach equlibrium, but the effect of these differences is beyond the scope of current work.

Heat-transfer Coefficient Variation

Considering the shape of the coolant channels (figure 18), it should not be surprising that the surface heat-transfer coefficient varies around the circumference of the pin. In fact what should surprise us is that, for turbulent flow, the variation is so small that, at the normal pitch-to-diameter ratio of 1.33, it is hardly significant.

The reason for the lack of variation is that turbulence causes a bulk rotation to be superimposed upon the axial velocity of the fluid (figure 19). This secondary vorticity transports momentum and energy tangentially along the rod surface. Fluid flows from the main bulk in the middle of the channel into the gap between the rods. It moves along the rod surface then returns to the middle of the channel. Heat transfer from the rod is enhanced near the inter-rod gap and reduced near the open channel.

Variation of shear stress and heat-transfer coefficient only starts to become strong at P/D ratios less than 1.1. Shear stress profiles normalised by average values are shown in figure 20. The profile obtained experimentally for the case where the rods are in contact is very similar in shape to the calculated profile for the pitch-to-diameter of 1.02. This gives confidence in the calculated flow conditions on which the heat transfer is based. These profiles are not sensitive to Reynolds number, provided that the flow is fully turbulent, but in the laminar-turbulent transition region the distributions become less uniform (Eichorn 1980).

Normalised heat-transfer coefficient profiles are shown in figure 21 for the uniform wall temperature case. With the exception of the case of touching rods, these profiles are the results of calculations performed by Rapley using a finite difference code incorporating an Algebraic Stress Transport model of turbulent flow (Rapley 1984). The results are not validated by experiment because it is not normal to obtain square pitched rod bundles at these pitch-to-diameter ratios. They are, however, qualitatively similar to triangular-pitched bundles, for which the calculation method has been successfully validated (Rapley 1980)

The variation of heat-transfer coefficient around the periphery of the fuel rod depends upon the heat-flux profile. Correlations were therefore obtained for both constant-heat-flux and constant-wall-temperature conditions. Local heat-transfer coefficients, calculated by Rapley (1984), were normalised by the azimuthal average and were fitted using the first two terms of the Fourier series. The resulting correlation-derived profiles are compared with finite-difference based predictions in figures 22-28. Results of the constant-wall-temperature correlation are compared with both the constant-heat-flux and the constant-wall-temperature finite difference predictions, for a number of pitch ratios, in figures 22-24. The constant-wall-temperature expression follows:

for P/d<1.18

$$h = \bar{h}\,(1 + a2\cos 4x + a3\cos 8x) \qquad 3.22$$

$$a2 = -0.23(1 - 5.5(p/d - 1)) \qquad 3.23$$

$$a3 = -0.77(1 - 5.5(p/d - 1)) \qquad 3.24$$

The constant-heat-flux correlation is compared with the data in figures 25-28. The expression used follows:

$$h = \bar{h}\,(a1 + a2\cos 4x + a3\cos 8x) \qquad 3.25$$

where;

$$a1 = \left({}_0\int^A \Delta T\, dA \right) \left({}_0\int^A 1/\Delta T\, dA \right) \qquad 3.26$$

where ΔT is the local clad-fluid temperature difference.

$$a2 = -1.1 \exp(-9.6\,(p/d - 1)) \qquad 3.27$$

$$a3 = -0.05 + 0.16 \exp(-15.3\,(p/d - 1)) \qquad 3.28$$

Note that, in the case of uniform heat flux, the average value of the heat-transfer coefficient differs from the overall value by the factor a1. This is because the overall heat-transfer coefficient is based upon the average temperature difference, while the true average is based on the ratio of heat-flux to temperature difference. The calculation of a1 is formulated in such a way that, if the cladding has a uniform temperature, rather than a uniform heat flux, the value of a1 would be unity and the specification of a constant-heat-flux boundary condition would not result in an error in the total heat transferred.

3.5 Thermal Properties

The material properties used are taken from the data assembled by NRU and published in their handbook MATPRO 11 (Hagrman 1979).

3.5.1 Zirconium

1 Specific Heat Capacity

A piecewise-linear function of temperature is used. The data on which this is based is shown in Table 1. The function is based on experiments using vacuum-purged material, so no account is taken of the effect of dissolved hydrogen. The standard error for temperatures below 970^0C is 2.8 J/KgK. The error in enthalpy in the two-phase region is more complicated. The standard error in the data is about 10 J/KgK, but heat capacity is affected by the enthalpy of phase change. The thermal part of the code takes no account of the departure of the material from its equlibrium composition, so a small error in cladding temperature may exist, for a short time, in rapid high-temperature transients.

2 Thermal Conductivity

The thermal conductivity is given by the following polynomial:

$$k=7.51 + 2.09E\text{-}2\,T - 1.45E\text{-}5\,T^2 + 7.67E\text{-}9\,T^3 \qquad 3.29$$

where k is in W/mK and T is the absolute temperature. (Hagrman 1979)

Experiments showed little measurable difference between the properties of Zircaloy-2 and Zircaloy-4. The material texture may have some effect on the conductivity of alpha phase zirconium, but insufficient data is available to model this. The standard error in the data used is estimated to be 1.01W/mK.

3.5.2 Uraniumdioxide

The pellets were assumed to be made of stoichiometric uranium dioxide of 95 percent theoretical density.

1 Specific Heat Capacity

The fuel specific heat capacity is calculated using the relationship below:

$$C_V = \frac{c1\,T_e^2\,\exp(T_e/T)}{T^2(\exp(T_e/T)-1)^2} + c2\,T + \frac{c3\,ED\,\exp(-ED/R\,T)}{R\,T^2} \qquad 3.30$$

where

$c1=296.7\ J/KgK$ $\quad c2=2.43\times10^{-2}\ J/KgK^2$

$c3=8.745\times10^{7}\ J/Kg$ $\quad T_e=535.285K$

$ED=1.577\times10^{5}\ J/mol$ $\quad R=8.314\ J/molK$

T is the pellet absolute temperature and c_v is the specific heat capacity in J/KgK.

The standard error is estimated to be 3 J/Kg K. (Hagrman 1979)

2 Thermal Conductivity

The following correlation was used:

$$k = \frac{c1}{c2 + T} + c3 \exp(c4\ T) \qquad 3.31$$

where;

c1=40.4W/cm
c2=464°C
c3=1.216×10^{-4} W/cmK
c4=1.867×10^{-3} 1/K

k is the thermal conductivity in W/cm K and T is the temperature in degrees celsius. (Hagrman 1979)

Chapter 4

Contents **Page**

Calculations with the ADVICE Code

Tests were carried out both on specific routines and on the code as a whole (Details are given in appendix 5). The code was then used to model the NRU MT3 experiments and the predictions made were compared with both those of the MABEL code, and the results of the experiment.

Modelling the MT3 Experiment

The MT3 experiment was chosen as a subject for modelling because it used a large bundle of nuclear heated rods and they were subjected to a temperature transient similar to that of the fuel in a real PWR during a large-break loss-of-coolant accident. The experiment has been used to obtain the values of pellet-cladding relative offset required to run clad-ballooning codes (Healey 1983) and considerable work has been carried out analysing the test results. Unfortunately the instrumentation did not prove totally satisfactory, so judgement needs to be exercised in specifying the experimental boundary conditions, but comparison with other calculations provided additional validation of ADVICE.

Six different calculations were carried out and each has been designated a run number in the range R1 to R6. The conditions used in each calculation are summarized in Table 2. The purpose of each calculation is described briefly below and a more detailed discussion of each run is presented later.

Run 1

A post-experiment prediction of the failure strain and temperature history was made. The observed pressure history was used directly, despite a large post-calibration error, and the heat transfer coefficient history was constructed to provide the best available representation of the experiment.

Run 2

The same conditions as Run 1 were used, but in this case radiation heat transfer across the gap between the pellet and the cladding was assumed to be radial only. This calculation demonstrates the consequences of ignoring azimuthal radiation heat transfer when clad bowing is calculated.

Run 3

The same conditions as Run 1 were used except that the fuel pin radiation heat-transfer model was omitted completely.

Run 4

The MT3 experiments were carried out with cladding tubes supplied by NRU. The NRU material is significantly stronger than other zircaloy cladding (Donaldson 1983), so the effect of using the more common Westinghouse cladding was investigated.

Run 5

The thermo-hydraulic data set used in MABEL calculations (Haste 1982) was input to ADVICE in its unmodified form and the results were compared with those obtained using MABEL. The pin pressure history calculated by MABEL was not available, so this was estimated.

Run 6

A study of the effect of cladding thickness variation was made. Uniform cladding was compared with cladding containing the maximum thickness variation observed in studies of ORNL test tubing (Johnston 1976). Westinghouse material was assumed, so the study was not specific to the MT3 tests.

4.1 Specification of Boundary Conditions

The input data is shown in Table 1. Several parameters are subject to some uncertainty:

1. Cladding Thickness

A cladding thickness of 0.61 mm was used by Haste in MABEL calculations while Donaldson used 0.58 mm. The cladding was assumed to have a uniform thickness of 0.61mm in the present work.

2. Fuel Rod Internal Pressure

Donaldson recommended a cold fill pressure value of 550 psi. Gibson reported a cold fill pressure of 550psig (564psi) (Gibson 1982). The pressure transducers all failed to provide accurate measurements. The best transducer showed a post-calibration error of 75psi and read 8.9 MPa at the start of the transient. Haste used a pressure of 8.2MPa at the start of the transient (based upon the fill pressure). The present work used the pressure histories shown in figure 30. The top curve represents the pressure measurements reported by Donaldson, with no post-calibration correction, and the lower curve results from a uniform change to these values made to obtain agreement with the initial value used by Haste.

3. Thermo-Fluid Boundary Conditions

Heat-transfer coefficient and fluid temperature boundary conditions were taken from RELAP calculation results (Haste 1983). Calculations were performed for axial level 15 in the experiment (the position at which the highest cladding temperatures were observed). An anomoly was detected in the RELAP results. The RELAP calculations predicted that a cold slug of water would pass through the test section when reflooding started at 30s. The cold slug was predicted to cause significant cooling of the rods, but no enhanced cooling was observed in the experiment. Temperature measurements at level 15 in the test rig are shown in figure 32. The cladding does not show increased cooling at 30 seconds. Furthermore no appreciable cooling was detected by the shroud thermocouple (figure 33) until 50 seconds.

When the purpose of the calculations was to make comparisons with the experiment, the cladding was assumed to be cooled by steam for the first 50 seconds of the transient.

4. Power

Rod power was found by heating the rods adiabatically prior to the ballooning experiment. The adiabatic heat-up-rate data is shown in figure 31 (Gibson 1982). Iterative calculation showed the rod power at level 15 to be between 1.71 and 1.89 KW/M. The power generation figure of 1.77 KW/M used by Haste is consistent with this, and was used in all of the calculations presented here.

5. Material Properties

Creep parameters were those used by Haste in the MABEL code, with the exception of the anisotropy coefficients which were set to typical values for cold worked fuel cladding (Sills 1979).

4.2 Calculation Results

Run 1: Comparison of Calculated Results with Experiment

The experimental conditions were duplicated as closely as possible. The heat transfer data predicted by RELAP does not predict the cladding temperatures well, so it was modified. In reality the cladding heated up adiabatically until 50 seconds into the experiment and reached temperatures 50^{o}C higher than predicted using the MABEL input data set based on the RELAP calculations.

The calculation reported here was made assuming adiabatic conditions up to 40 seconds, followed by RELAP-predicted heat-transfer coefficients at later times. The pressure history used was the measured history for rod 2C (figure 9) without any adjustments.

The calculated temperature history shown in figure 34 and can be compared with the observed temperatures in figure 32. The predicted failure temperature was 1060K, which agrees well with the observed mean value of 1067K and the predicted failure time was 160 seconds, which is within the experimental range of 109-182 seconds.

The deformation proceeds fairly steadily for approximately two minutes before accelerating towards failure. The cladding strain localization is shown in figure 35 where the ratio of the peak to the average strain is plotted against strain. Despite an eccentric pellet stack, the deformation remains largely uniform until the rods start to approach each other. The proximity of other rods then affects the distribution of surface-heat-transfer coefficient and large azimuthal temperature gradients start to develop. At 25 percent strain the peak strain is still

only twice the average, but when contact with all four neighbouring rods occurs at 29 percent strain, the deformation has already become localized at the point of contact. The strain achieved at the failure site exceeds 200 percent but, because the deformation is confined to a small proportion of the cladding, the effect of this strain on the diameter of the cladding is small.

The relative movement of the cladding and the pellet is shown in figure 36. Initially the pellet is completely offset in the cladding and temperature variation in the cladding causes the creep rate to vary, resulting in rapid bowing. Since the rods are constrained, bending moments are set up to oppose the bowing, causing it to slow down. As the cladding deforms the clad diameter increases and bowing of the cladding is not sufficient to maintain contact with the pellet. The eccentricity of the cladding and the pellet therefore decreases as the cladding diameter increases. This leads to a reduction in azimuthal temperature gradients and hence a further reduction in the rate of bowing. Nevertheless, the displacement of the cladding increases until the rod comes into contact with its neighbour at 27% strain. The subject rod is then pushed back to its original position and the original pellet offset is re-established. Deformation proceeds so rapidly at this stage that subsequent changes in geometry do not have time to effect the temperature field before failure occurs.

Assuming a local ductility of 200%, the cladding fails at a true strain 39% (48% engineering) which is within the experimentally observed range of between 30% and 53% engineering strain (Mohr 1983). The fact that failure occurs near the top of the range of observed strain is to be expected. The calculation assumed uniform cladding thickness, while in practice some variation in thickness occurs, leading to earlier failure.

Run 2: Calculation using Radial Radiation Heat Transfer Only

A model of radiation heat transfer in the gap between the pellet and the cladding is necessary because this mechanism can account for up to 40% of the total heat transfer. ADVICE normally uses a two-dimensional model, but Run 2 was made using the thin gap approximation (ie. radial configuration factors equal to 1). The results of this calculation are compared with those of the normal model to determine the degree of complication required in a model containing mechanistic treatment of clad bowing.

The cladding average temperature was not changed significantly by omitting azimuthal radiation transfer, but the deformation behaviour was somewhat different. Failure occurred earlier in the case of the calculations using the thin gap approximation and the failure strain was lower.

The average strain history, for Run 2, is shown in figure 37. The strain history is almost indistinguishable from that of the more complex model until failure, but the simple model predicts failure about 3 seconds earlier. Moreover, the simple model predicts a true strain of 30%, rather than 39% in the case of the model which included tangential radiation transfer. The difference in failure strain results from different bowing behaviour.

The pellet offset predicted in Run 2 is shown in figure 38. The Clad bowing is not calculated to stabilize at a cladding displacement of 0.3 mm as the full model predicted. Instead azimuthal temperature gradients develop which permit further bowing until contact is made with another rod at a pellet offset of 0.6 mm. The cladding is then pushed back to its original position and starts to flatten. By this time the deformation has become localized and failure is predicted before serious channel blockage.

The strain localisation is shown in figure 39. Deformation is always less uniform when the thin gap approximation is used than with the 2D model. When the neighbouring rod is contacted at 22% strain, the peak strain is already twice the average and failure approaches rapidly. The choice of model clearly has an effect on failure strain predicted and should be made with care.

Run 3: Calculation Assuming no Radiation Heat Transfer

The cladding temperature history is shown in figure 40. Little difference in the average cladding temperature can be observed when this calculation is compared with that of the full model, except that the cladding failure is early and no increase in cladding temperature occurs immediately prior to failure because the failure strain is too low to cause significant coolant channel blockage.

The pellet offset history is shown in figure 41. This differs considerably from the results of Run 1. The pellet offset develops rapidly as deformation proceeds and the pellet eccentricity remains close to 1. Bending moments resulting from the constraint have little effect. The offset of the pellet results in large azimuthal temperature gradients which cause further bowing and more localised deformation. The cladding is calculated to contact its neighbour at 2l% strain then to straighten, but by this time failure is imminent.

The strain localisation is plotted against strain in figure 42. From the start of ballooning the deformation becomes increasingly localised and, in the absence of heat transfer by radiation, the cladding fails at 25% strain.

Run 4 : The Use of Westinghouse Material

Calculations were performed using the alpha phase creep constants which describe the Westinghouse fuel cladding. This cladding is significantly softer than NRU material and consequently failed much earlier at 108 seconds. Cladding strain is shown as a function of time in figure 43.

The strain commences at about 40 seconds, and reaches 4% before the rapid rise in clad temperature finishes at 60 seconds. The deformation rate steadily increases until 30% strain is obtained. Then it slows down as the rod flattens because the support provided by adjacent rods causes a reduction in stress. Finally the deformation accelerates again when the clad temperature rises as coolant channel blockage is approached.

The pellet offset is shown in figure 44. In the early stages of deformation the cladding surface is almost adiabatic. Temperature gradients are therefore smaller than in the case of NRU material at the same strain and the cladding bows less than the NRU material initially. As strain progresses the bowing increases and the difference in the behaviour of the materials is reduced. When contact is made with the neighbouring rod at 26% strain the pellet offset is similar to that of the NRU material. The lack of temperature gradients early in the deformation leads to less rapid strain localisation (figure 45). This results in a predicted true strain greater than 44% and a predicted channel blockage greater than 90% for uniform thickness material.

Run 5 Comparison with MABEL Results

Haste carried out a number of calculations with different assumptions about the behaviour of surrounding rods, but ADVICE calculations have been limited to the assumption that all of the surrounding rods strain at the same rate as the subject rod. MABEL results for this assumption are shown in figure 46. ADVICE results for the axial level corresponding to node 14 in the MABEL grid are shown in figure 47. Close agreement between the temperature histories is evident.

The initial cladding temperature is 420^{o}C and after 15 seconds it rises rapidly. After 30 seconds the rate of increase is limited, for a short time, by a temporary improvement in heat transfer resulting from the injection of a large quantity of water at the start of reflooding. After 40 seconds the cladding temperature rise becomes progressively slower, until at about 170 seconds the cladding reaches the phase transition temperature. Rapid deformation of the cladding then reduces the heat transfer from the fuel and increases the surface exposed to the coolant, so the cladding temperature drops. The cladding temperature is shown, as a function of strain, for the ADVICE calculations, in figure 47. As rod interaction starts the area of cooled surface drops and the cladding temperature rises again until ADVICE terminates calculations when 90% of the coolant channel is blocked.

The failure strain predicted by the MABEL code depends upon the pellet eccentricity value selected and predicted strain varies from 29% engineering strain to complete channel blockage at 60% engineering strain. The failure time only varies between 181 and 200 seconds and this agrees with the ADVICE result of 190 seconds.

When comparing the deformation histories shown in figures 46 and 47, two points are worthy of note:

1. The cladding deformation calculated by the ADVICE code shows a temporary increase in strain rate between 8 and 18 percent strain. This results from a short time spent above the phase transition temperature. This change is also present in the MABEL calculations, but it is much smaller. The difference is probably a result of a slightly higher temperature calculated by the ADVICE code because it makes no allowance for the effect of deformation on the overall surface heat transfer coefficient.

2. The ADVICE code does not predict a reduction in the deformation rate as coolant channel blockage occurs. This may be due to the fact that ADVICE models the heating of the cladding caused by plastic deformation, but some difference in the deformation behaviour predicted by MABEL and ADVICE is inevitable because the pressure history, calculated by MABEL was not available and had to be estimated. The amount of agreement obtained is encouraging.

The strain localisation calculated by ADVICE is shown in figure 48 as a function of strain. The assumption that cladding material becomes isotropic once the phase change starts resulted in a prediction that the pellet stack would remain almost concentric in the cladding. The deformation is consequently predicted to be stable and uniform. The sharp increase in deformation rate, resulting from the start of the phase change, is the only major source of destabilization. The local strain is not predicted to exceed 100% before channel blockage occurs.

This prediction disagrees with experiment (Barlow 1983). The increased sensitivity of the deformation to temperature, caused by the phase change, results in a reduction, and not an increase, in failure strain after the transition to the beta phase has commenced. The Anisotropy data published by Hindle also contradicts the assumption of an immediate return to isotropy. Insufficient data exist to make definite conclusions about anisotropy of mixed-phase material, but a linear drop in anisotropy with composition would probably be a better approximation than an immediate return to isotropy at 820^{o}C.

Run 6 Effect of Thickness Variation

The thickness of cladding tubing used by the NRC has been found to vary by up to 0.04 mm in any one tube (Johnson 1976). In order to investigate the effect of this variation two calculations were made. In one calculation uniform cladding was assumed and in the other the cladding thickness was assumed to vary as the cosine of the angle, between 0.63mm and 0.59mm.

The temperature histories for the uniform and varying thickness cladding are shown in figure 49. They both deform in the high alpha phase temperature range, but the non-uniform cladding fails at relatively low strain, so no increase in cladding temperature was predicted in this case.

The strain histories, for the two cases, are shown in figure 50. The uniform cladding deforms at essentially the same rate as the non-uniform cladding until 20% strain is reached. The deformation rate for the non-uniform case then starts to accelerate, leading to failure at 110 seconds. The uniform cladding continues to deform until 90% channel blockage is calculated to occur at 135 seconds.

Pellet offset histories are compared in figure 51. The cladding behaviour is qualitatively similar. Both rods bow rapidly initially, then the effect of bending moments limits the bowing and the pellet eccentricity drops from near 1 to a low value. The uniform cladding achieves a displacement of 0.2 mm, while the non uniform cladding achieves 0.4 mm, before being pushed back to its original position by contact with the neighbouring rod.

The difference in bowing behaviour results in a difference in azimuthal temperature range. The cladding circumferential temperature variations are compared in figure 52. The temperature difference in the non-uniform case is substantially greater and rises sharply as a result of localised plastic work immediately prior to failure.

The extent of strain localization is compared in figure 53. The deformation of the non-uniform cladding is always considerably less uniform, and the onset of instability occurs at 20% strain. This happens at 30% strain in the case of the uniform cladding. Failure is not calculated to have occurred in the uniform case, but it is imminent when blockage is reached because the local deformation is 4 times the average and the difference is increasing rapidly. The failure of the non-uniform material occures at 33% true strain before serious channel blockage.

Chapter 5

Contents **Page**

Discussion and Conclusion

The ADVICE computer code has been constructed to reduce the need for empirical approximations in the prediction of cladding failure strain.

Two processes which destabilize the deformation are modelled: A correlation has been developed to calculate the local heat transfer coefficient at the fuel pin surface and a model of clad bowing has been introduced to predict pellet eccentricity. Both of these models involve assumptions that are based upon limited experimental evidence.

5.1 Variation of Heat-Transfer coefficient

Data on the variation in surface heat transfer has been obtained from the results of turbulence modelling calculations, rather than experiment, and despite the fact that these calculations have been demonstrated to be reasonably accurate in rod bundles (Rapley 1980), the assumption that the flow pattern in the neck of a blockage is fully developed is not justified for the case of short balloons. Nevertheless some assumption is necessary in the absence of more detailed information, and fully developed turbulence leads to more uniform heat flux than would arise in the absence of secondary flows. This approximation is therefore likely to under-prediction of the variation of the cladding temperature and hence over-prediction of the diametral failure strain.

Neglecting cross flow leads to less predictable results. If a large coplanar blockage develops, there will be no nett cross flow in the centre of the blockage, but observed blockages tend not to be uniform and cross flow between the coolant subchannels surrounding the rods could cause more uniform heat-transfer coefficient profiles than the analysis predicts (leading to higher cladding strains).

5.2 Bowing of the Cladding

The ADVICE code uses cladding curvature at a single axial position to calculate the bowing of a rod and hence the relative offset of the cladding and the pellet stack. This cannot be expected to result in highly accurate predictions of cladding strain. Clearly a three-dimensional model that calculates cladding curvature as a function of axial position is desirable. Nevertheless the use of even a crude model of clad bowing is a step forward when compared to codes which require the specification of pellet eccentricity or cladding azimuthal temperature range. Clad bowing is affected by a complex interaction between the stress and temperature distributions in the material, so studies of the effects of changes in conditions could result in inaccurate conclusions if the effect of these changes on the bowing process is not considered. One illustration of this possibility is provided by the study of the effect of non-uniform clad thickness on failure strain (Run 6).

The study demonstrated that the high stress in the thinnest part of the cladding, while not enough to cause failure in itself, results in increased bowing of the cladding and higher temperature gradients. Conventional clad-ballooning computer codes would have implicitly assumed that the thickness variation did not affect the bowing and would have under predicted the importance of this effect.

The results of Run 6 suggested a likely range of engineering strain of between 39 and over 57%. Run 6 was meant to represent typical LOCA conditions, and the conditions assumed were not identical to those of the MT3 experiment, but the strains predicted are similar to the range of 30-53% engineering strain observed in the MT3 experiment.

5.3 Performance of the Code

The code was tested in a number of ways:

1 The rod power was found independently by MABEL and ADVICE from MT3 adiabatic heat-up data and the same result was obtained.

2 When an anomaly in the MABEL input data was removed the MT3 rod temperature behaviour was well predicted (Run1).

3 Run 5 was a made using the same input data as the MABEL computer code and the predicted cladding temperatures were almost identical to those of the MABEL calculations until MABEL started to modify the input heat-transfer coefficients.

The prediction of cladding deformation in the mixed-phase region was, however, inaccurate (Run 5). The supposed return to isotropic deformation lead to symmetrical ballooning and to low temperature gradients. This caused an over prediction of diametral strain at failure. If the anisotropy data published by Hindle (1983) were included in the code, this would be corrected. Bowing would be calculated to occur after the phase change started and, since the deformation is more temperature sensitive in this region, the resulting temperature gradients would limit the diametral failure strain.

The predicted rod behaviour in the MT3 experiment was within the observed range both of failure strain and failure time, but this is not a rigorous test given the wide range in both. Two-phase reflooding experiments are probably not the best way of validating ballooning codes because our lack of understanding of the flow increases uncertainty. Also in-core pressure measurement needs to be improved.

5.4 Effect of Modelling Changes

The effect of introducing a detailed model of radiation across the pellet-clad gap was to increase the failure strain from a true strain of 25% in Run 3 to over 45% in Run 1. (The one-dimensional model used in Run 2 resulted in a predicted true strain of 30%). This result is only relevant to models that include a description of the bowing process and it demonstrates that detailed modelling of all sources of azimuthal instability is more important in a code that models bowing than in a conventional code. The reason for the increased sensitivity is that small errors in the description of the physical processes of azimuthal heat transfer can cause large errors in the strain profile by their influence on the stability of the deformation. Other factors which were found to be important include the model for transport of mass and energy across cell boundaries during non-uniform deformation and the inclusion of local calculation of phase change dynamics and deformation work. The process of validating ADVICE should be continued and sensitivity studies should be an important part of future code development.

5.5 Future Work with the ADVICE Code

1. The anisotropy model should be modified to take account of the gradual reduction of anisotropy as the phase change takes place. The current model over predicts failure strains in the mixed phase temperature region.

2. An oxygen embrittlement model should be developed to permit prediction of failure strain in the beta phase region.

3. A more detailed study of the effect of cladding thickness variation should be carried out. The statistical distribution of thickness within a batch of tube could be used to predict the likely distribution in failure strain resulting purely from this cause.

4. Ultra-sonic measurement of the cladding thickness distribution in individual tubes should be made and ADVICE should be used to predict the failure strain of these tubes.

5. The effect of surrounding rods could be investigated by changing the assumption that all rods deform at the same rate. This could be done by studying the effect of changing the calculation of pitch-to-diameter ratio.

6. The effect of the constraint model used in ADVICE should be studied. The rods should be permitted to move apart as they do in the MT3 experiment and the results of ADVICE calculations should be compared with those Haste obtained using MABEL (Haste 1984). MABEL does not model local heat transfer coefficients so some differences in results are likely.

7. The ADVICE code should be extended to include calculation of fluid flow and to permit a three dimensional model of clad bowing to be constructed. The bowing should only be permitted to occur in a specified plane because this permits the maximum deflection to be modelled as a scalar and allows a rapid solution to be obtained by the relaxation method used in ADVICE.

Table 1 : ADVICE Input Data Set

CREEP CONSTANTS

ALPHA PHASE

MIXED PHASE SUPER PLASTIC CONSTANTS

STRUCTURE CONSTANT	STRESS EXPONENT	ACTIVATION ENERGY
.5750E+07	1.500	.1785E+06

BETA PHASE

STRUCTURE CONSTANT	STRESS EXPONENT	ACTIVATION ENERGY
15.69	4.000	.1500E+06

PRIMARY CREEP CONSTANTS

0. 0.

OXIDE HARDENING FACTOR

50.00

OXIDE FRACTURE STRAIN	GAS CONSTANT
.2000E-01	8.314

PHASE CHANGE START	PHASE CHANGE END	DORN FACTOR
1093.	1253.	1.000

GENERAL DATA

NUMBER OF NODES

NSECTORS	NPELLET	NGAP	NTIME
24	5	2	8

GEOMETRY

DT	TOL	P/D	COLDLGTH
45.00	.1000	1.330	.2500

HOT LENGTH	RUFFNESS	PELRAD	CLADR
.5000E-01	.1000E-04	.4800E-02	.5150E-02

OFFSET	FREQUENCY	RELAX	STEP
.1000E-03	4.000	1.300	.1000E-01

NEUTRON DIFFUSION PARAMETERS

ABSORPTION CROSS-SECTION	DIFFUSION COEFFICIENT
16.90	.1616E-01

HILLS ANISOTROPY FACTORS

F,G,H+7.730000E-01 +5.320000E-01 +1.950000E-01

EMISSIVITIES; PELLET 8.000000E-01 CLADDING 8.000000E-01

TABLES OF TIME DEPENDENT VALUES

TIMES AT WHICH PROPERTIES ARE GIVEN

.0000E+00 45.00 90.00 135.0 180.0
225.0 270.0 315.0

FLUID TEMPERATURE HISTORY

473.0 573.0 623.0 673.0 723.0
773.0 823.0 873.0

POWER HISTORY

1.850 1.850 1.850 1.850 1.850
1.850 1.850 1.850

HEAT TRANSFER COEFFICIENTS

4.760 .1000E-06 .1206 .1206 .1206
.1206 .1206 .1206

PIN INTERNAL PRESSURE

8.000 8.000 8.000 8.000 8.000
8.000 8.000 8.000

EXTERNAL FLUID PRESSURE

0.3 0.3 0.3 0.3 0.3
0.3 0.3 0.3

Table 2

Conditions in Test Runs

Run	Start Pressure	Heatup Behaviour	Comments
1	8.2 MPa	Adiabatic	Experiment post-prediction
2	8.9 MPa	Adiabatic	Limited radiation model
3	8.9 MPa	Adiabatic	No radiation model
4	8.9 MPa	Haste data	Effect of material change
5	8.2 MPa	Haste data	Comparison with MABEL
6	8.2 MPa	Adiabatic	Effect of thickness Variation

Fig 1 Fuel Pin Assembly

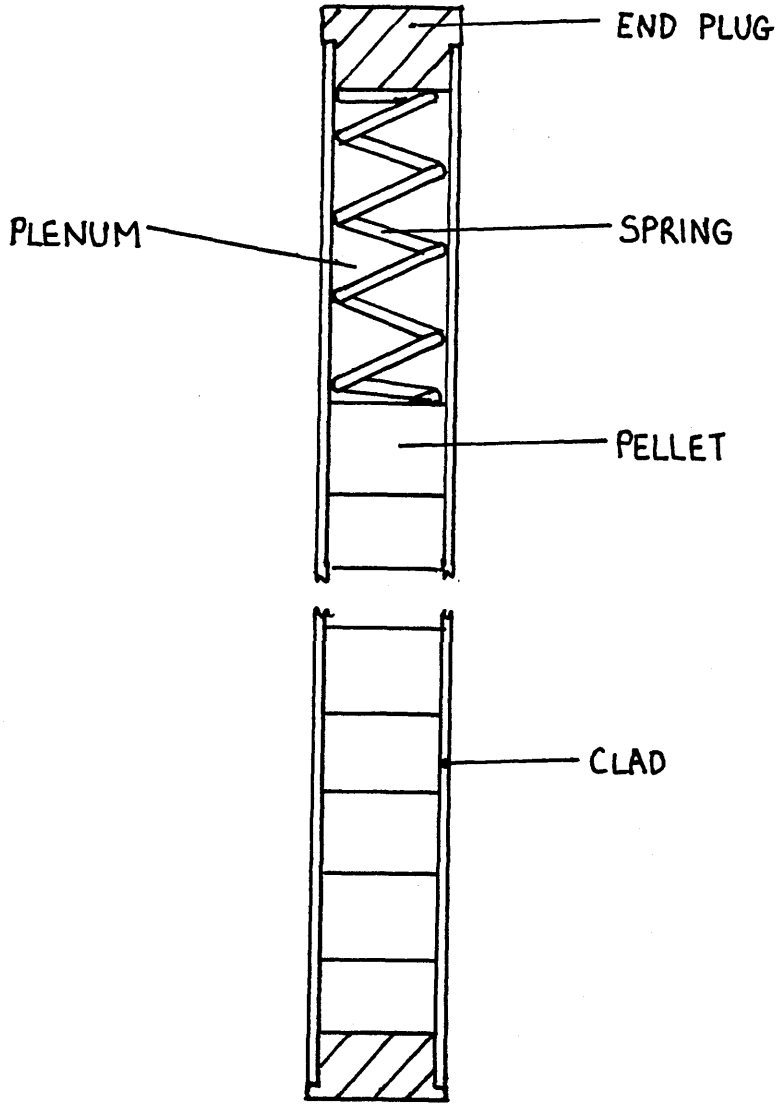

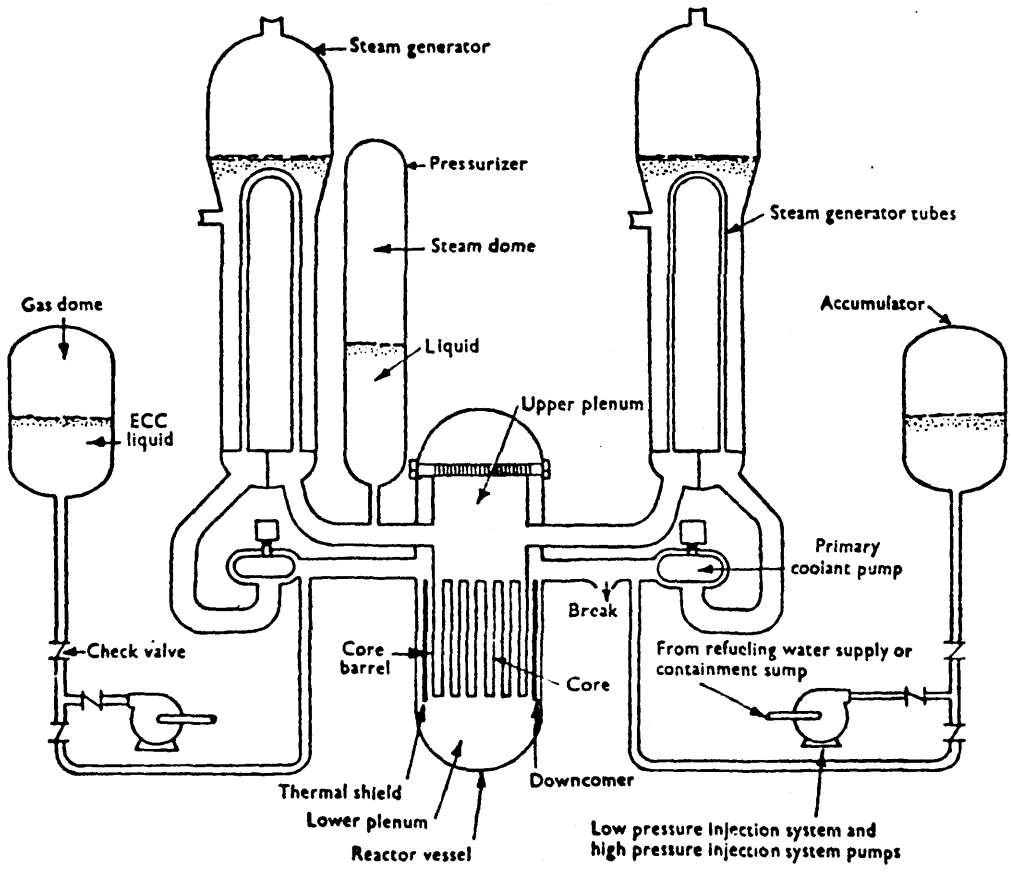

Fig 2 Multiple-loop PWR System During Reflood

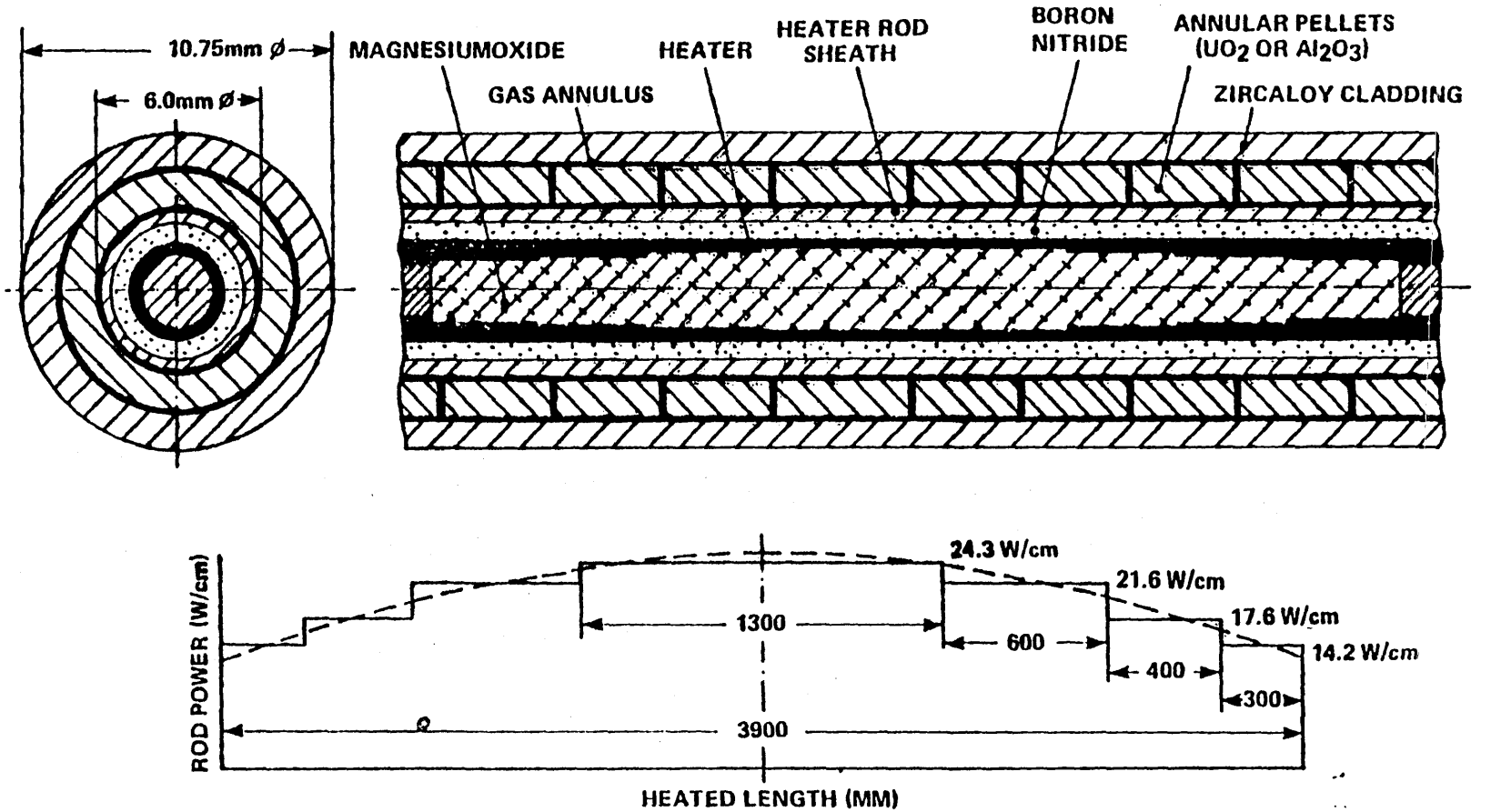

Fig 3 Fuel-rod Simulator (Mann 1982)

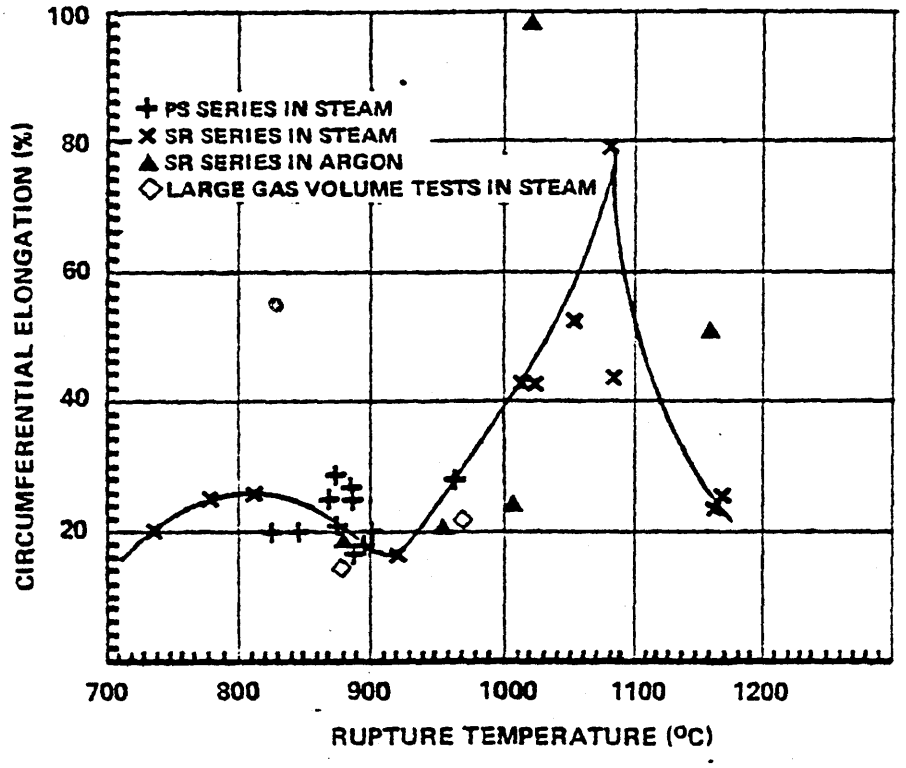

Fig 4 Average Rupture Strain From Single-rod Test Data

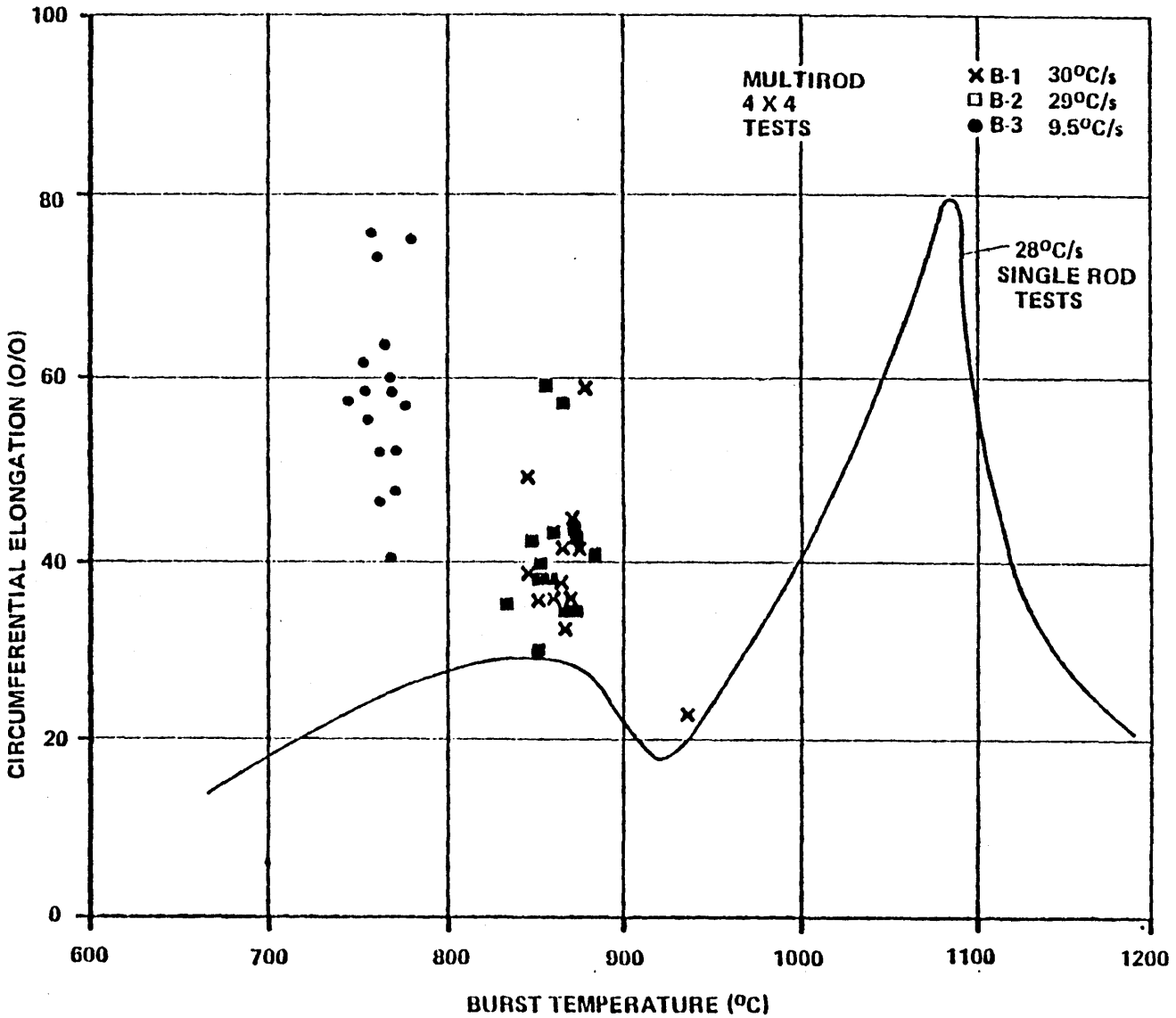

Fig 5 Comparison of Burst Strains in Rod-bundle and Single-rod Tests

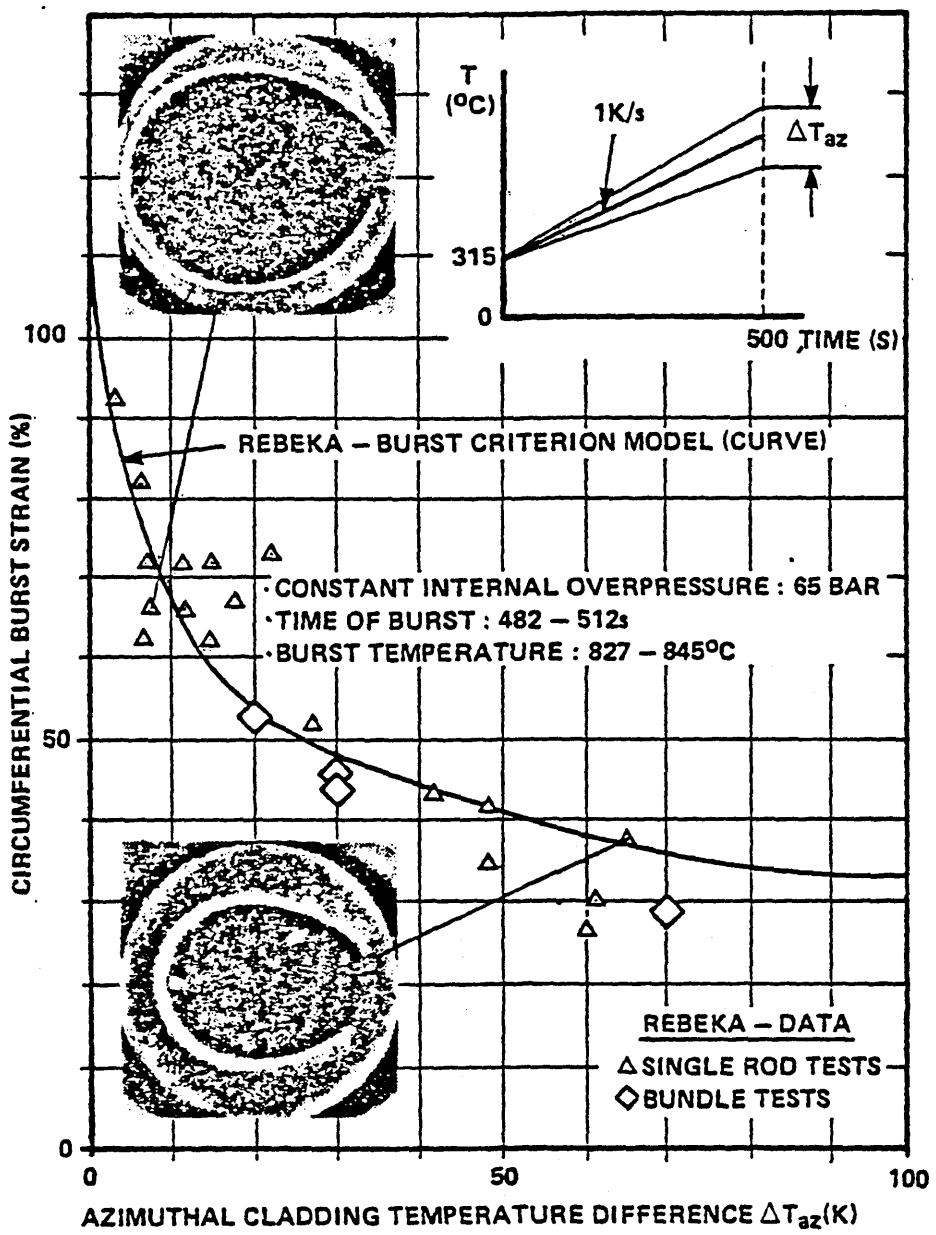

Fig 6 Burst Strain vs Azimuthal Temperature Difference (Mann 1982)

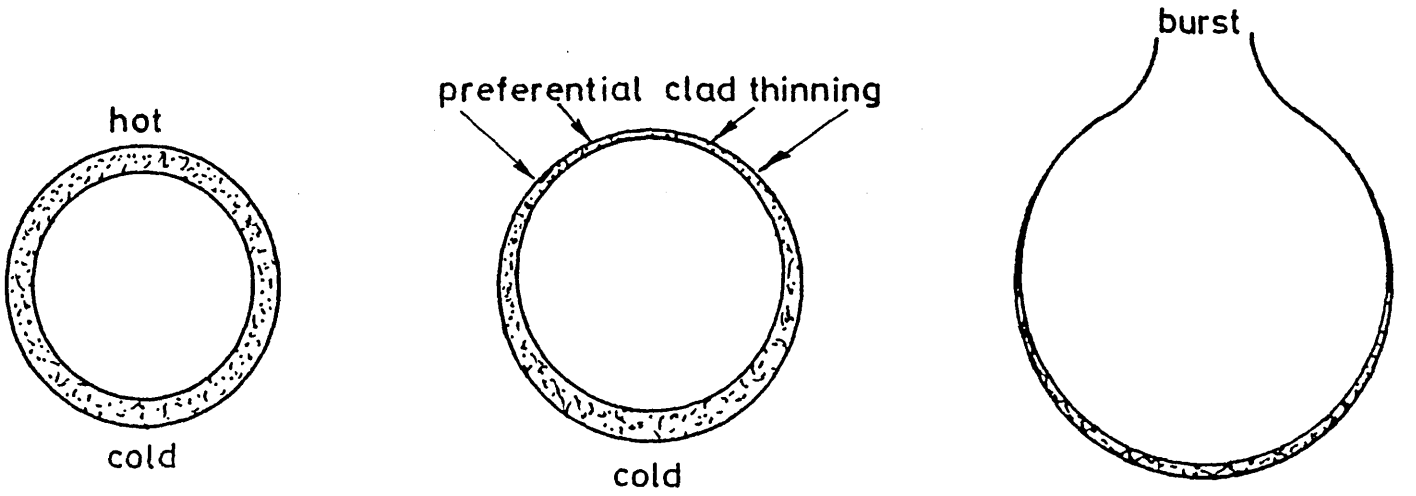

a) Non uniform temperature showing non-uniform thinning with burst at low strain.

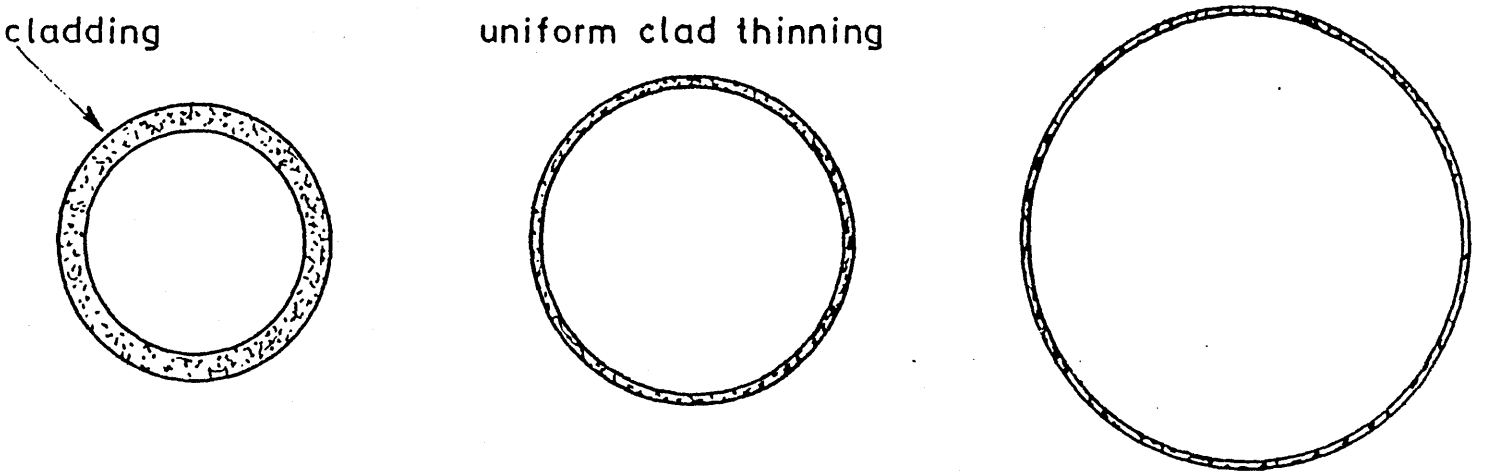

b) Uniform clad temperature showing development of large strain without burst.

Fig 7 Effect of Azimuthal Temperature Variation

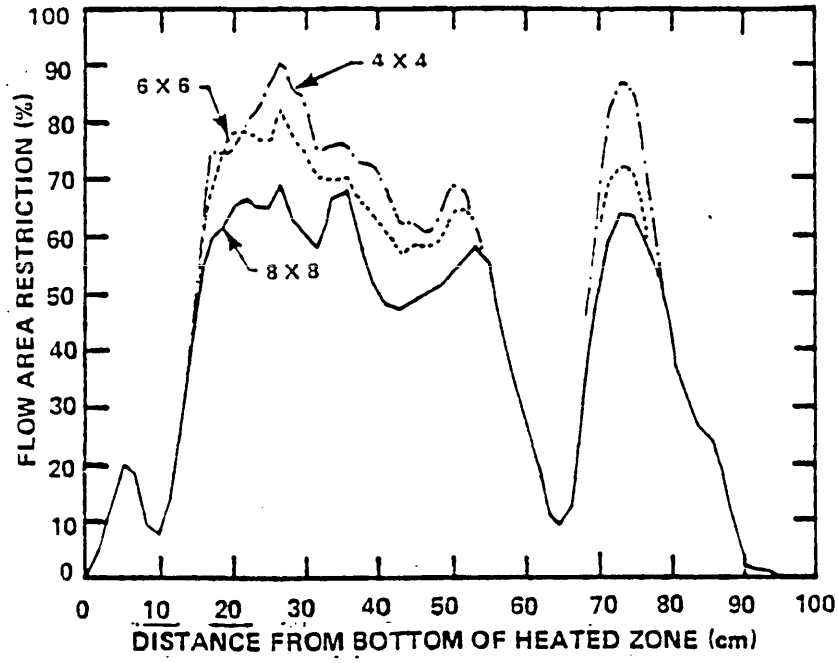

Fig 8 Subdivision of Rod Bundle Data Showing that Interior Subarrays Have Greater Flow Area Restriction

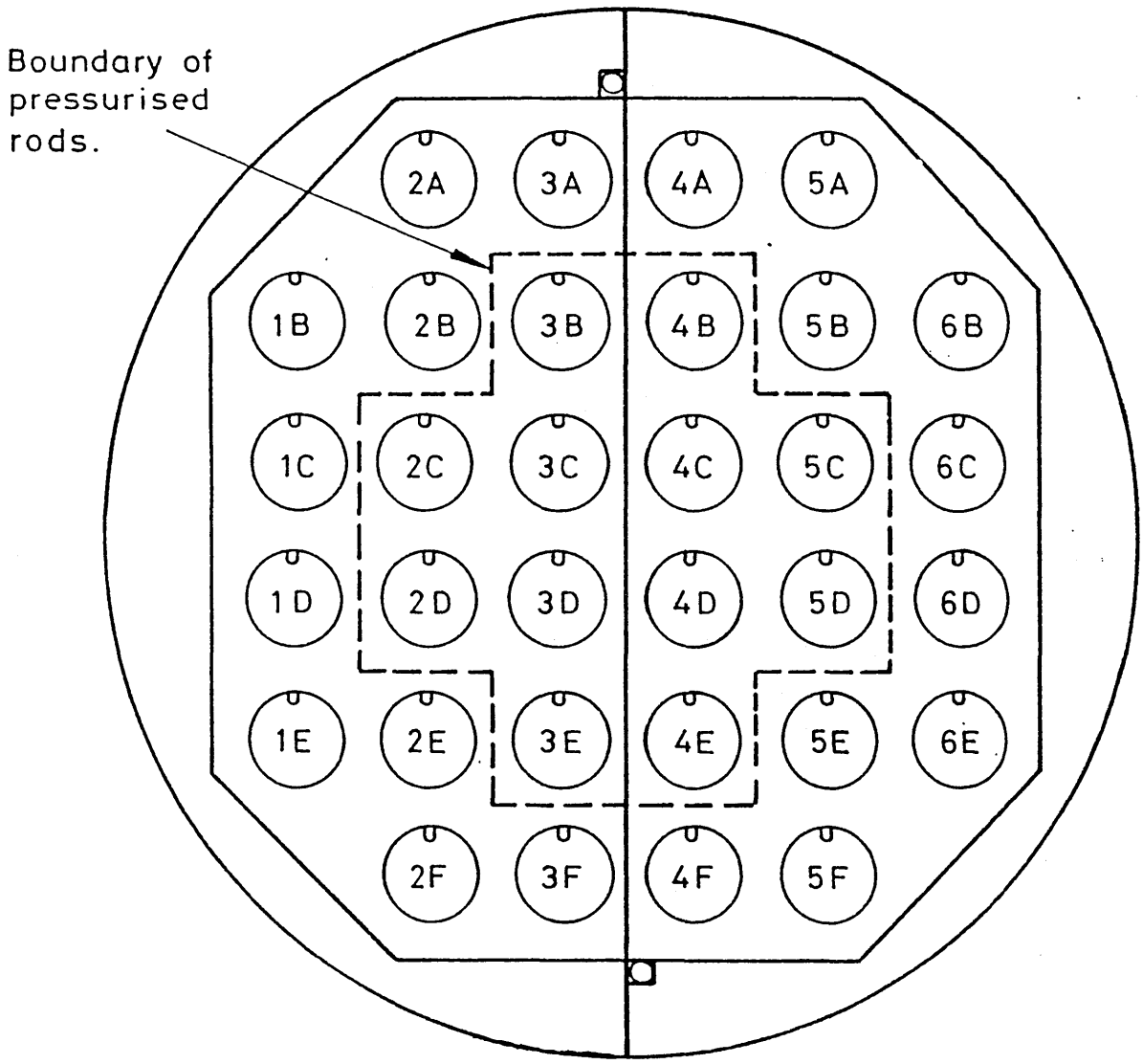

Fig 9 Schematic of MT3 Fuel Rod Array

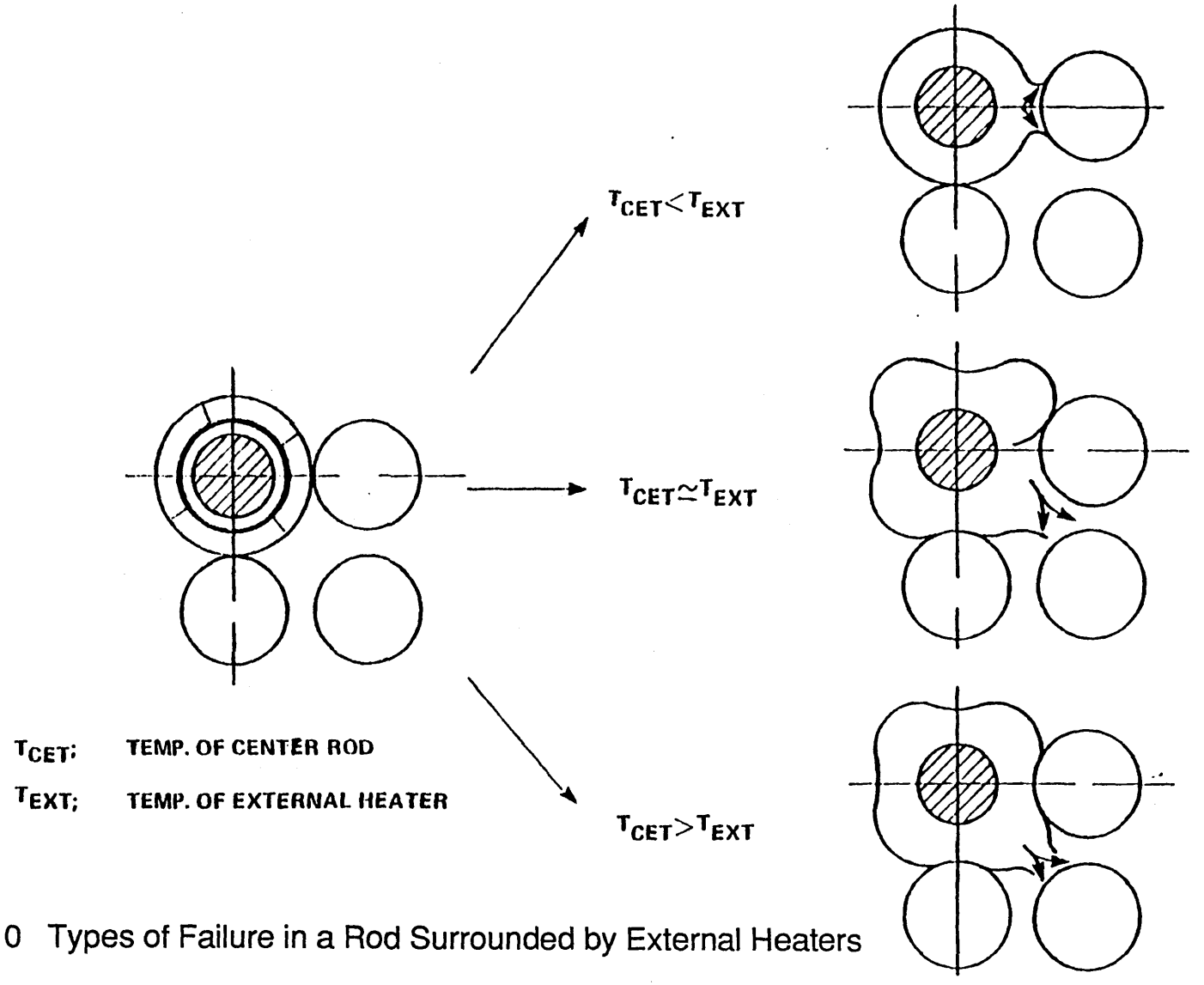

Fig 10 Types of Failure in a Rod Surrounded by External Heaters

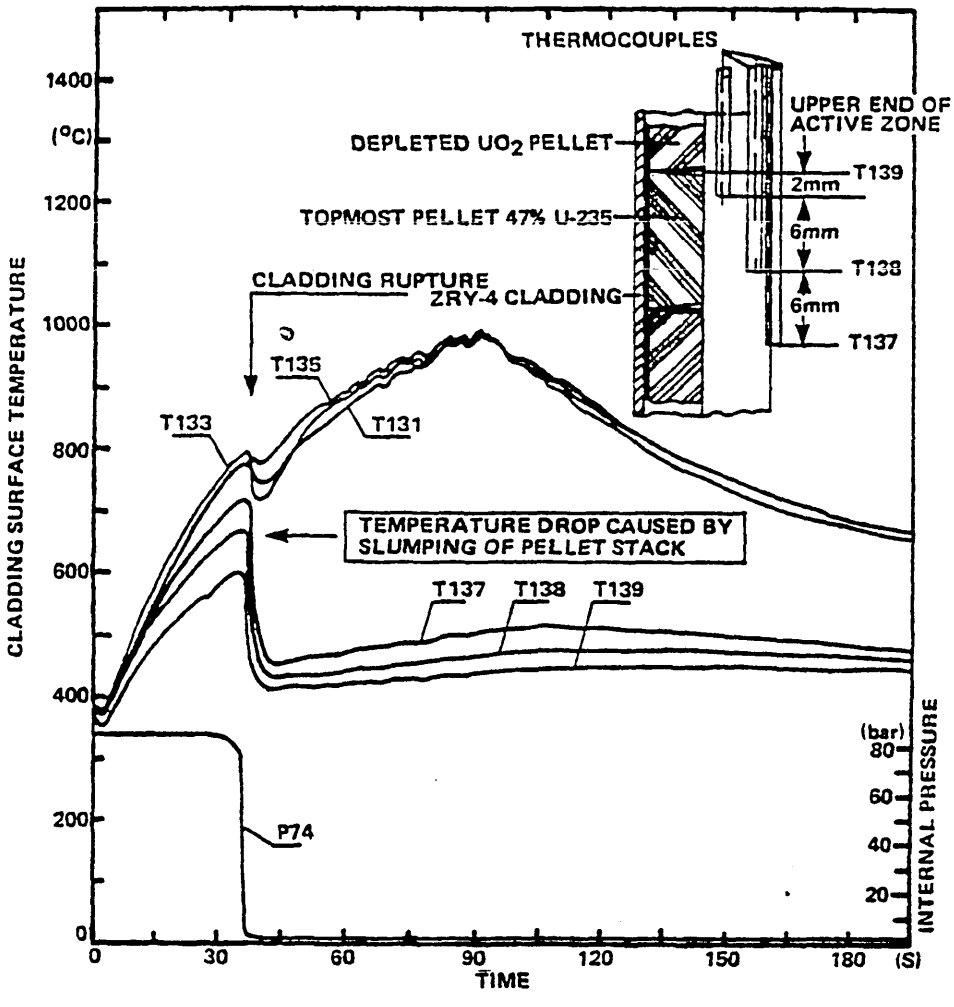

Fig 11 Temperature and Internal Pressure Histories During Ballooning Test

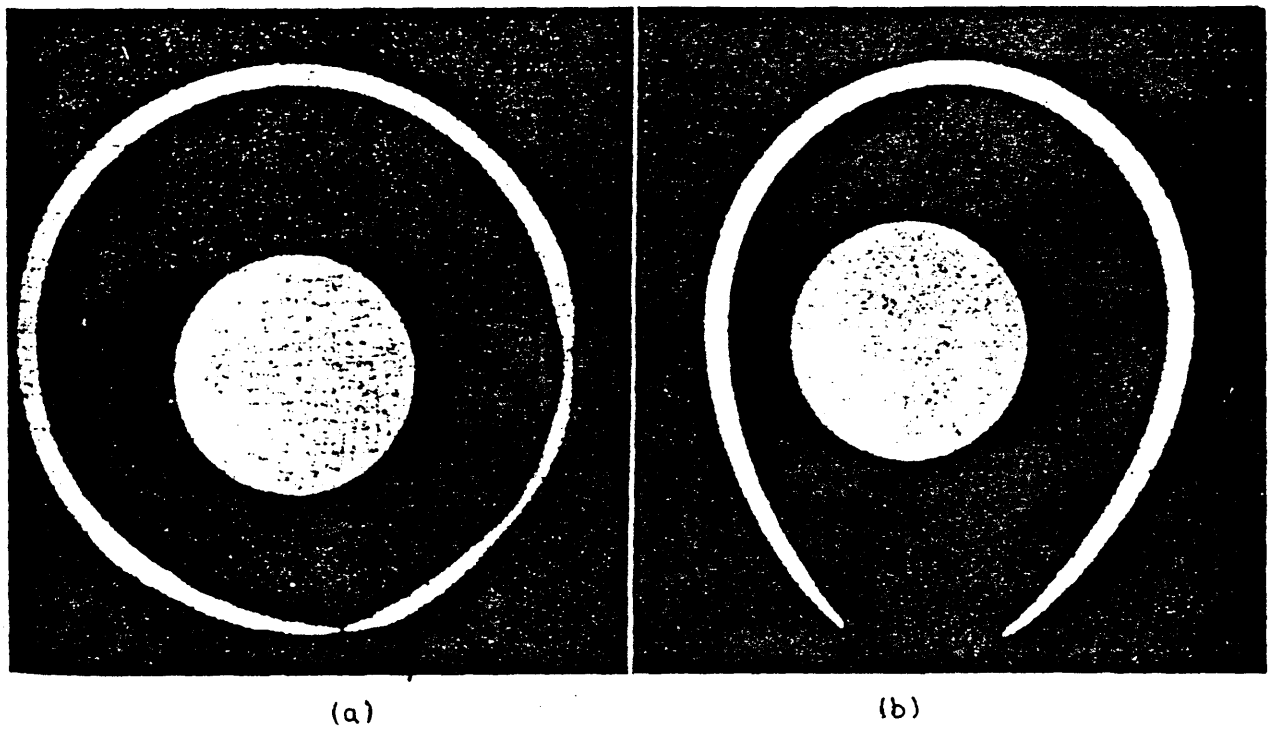

(a) *burst temperature 1135°C.* (b) *burst temperature 814°C.*

Fig 12 Cross Sections of Transient-burst Specimens Showing Multiple and Single-neck Behaviour

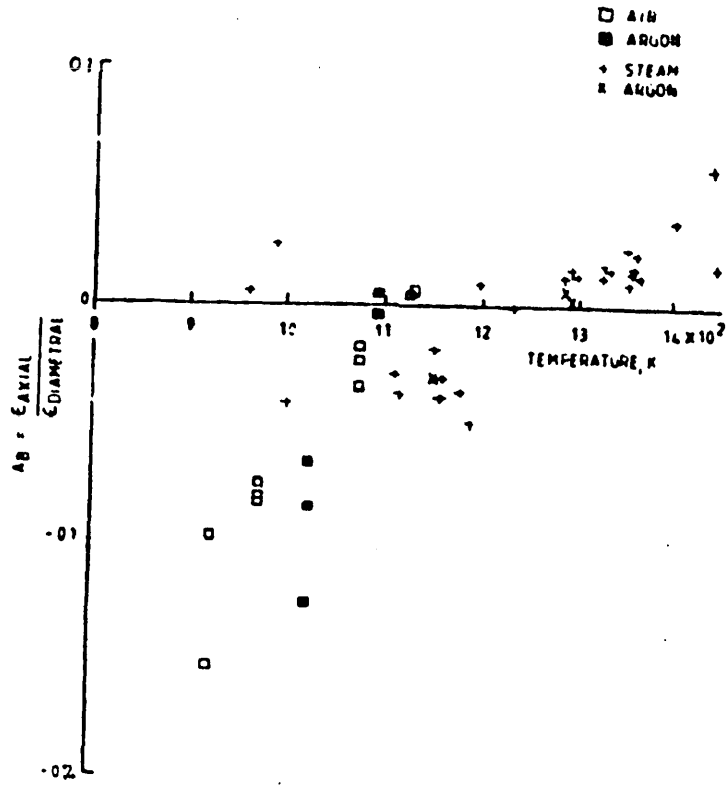

Fig 13 Maximum Circumferential Strain vs Burst Temperature in FR-2 Tests

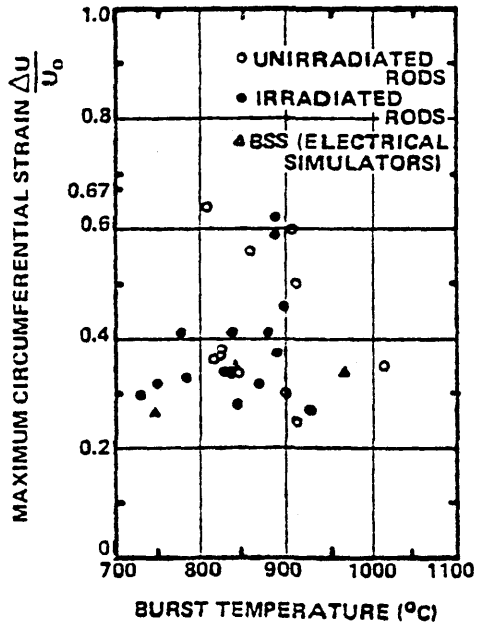

Fig 14 Zircaloy 4 Tube Anisotropy Factor vs Temperature

Fig 15 Flow Chart of the ADVICE Computer Program

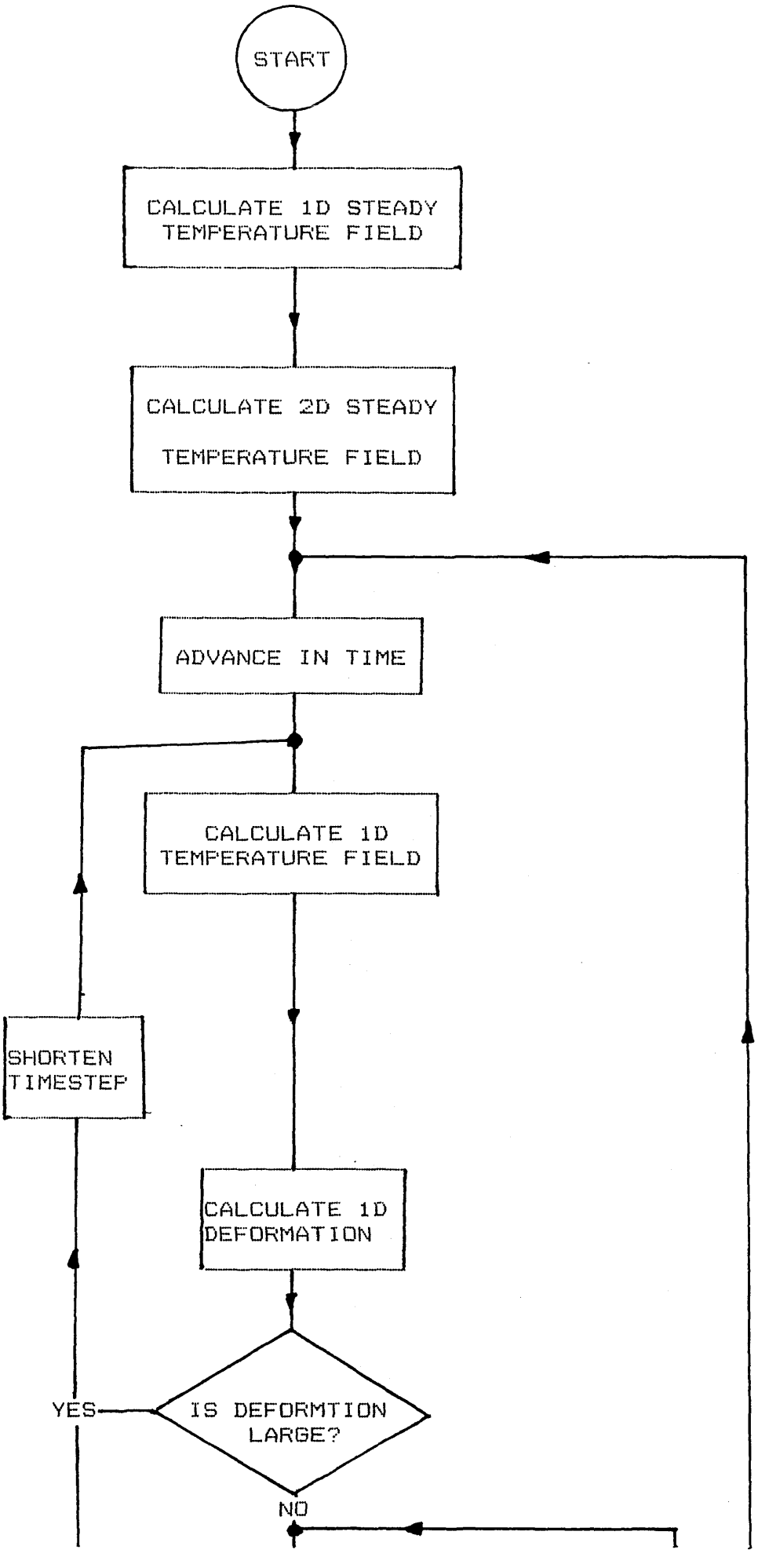

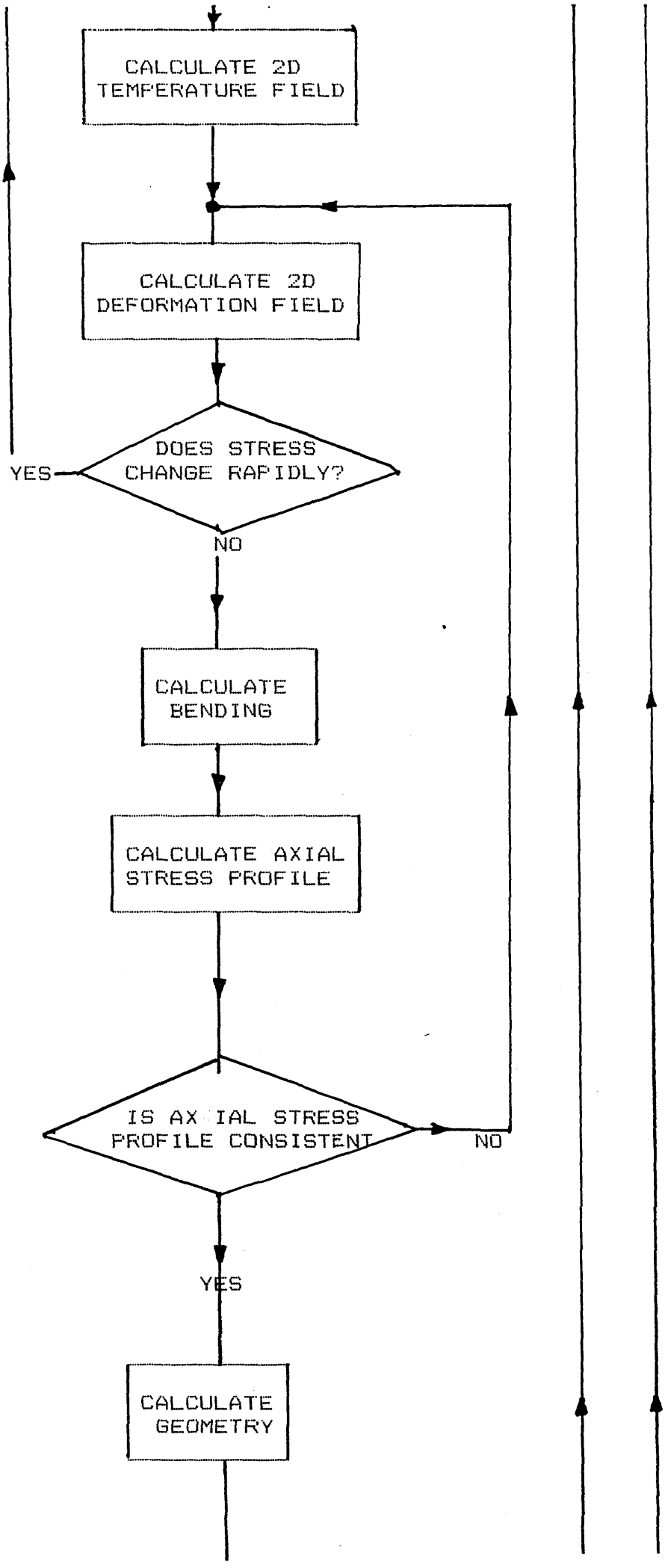
CALCULATE 2D TEMPERATURE FIELD
CALCULATE 2D DEFORMATION FIELD
DOES STRESS CHANGE RAPIDLY?
YES
NO
CALCULATE BENDING
CALCULATE AXIAL STRESS PROFILE
IS AX IAL STRESS PROFILE CONSISTENT
NO
YES
CALCULATE GEOMETRY

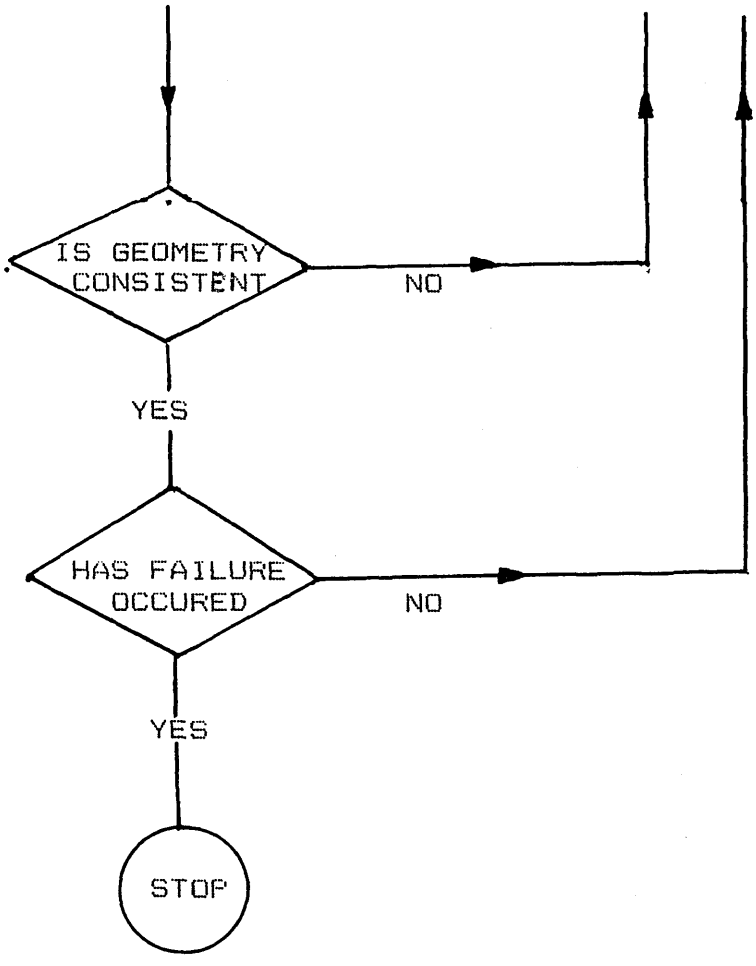
IS GEOMETRY CONSISTENT
NO
YES
HAS FAILURE OCCURED
NO
YES
STOP

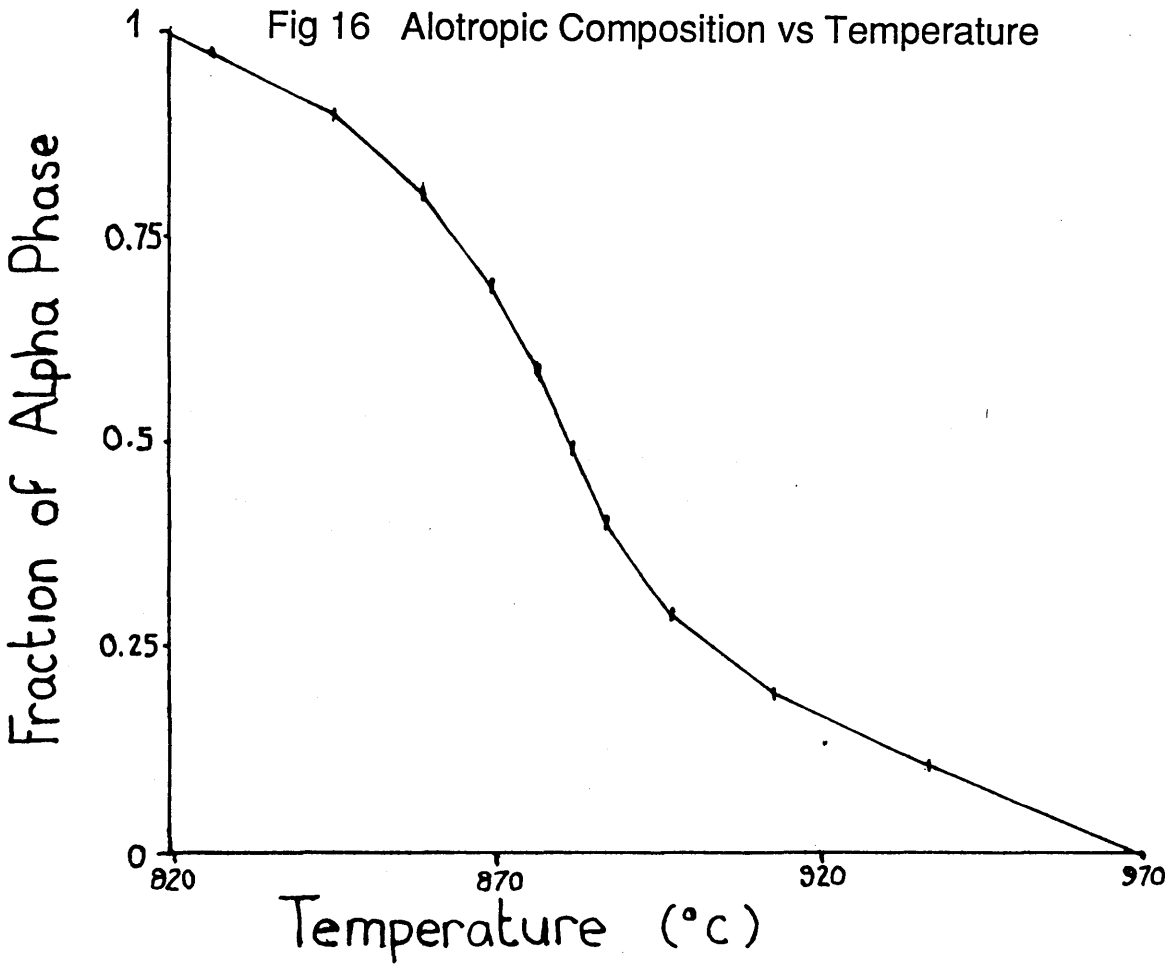
Fig 16 Alotropic Composition vs Temperature
Fraction of Alpha Phase
1
0.75
0.5
0.25
0
820
870
920
970
Temperature (°c)

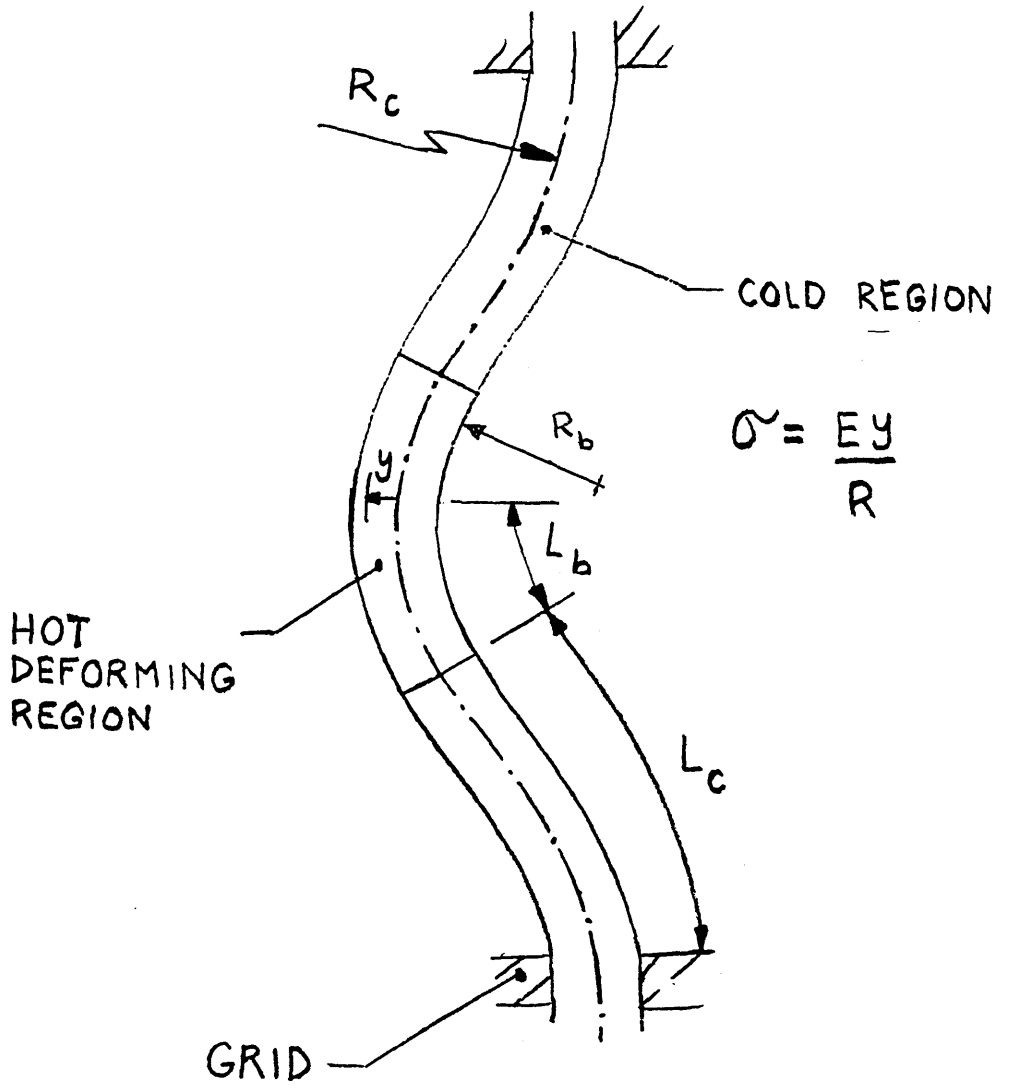

Fig 17 Diagram of the Bowing Model

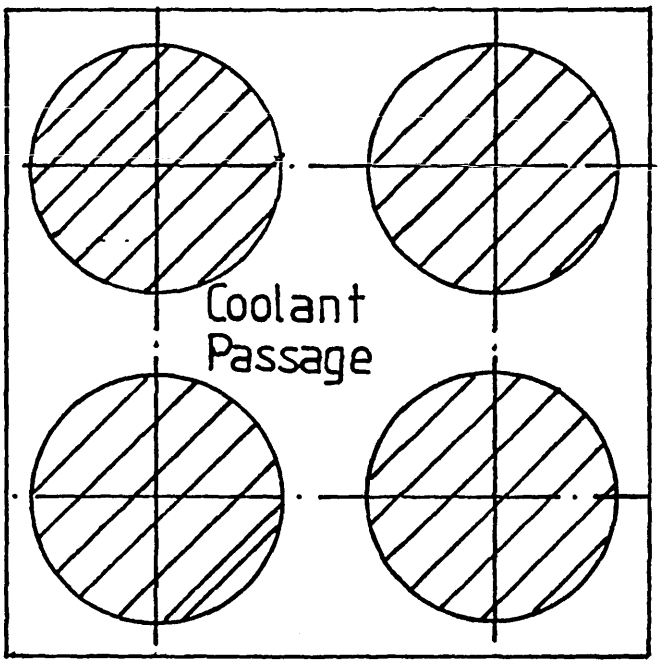

Fig 18 Diagram of a Coolant Passage

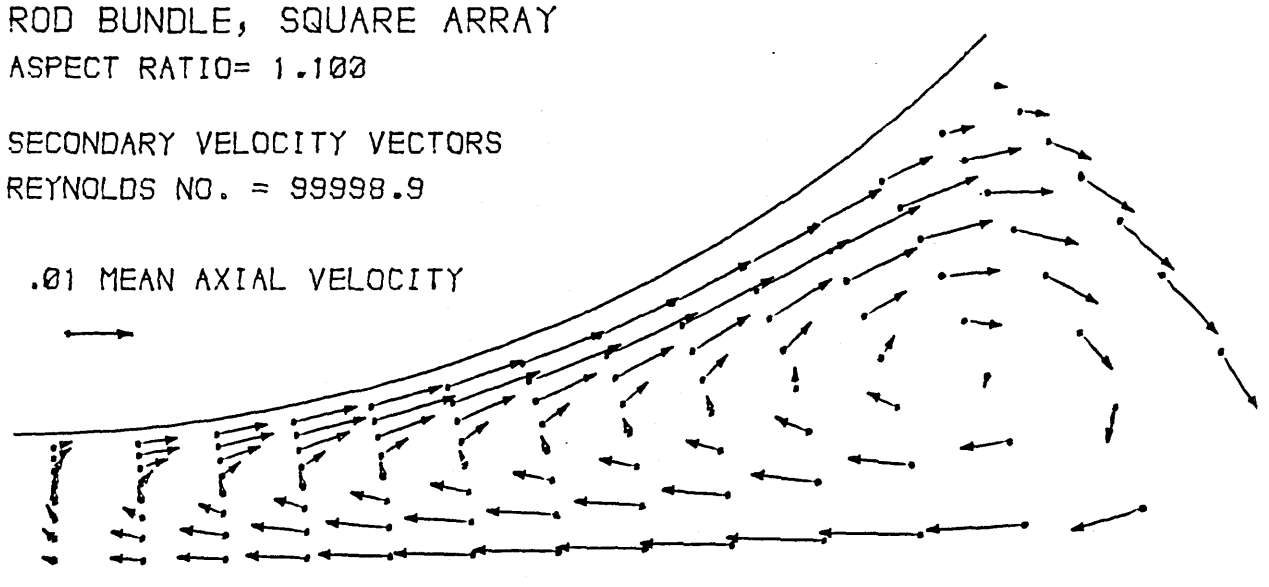

Fig 19 Secondary Velocity Distribution (Rapley 1984)

Fig 20 Fluid Shear Stress Profiles

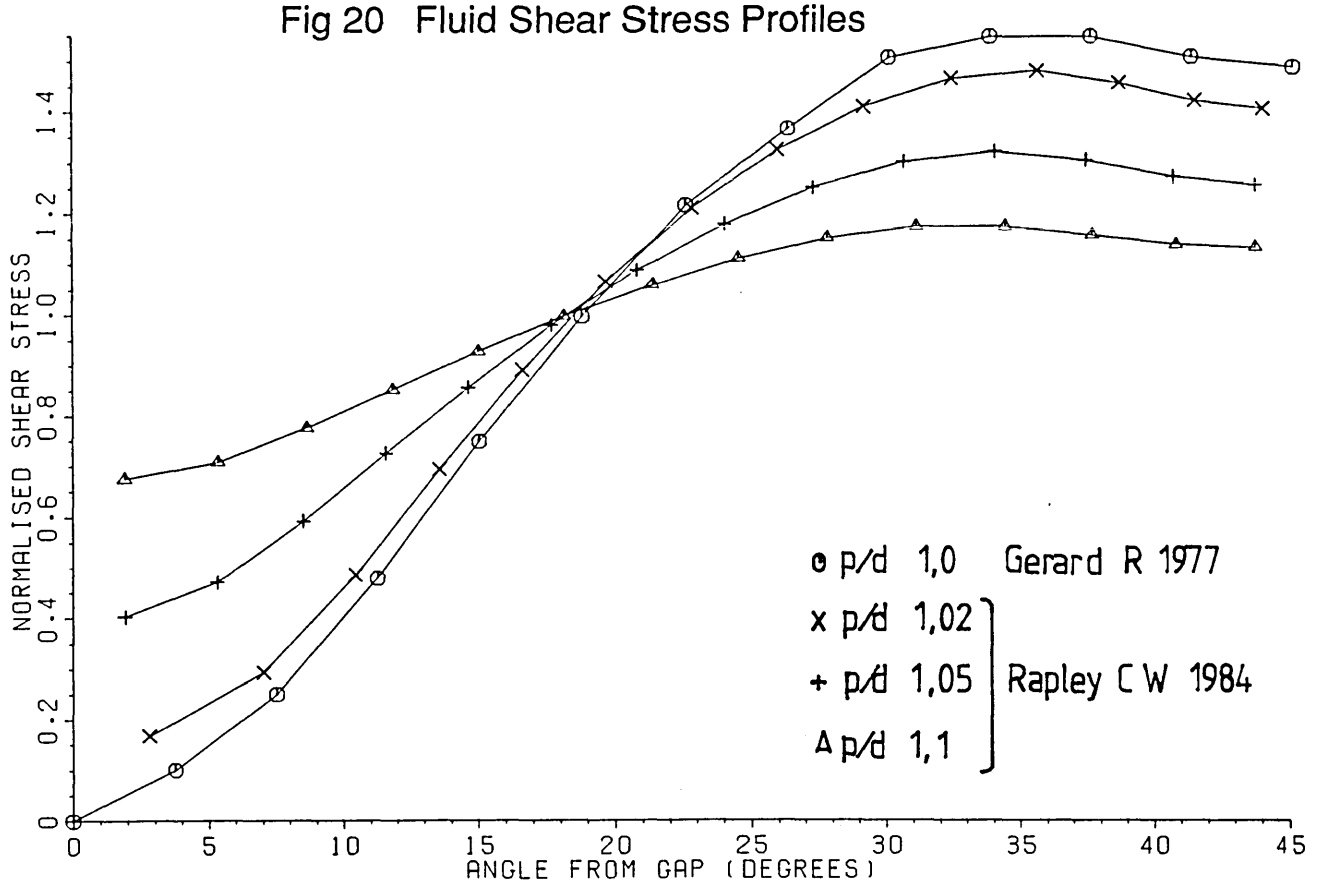

Fig 21 Heat-transfer Coefficient Profiles

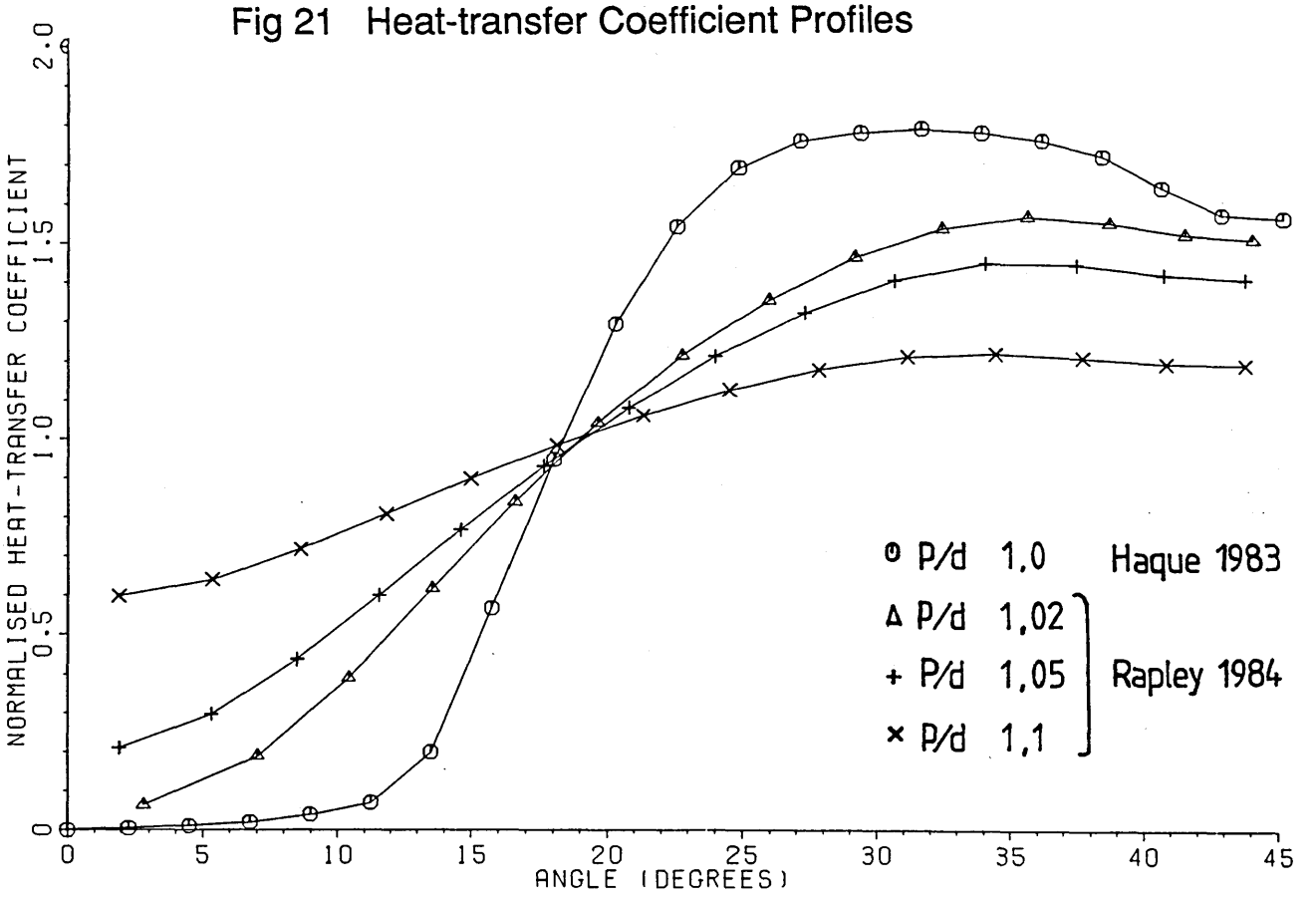

Fig 22 Comparison of Correlation 1 and Turbulent-flow Calculations P/d 1.1

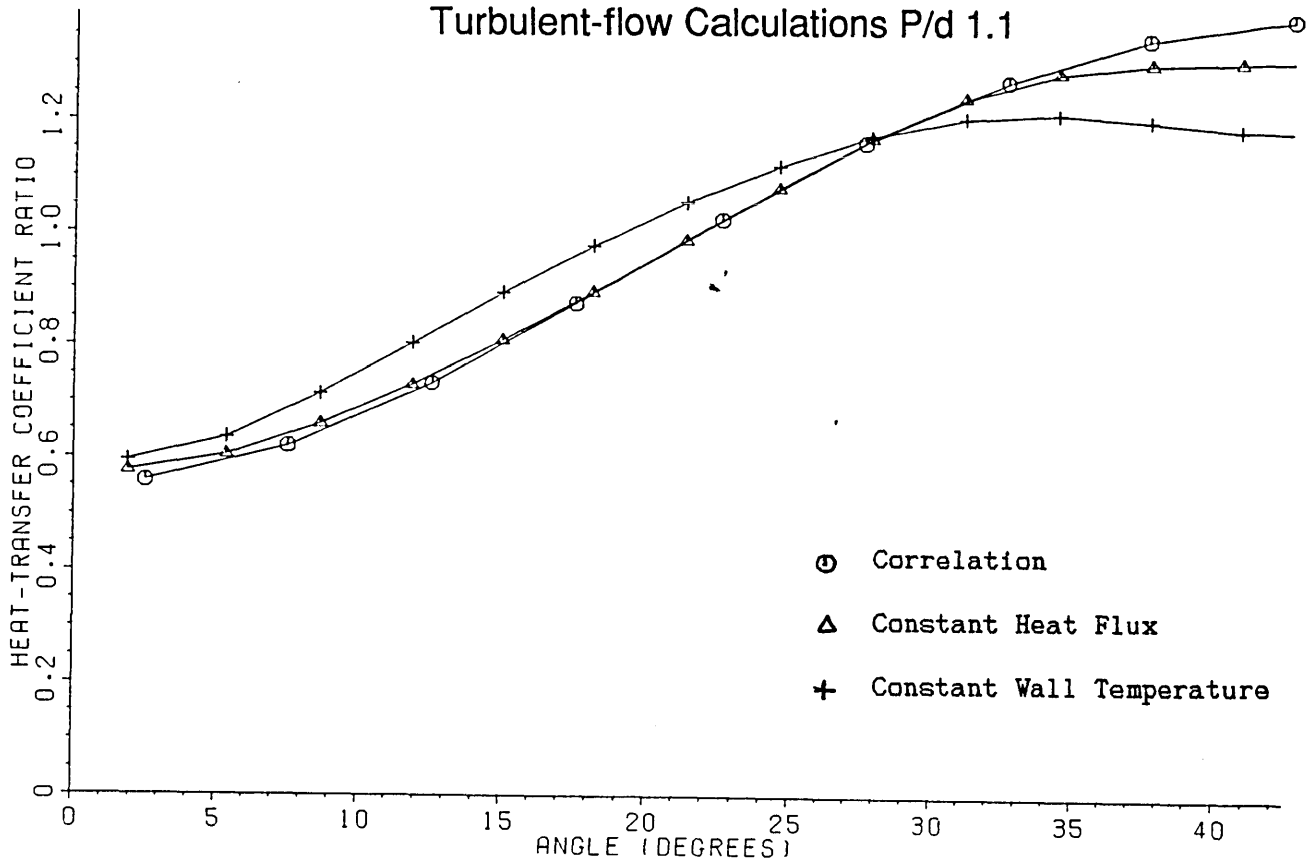

Fig 23 Comparison of Correlation 1 and Turbulent-flow Calculations P/d 1.05

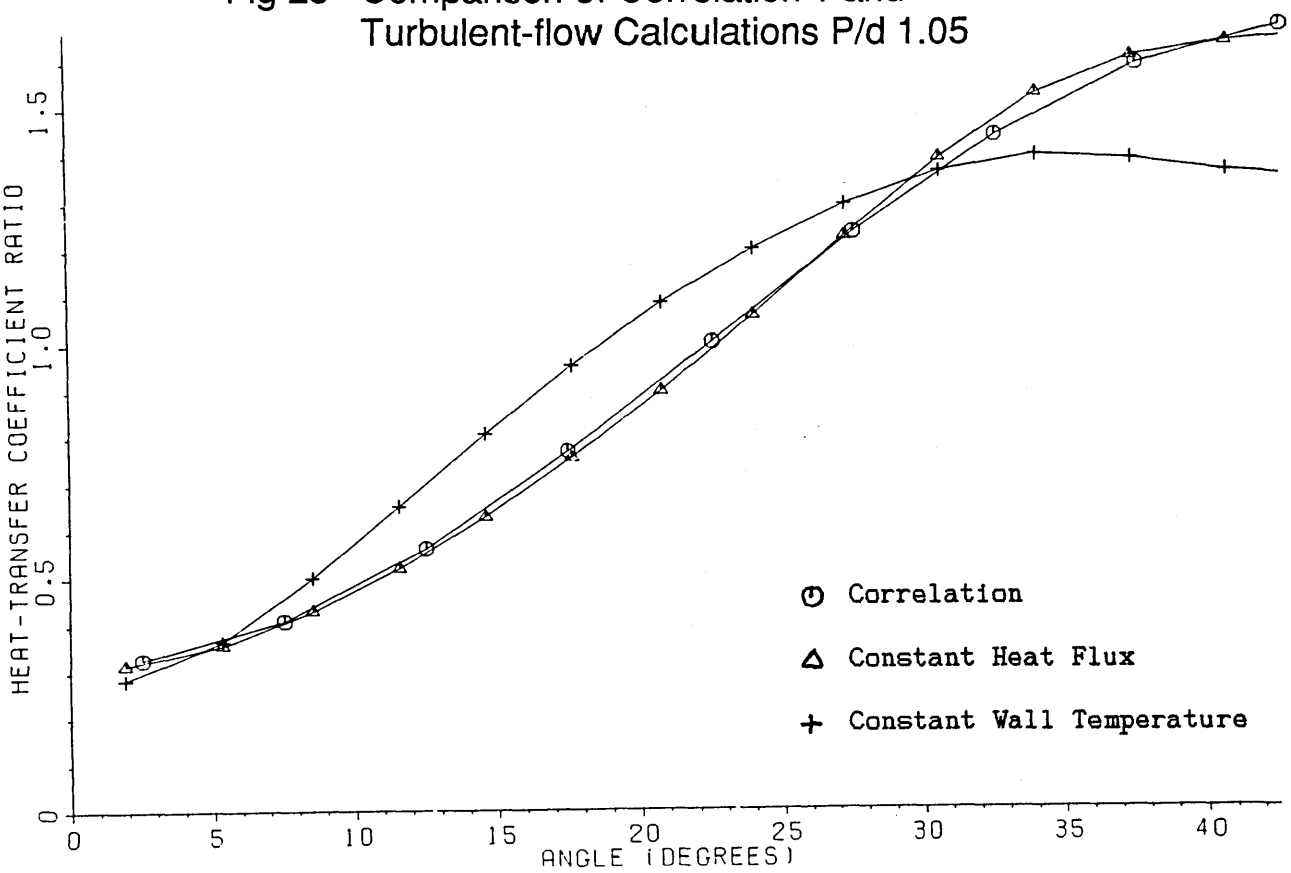

Fig 24 Comparison of Correlation 1 and Turbulent-flow Calculations P/d 1.02

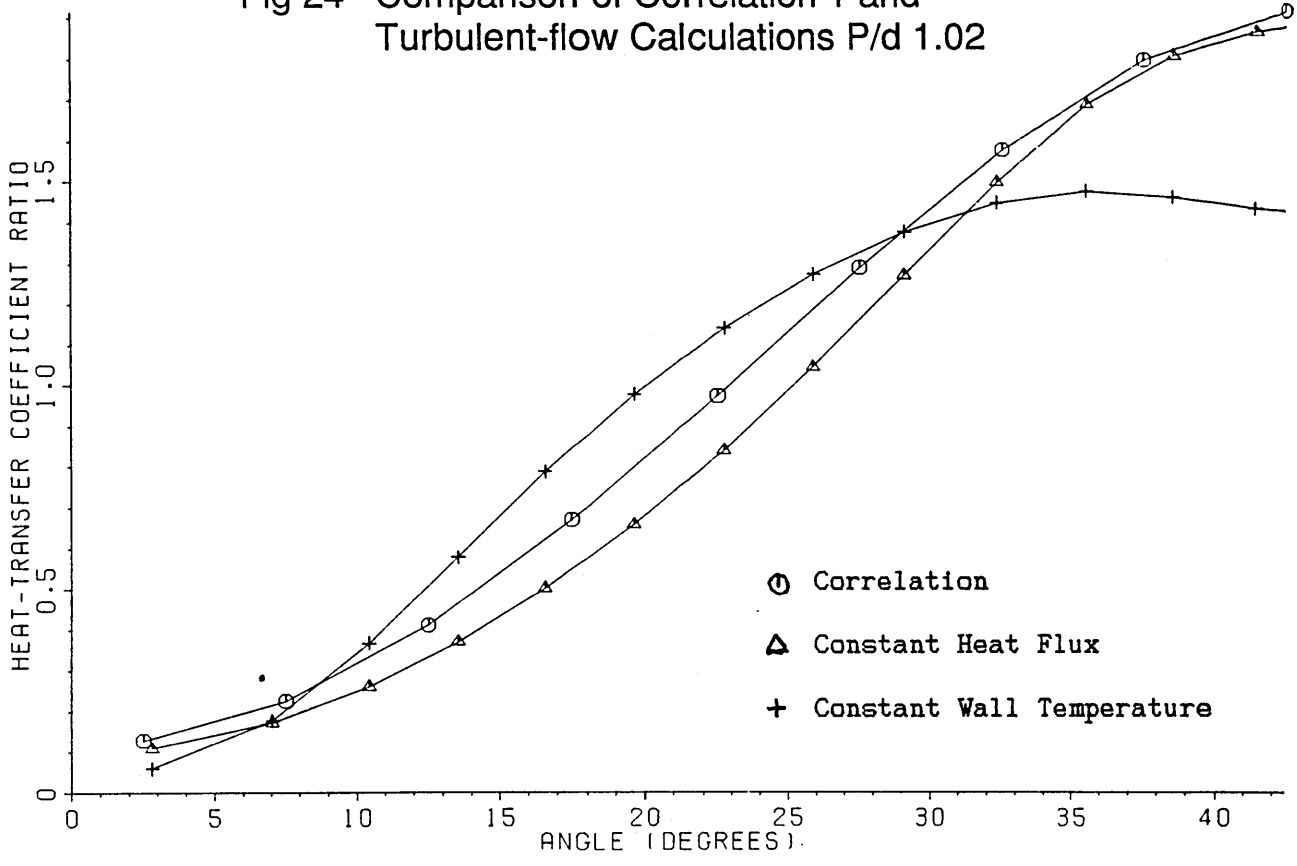

Fig 25 Comparison of Correlation 2 and Turbulent-flow Calculations P/d 1.1

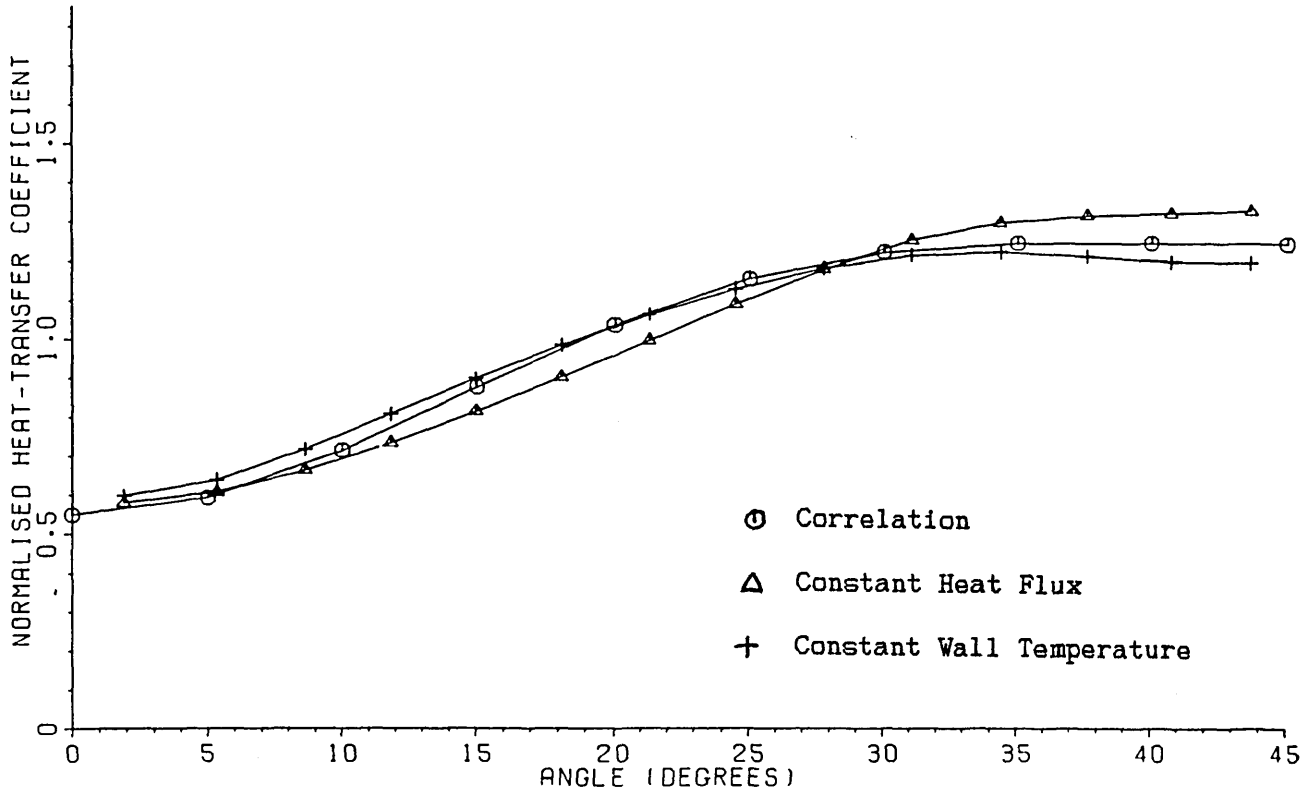

Fig 26 Comparison of Correlation 2 and Turbulent-flow Calculations P/d 1.05

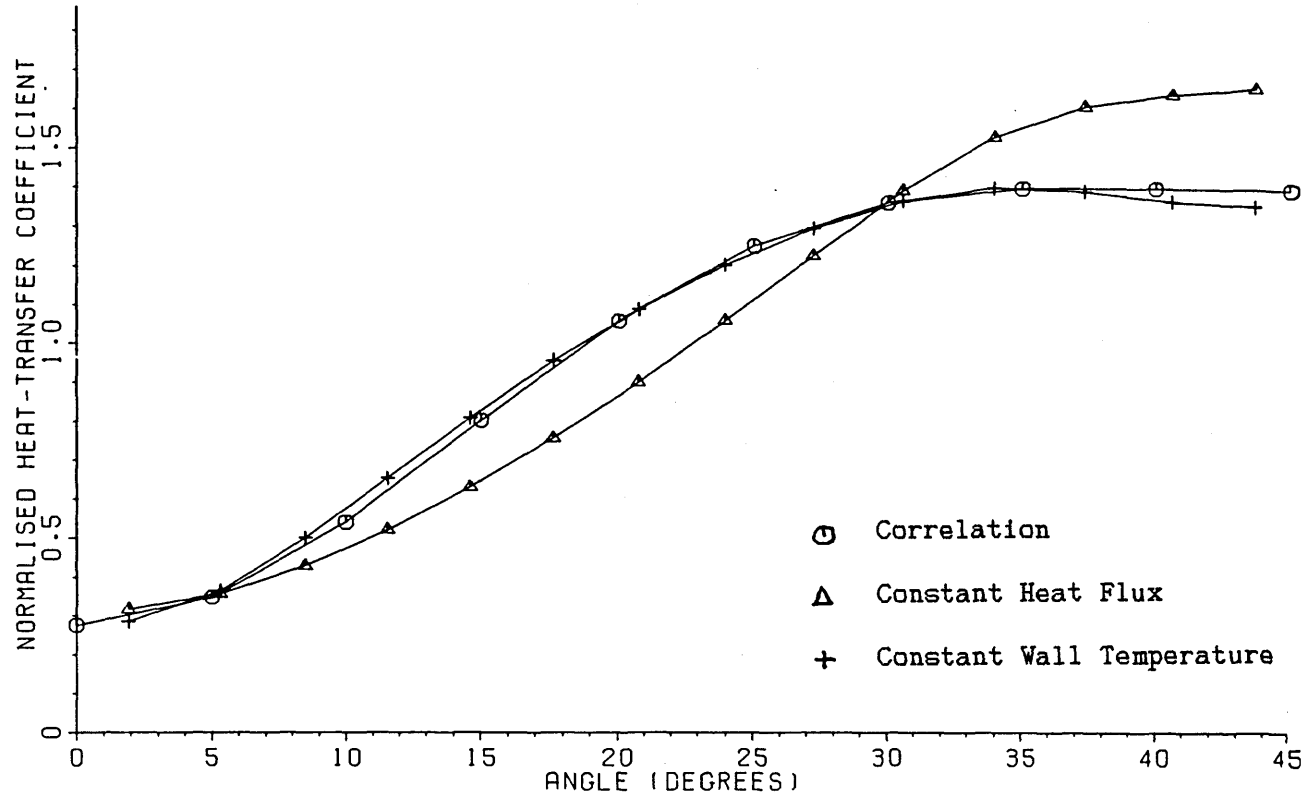

Fig 27 Comparison of Correlation 2 and Turbulent-flow Calculations P/d 1.02

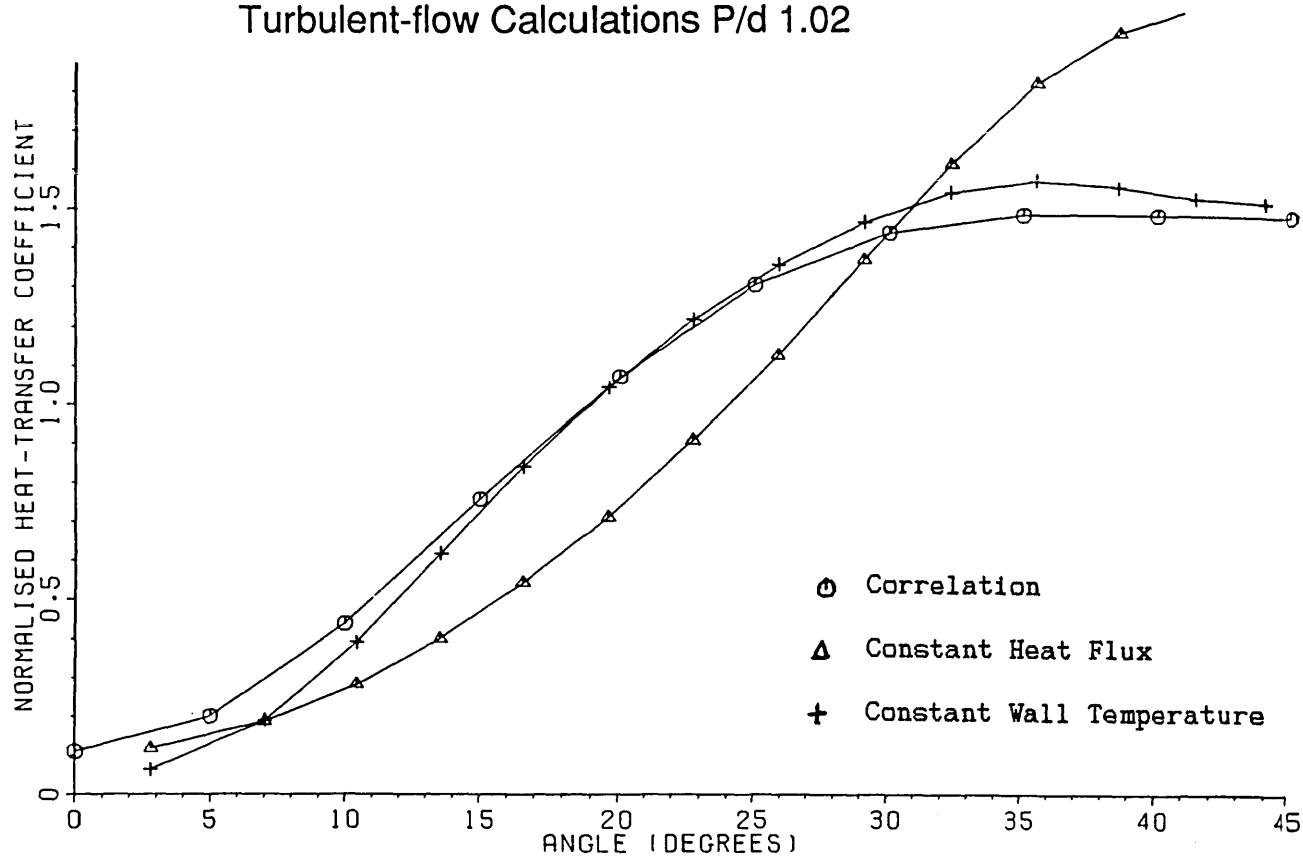

Fig 28 Comparison of Correlation 2 and Turbulent-flow Calculations P/d 1.0

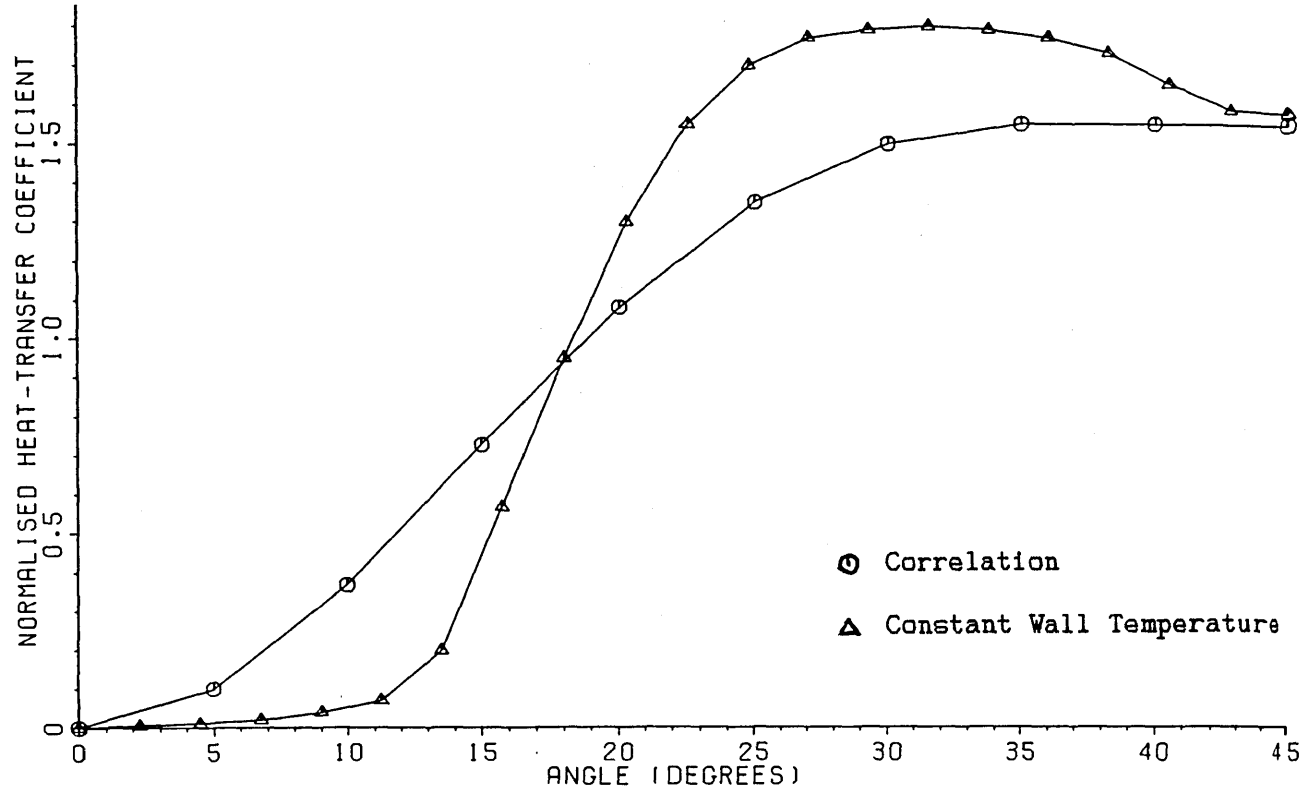

Fig 29 Effect of Mesh on Strain Localisation

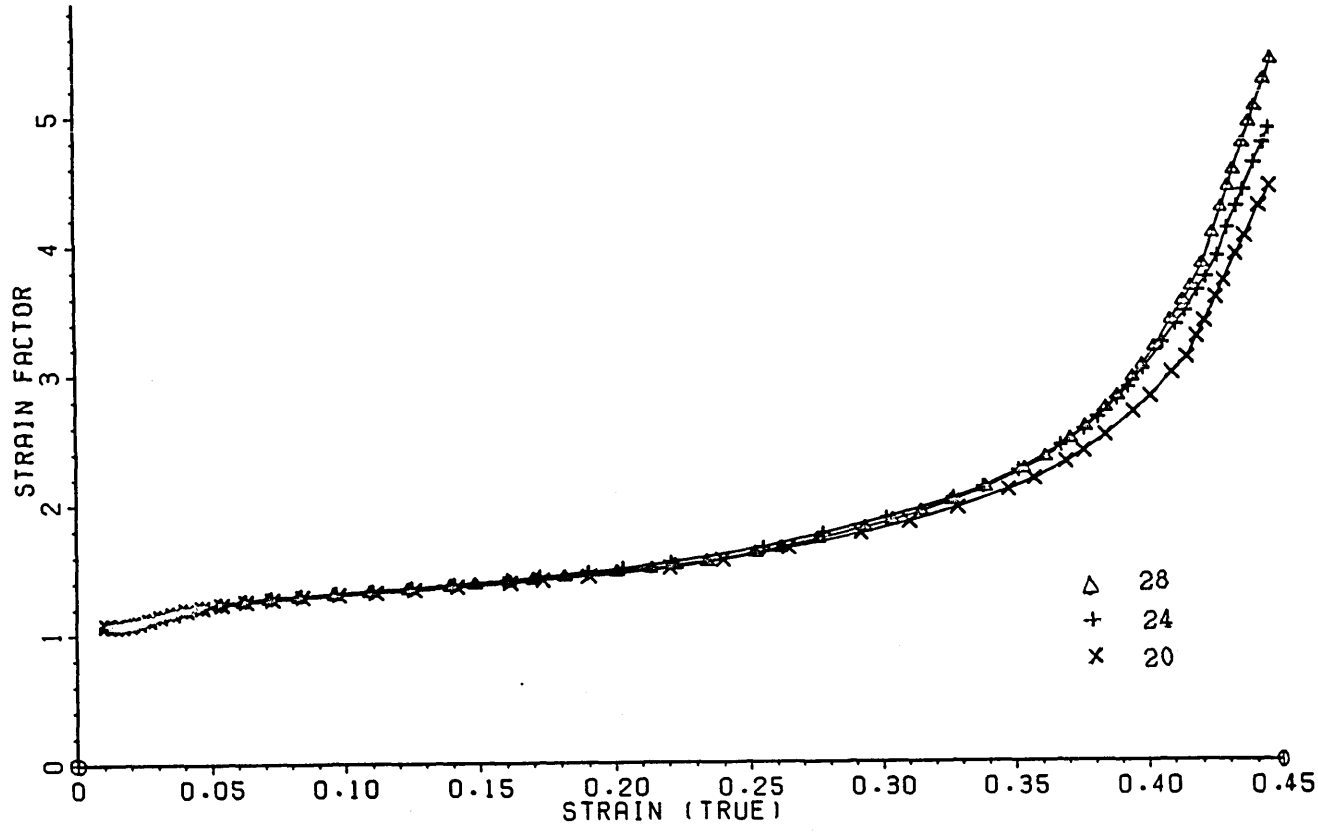

Fig 30 MT3 Pressure Histories

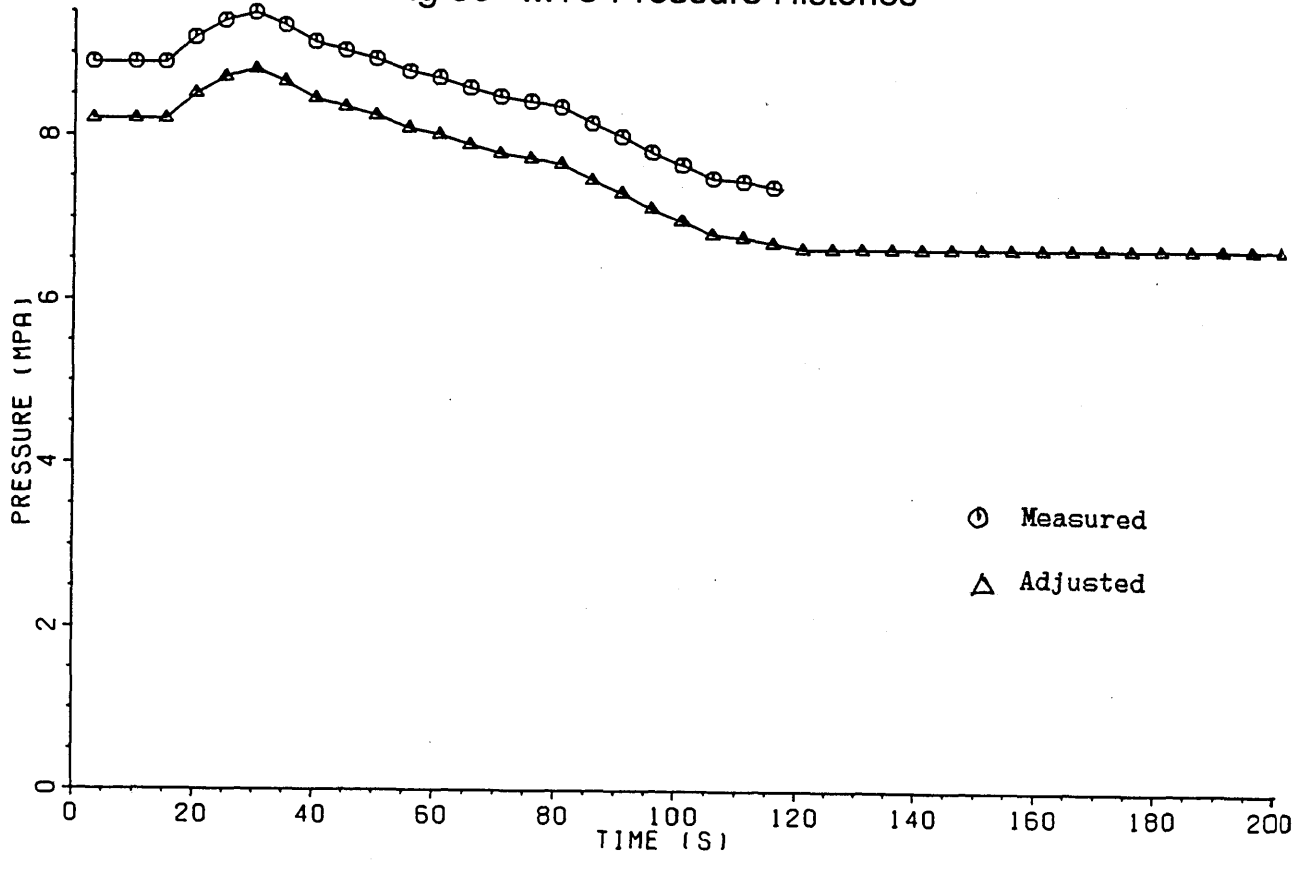

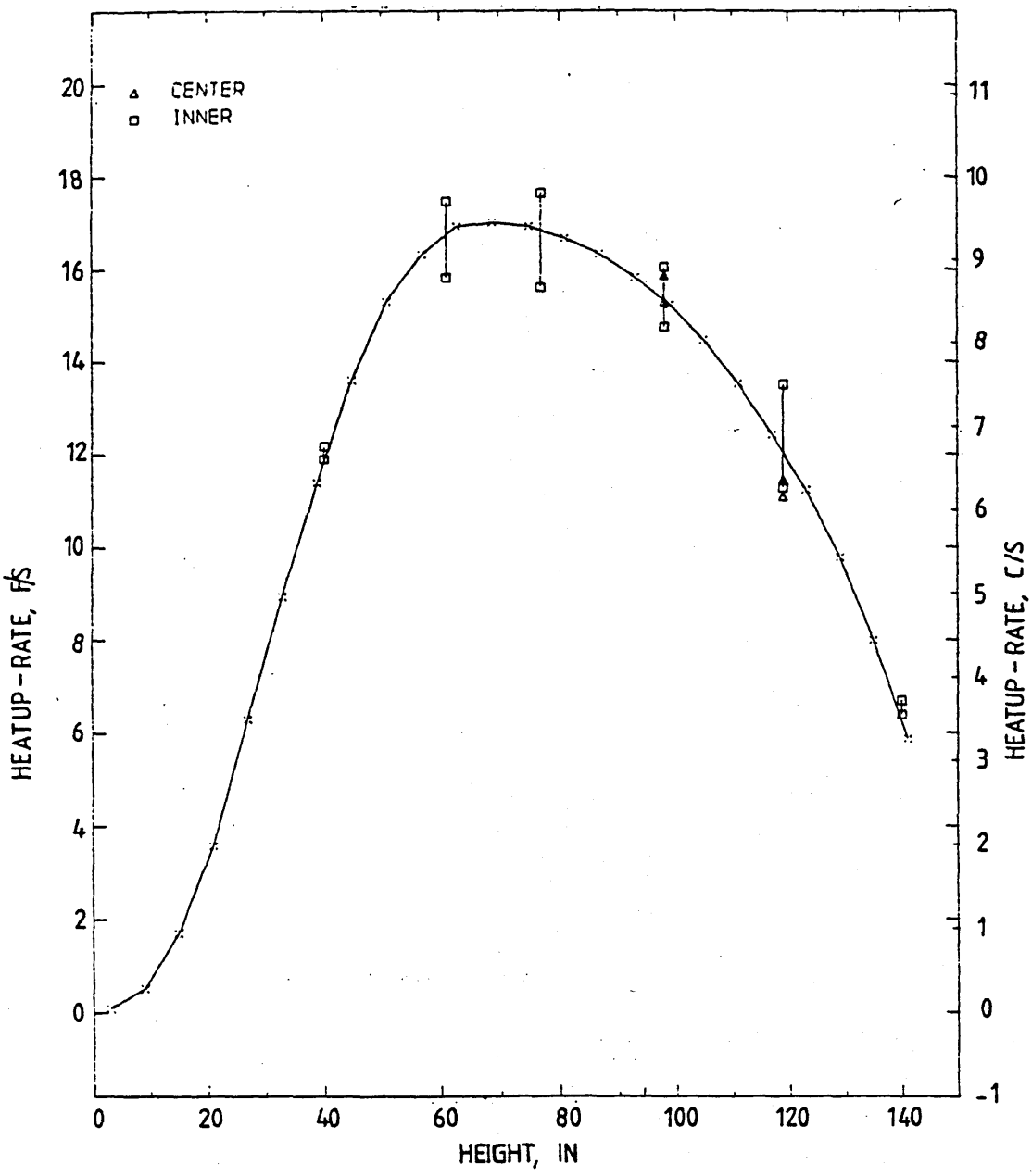

Fig 31 MT3 Heatup-rate Profile (Gibson 1982)

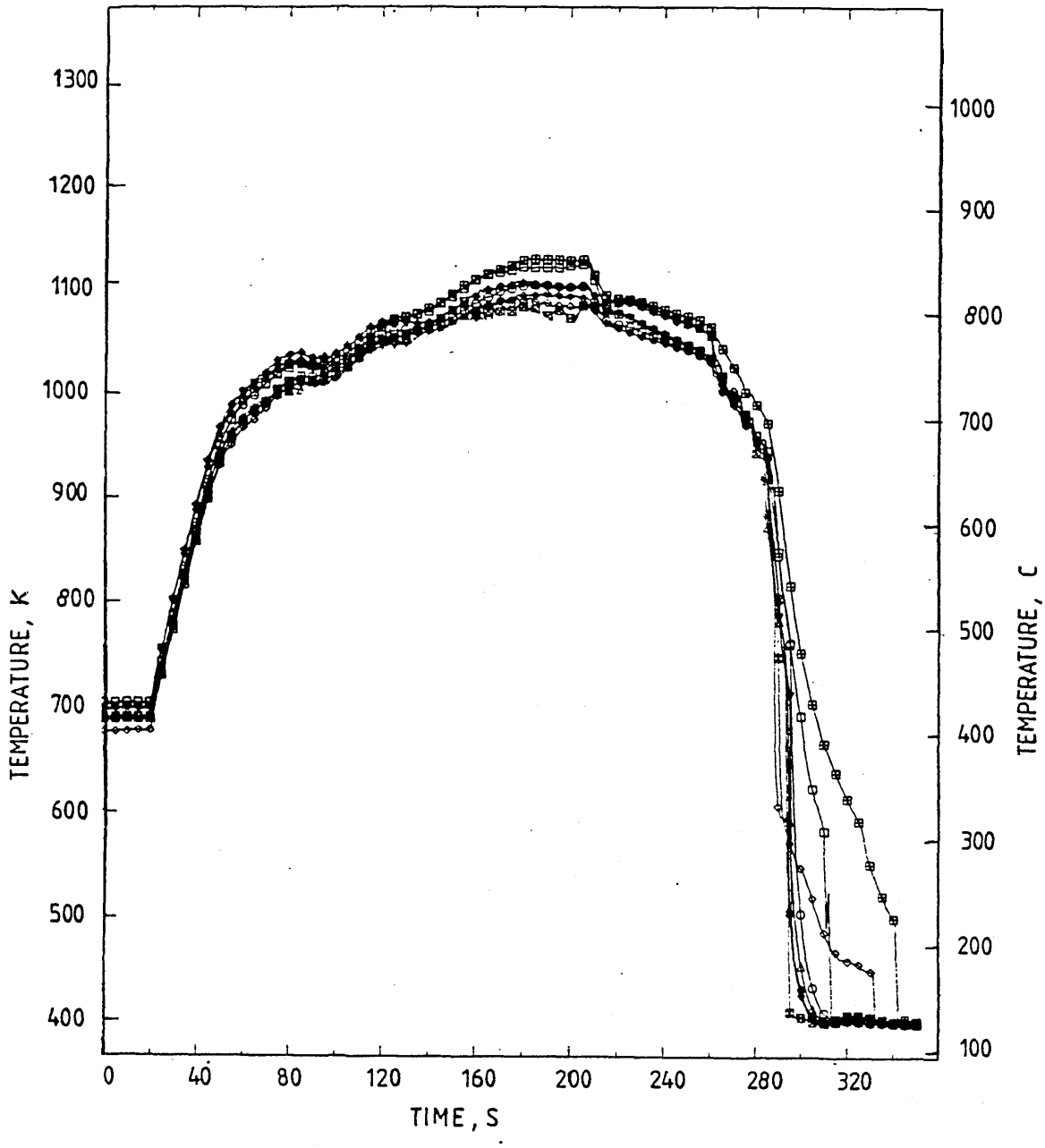

Fig 32 Experimental Clad Temperature Histories at Level 15 During the MT3 Ballooning Experiment

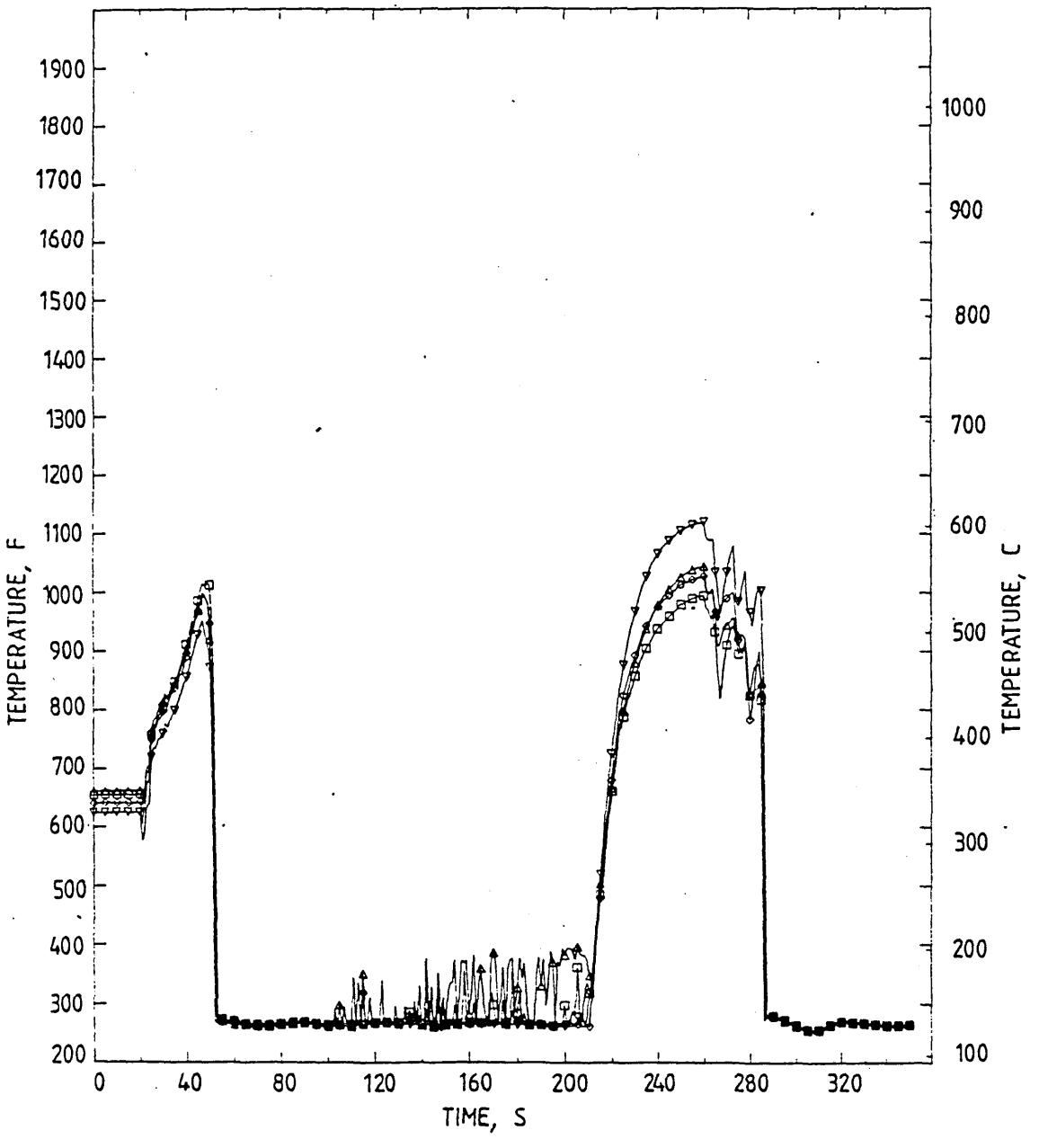

Fig 33 Experimental Shroud Temperature Histories at level 16 During the MT3 Ballooning Experiment

Fig 34 MT3 Cladding Temperature Prediction Run1

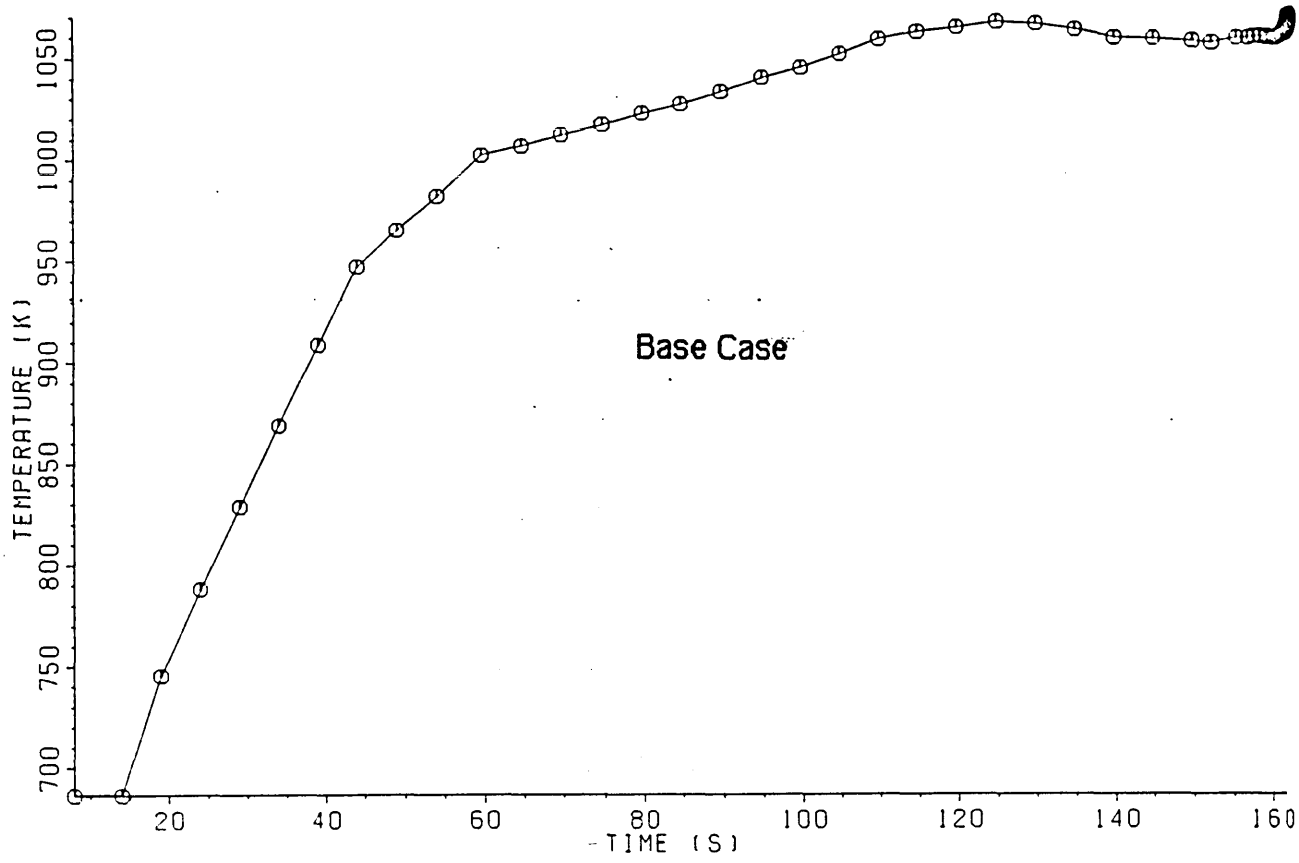

Fig 35 MT3 Strain Localisation Prediction Run1

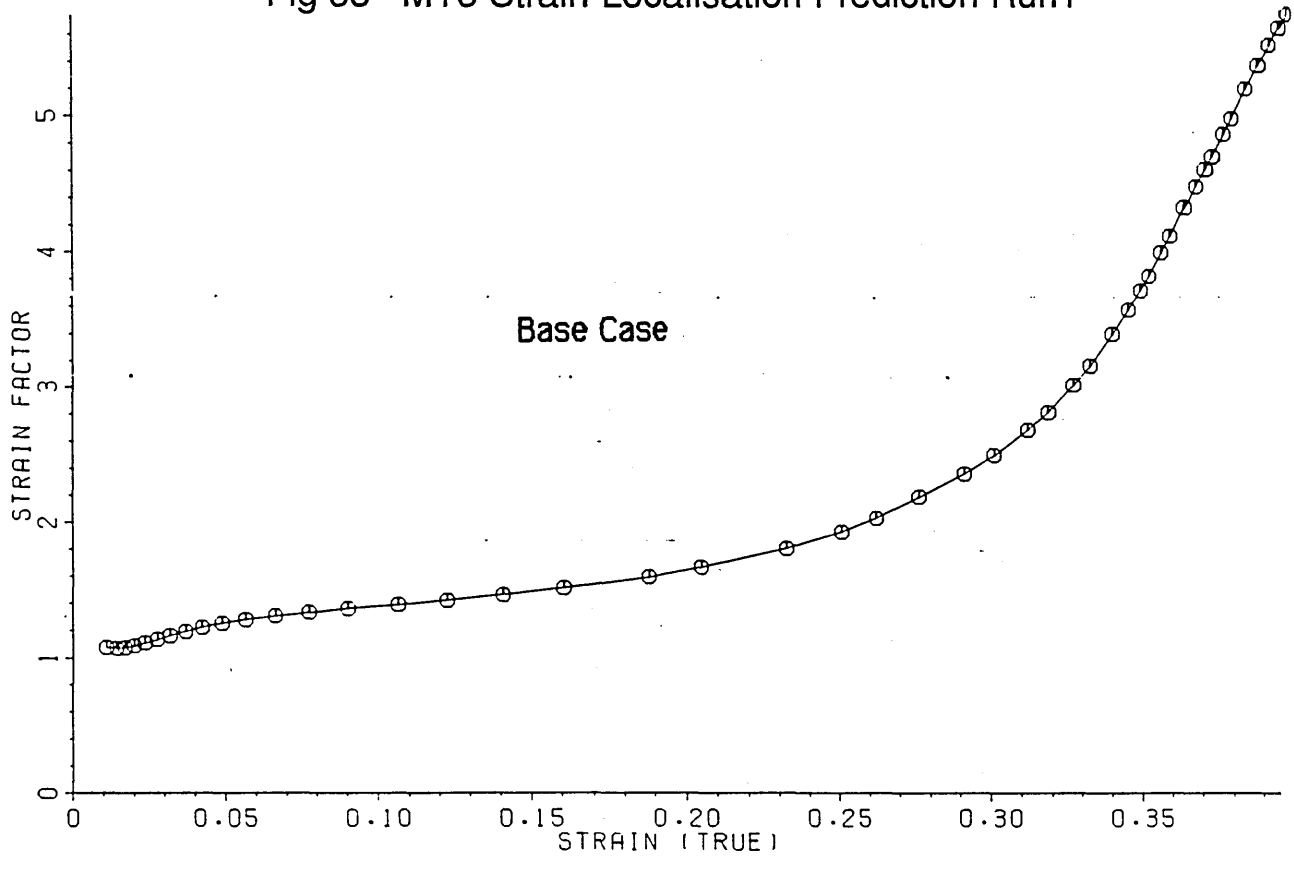

Fig 36 MT3 Pellet Offset Prediction Run1

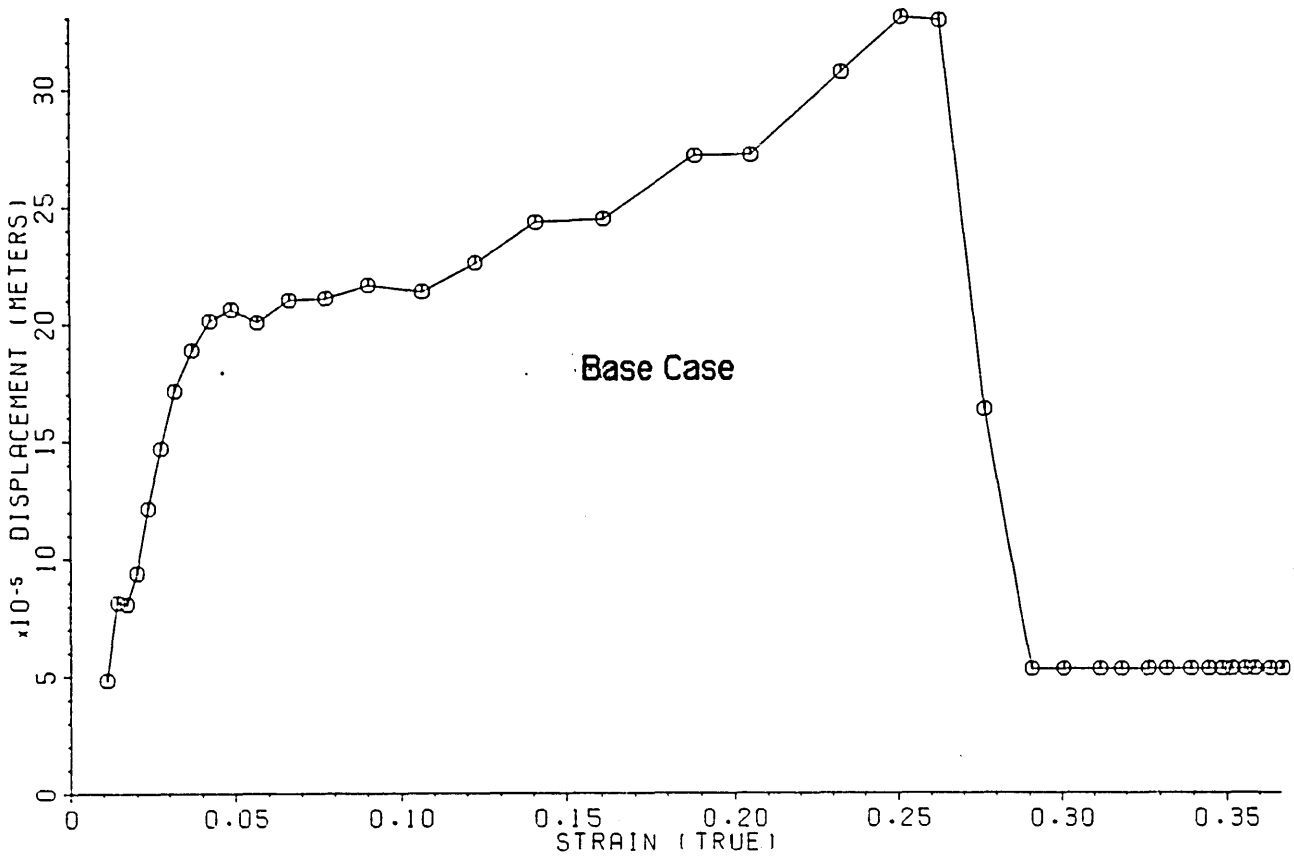

Fig 37 MT3 Strain History Prediction Run2

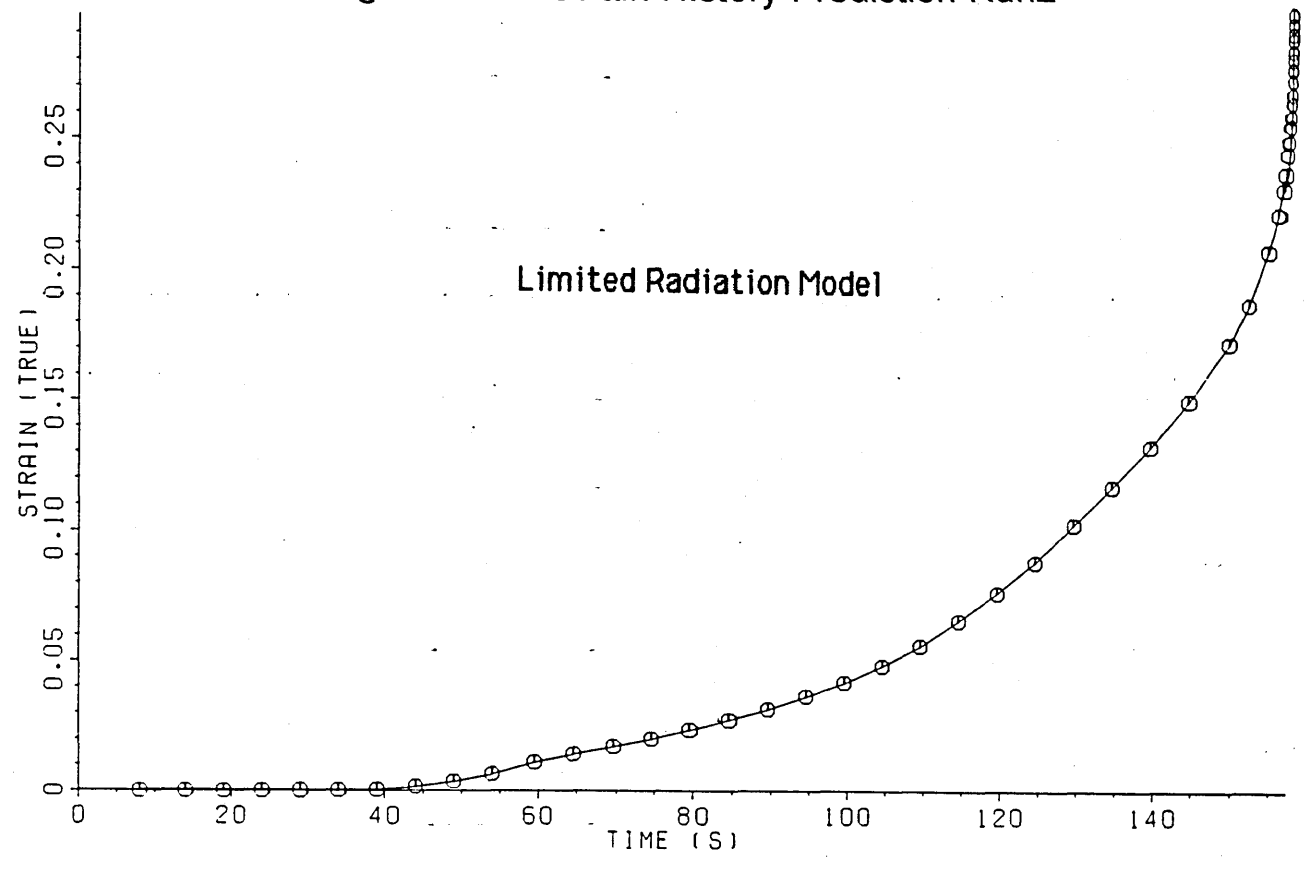

Fig 38 MT3 Pellet Offset Prediction Run2

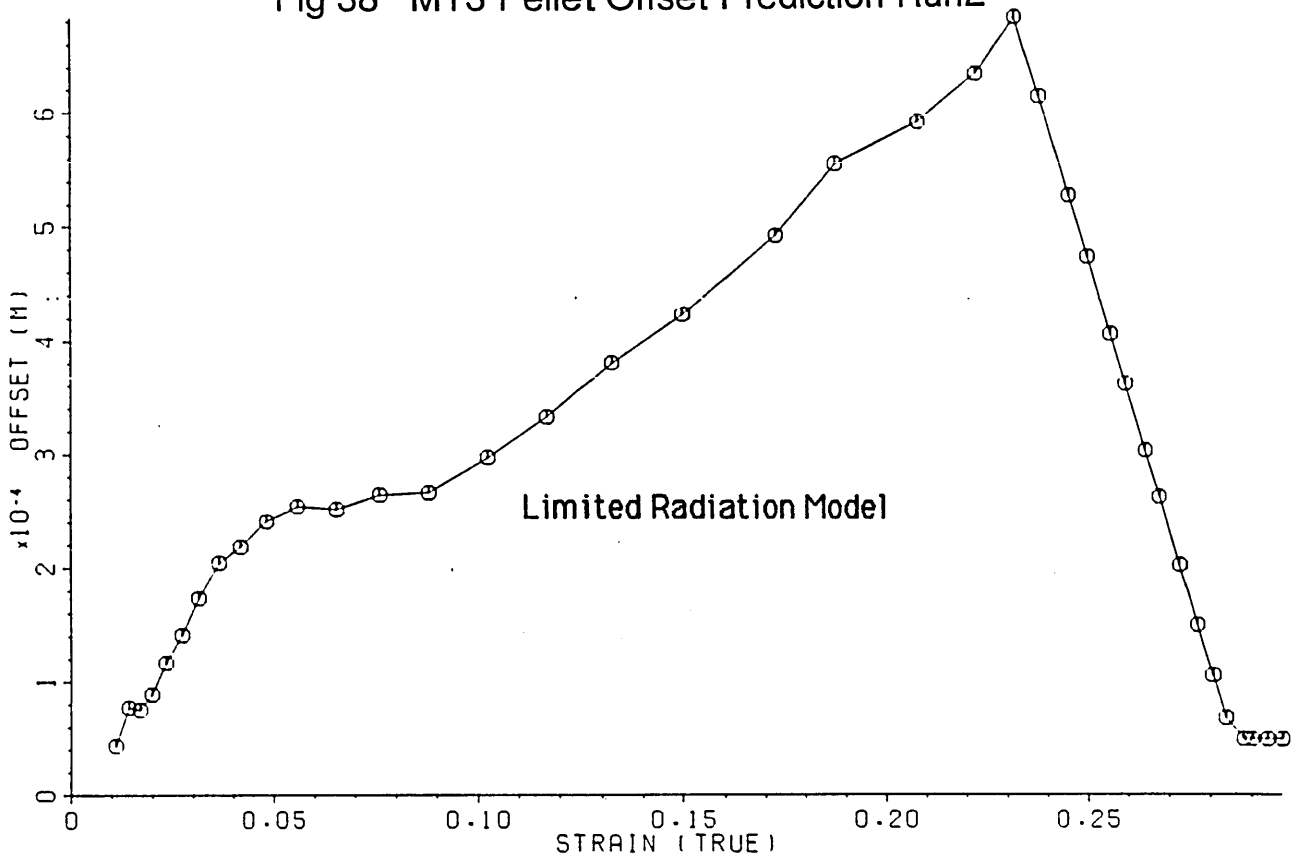

Fig 39 MT3 Strain Localisation Prediction Run2

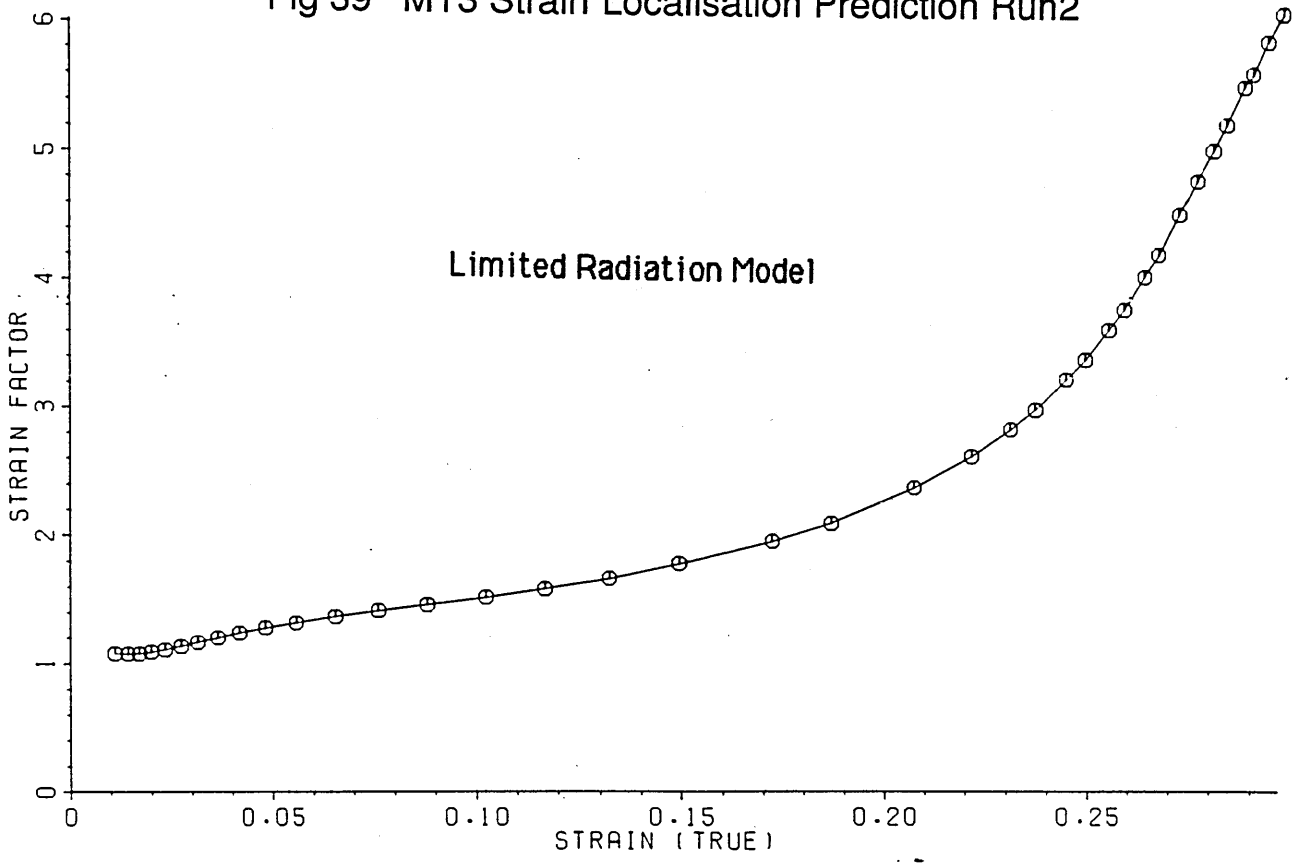

Fig 40 MT3 Temperature History Prediction Run3

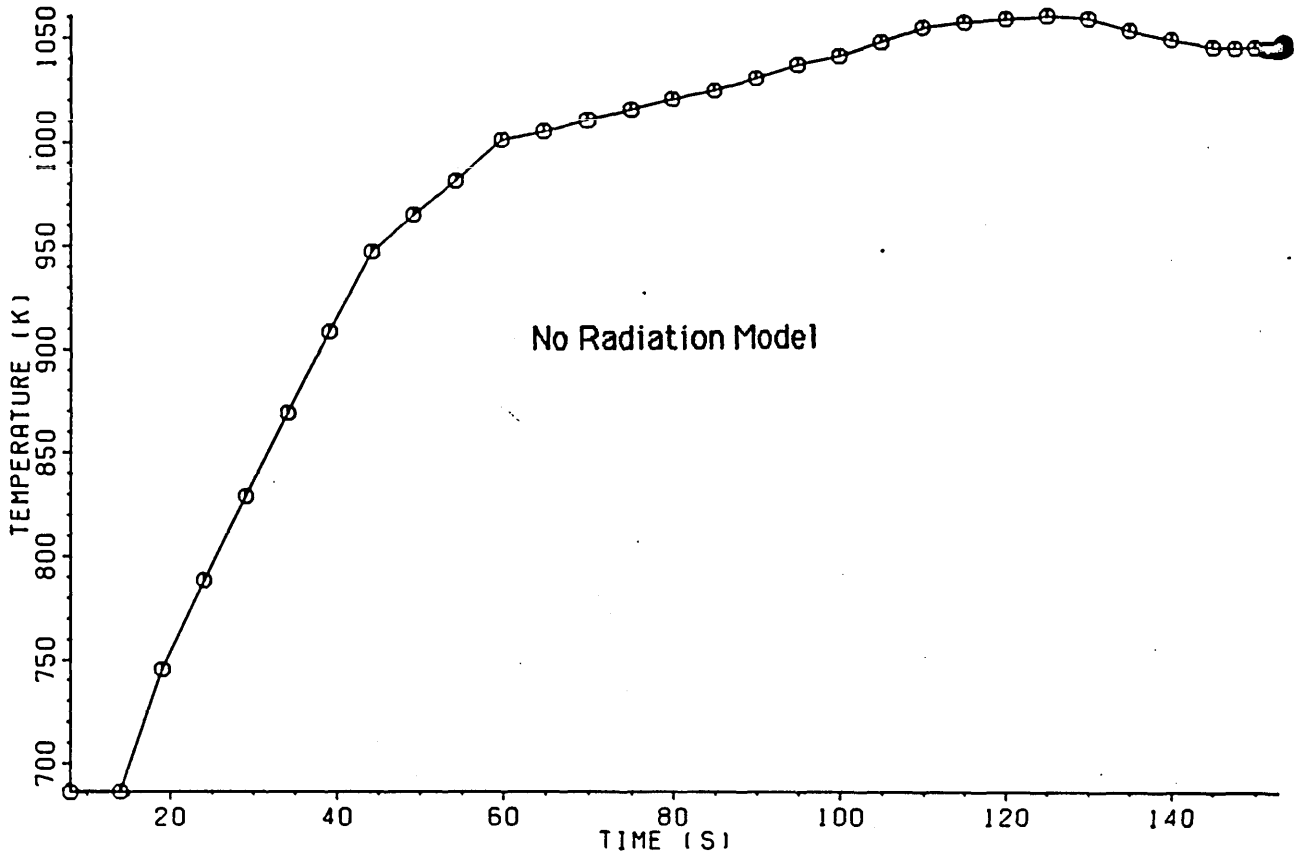

Fig 41 MT3 Cladding Displacement Prediction Run3

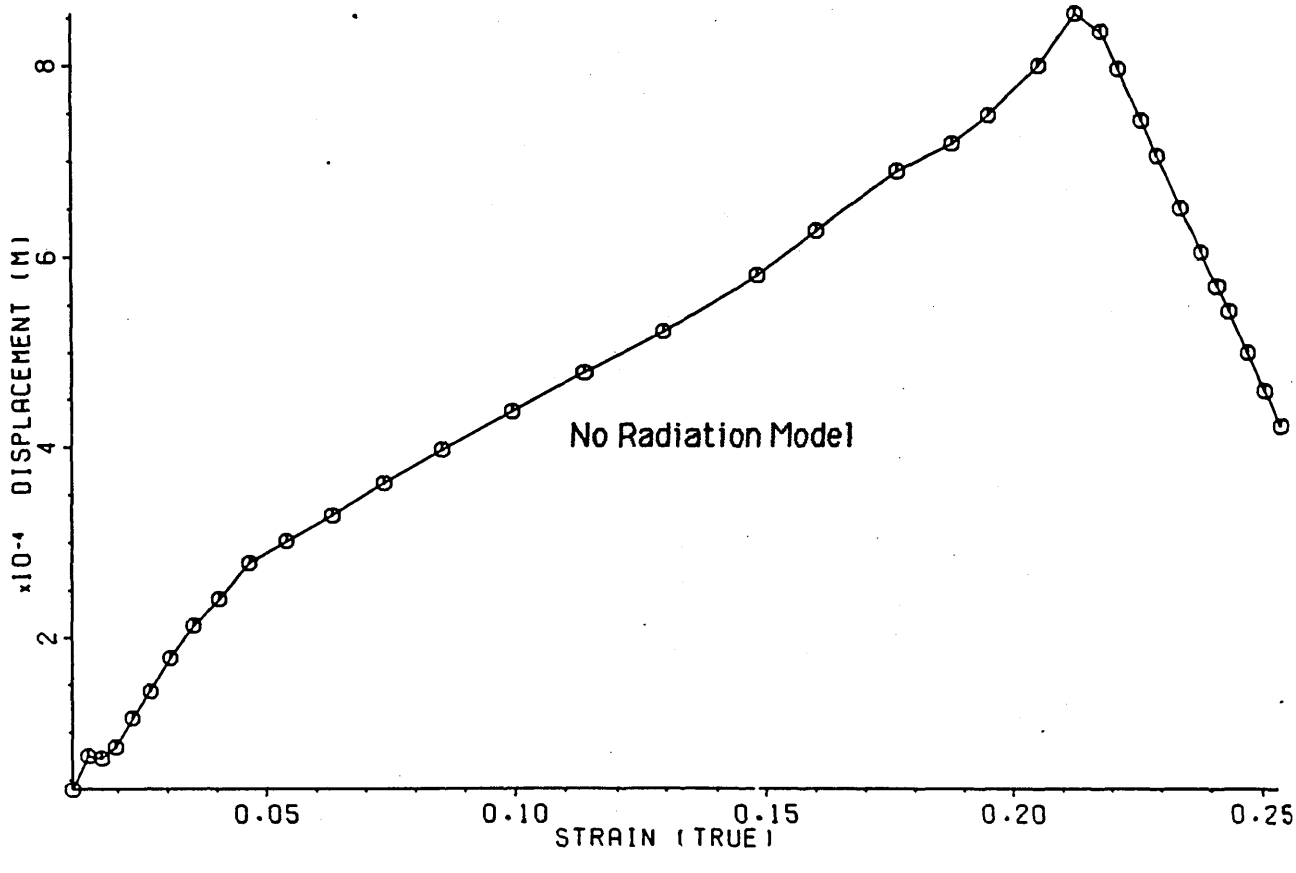

Fig 42 MT3 Strain Localisation Prediction Run3

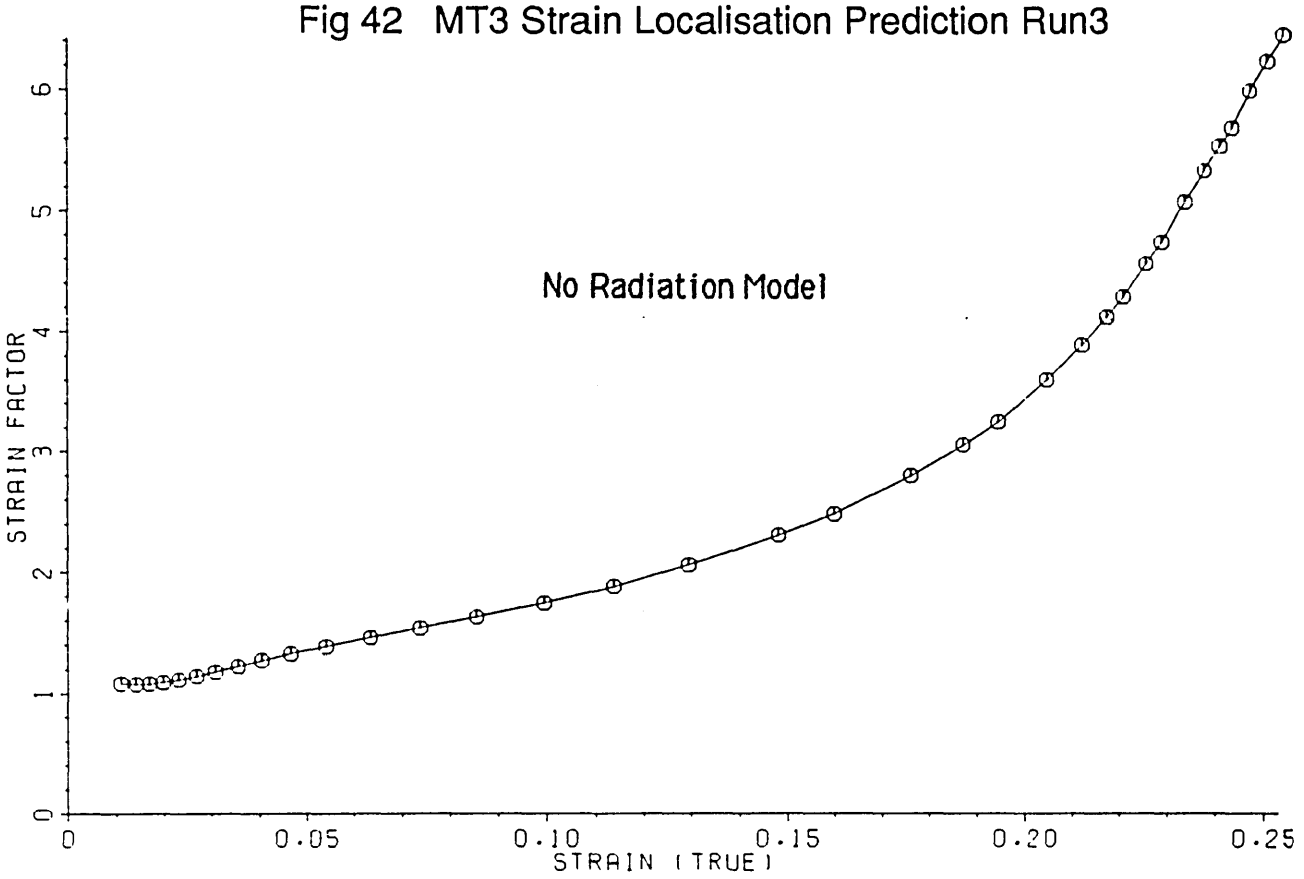

Fig 43 MT3 Strain History Prediction Run4

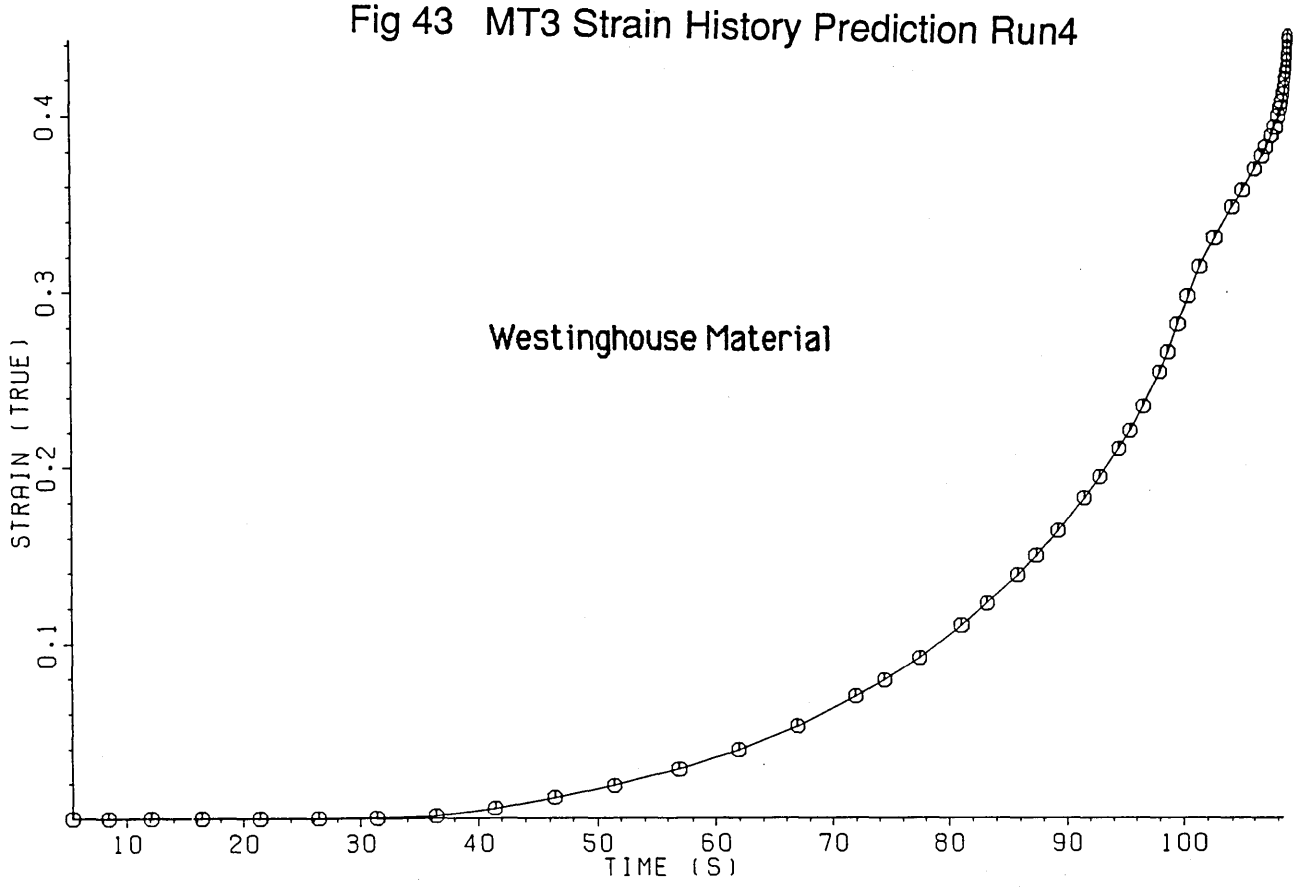

Fig 44 MT3 Pellet Offset Prediction Run4

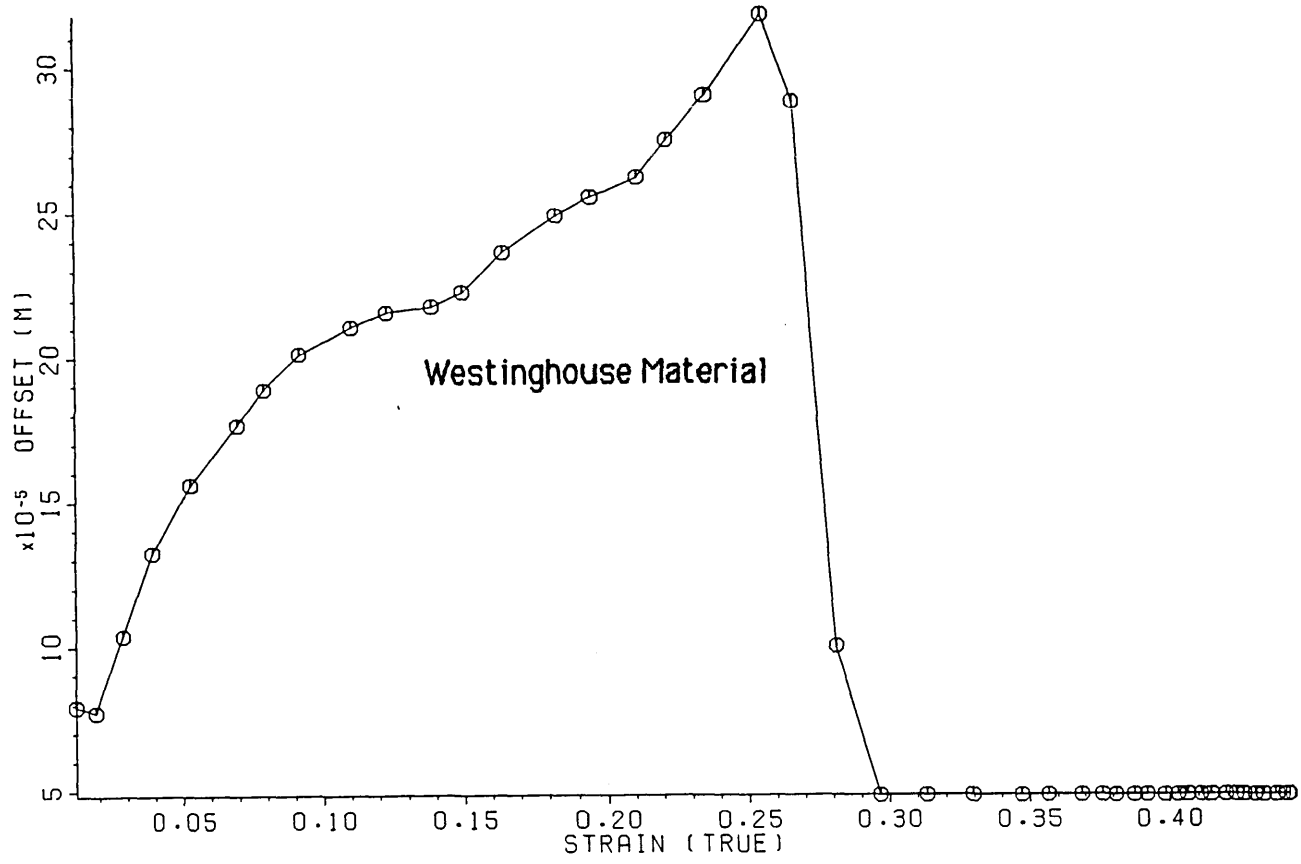

Fig 45 MT3 Strain Localisation Prediction Run4

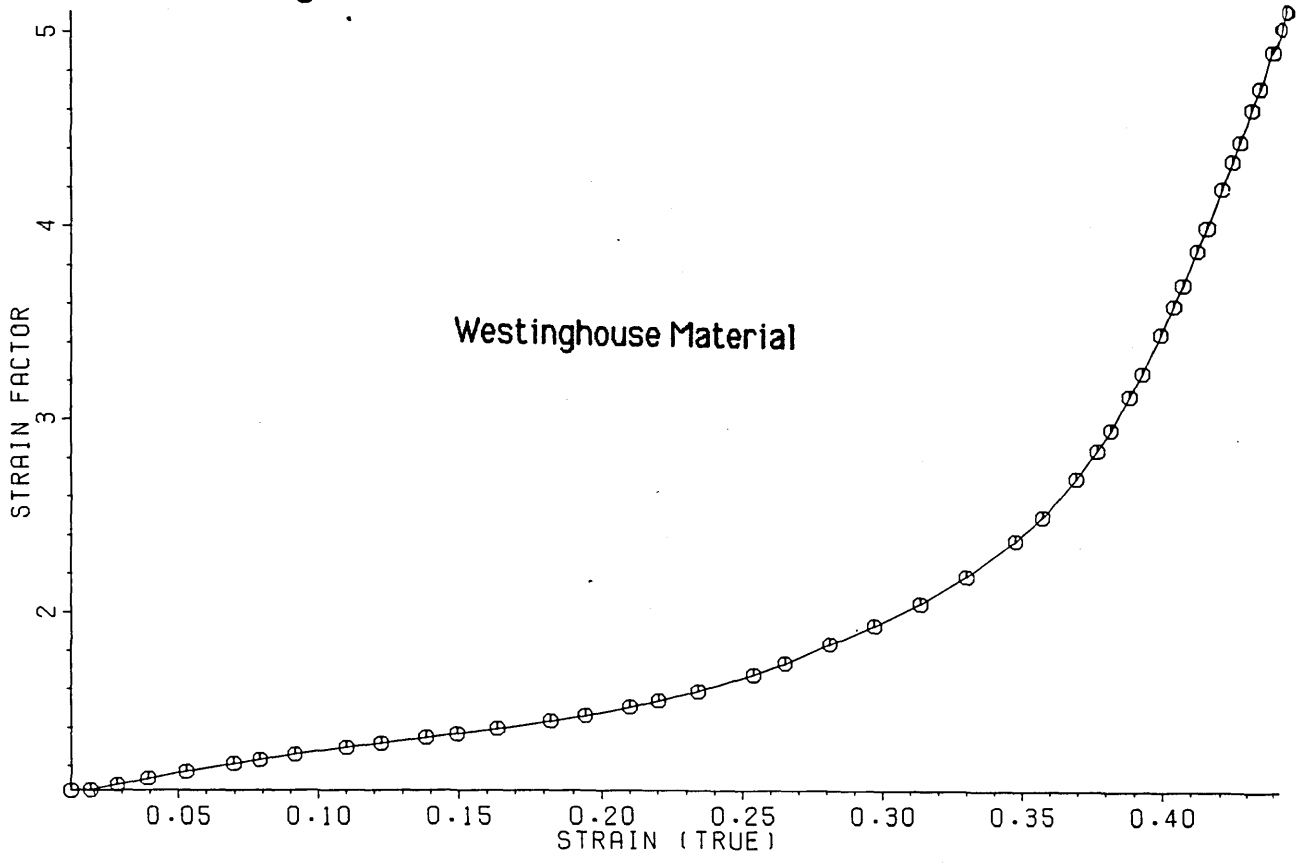

Fig 46 MABEL Calculation Results (Haste 1984)

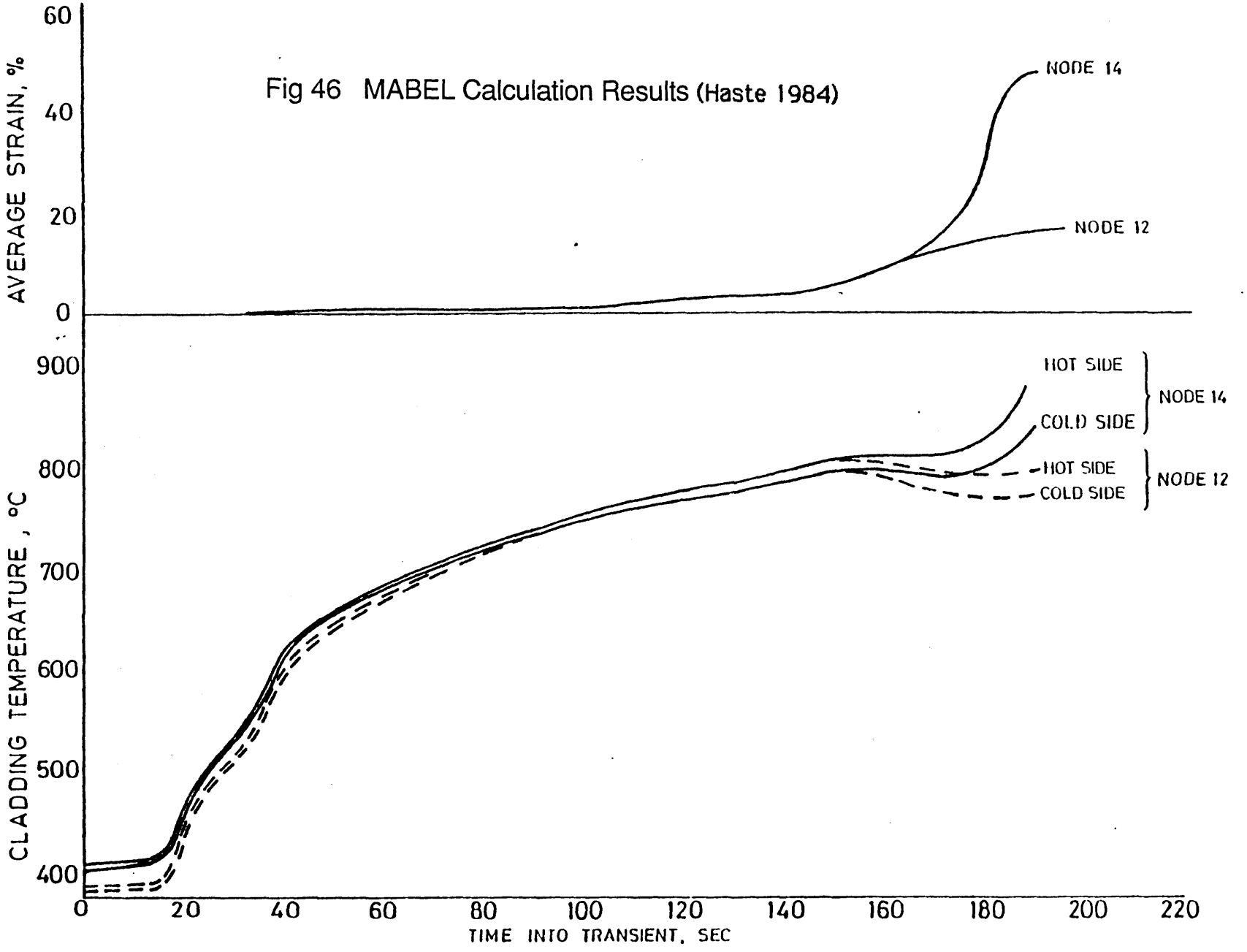

Fig 47 MT3 Strain and Temperature History Predictions Run5

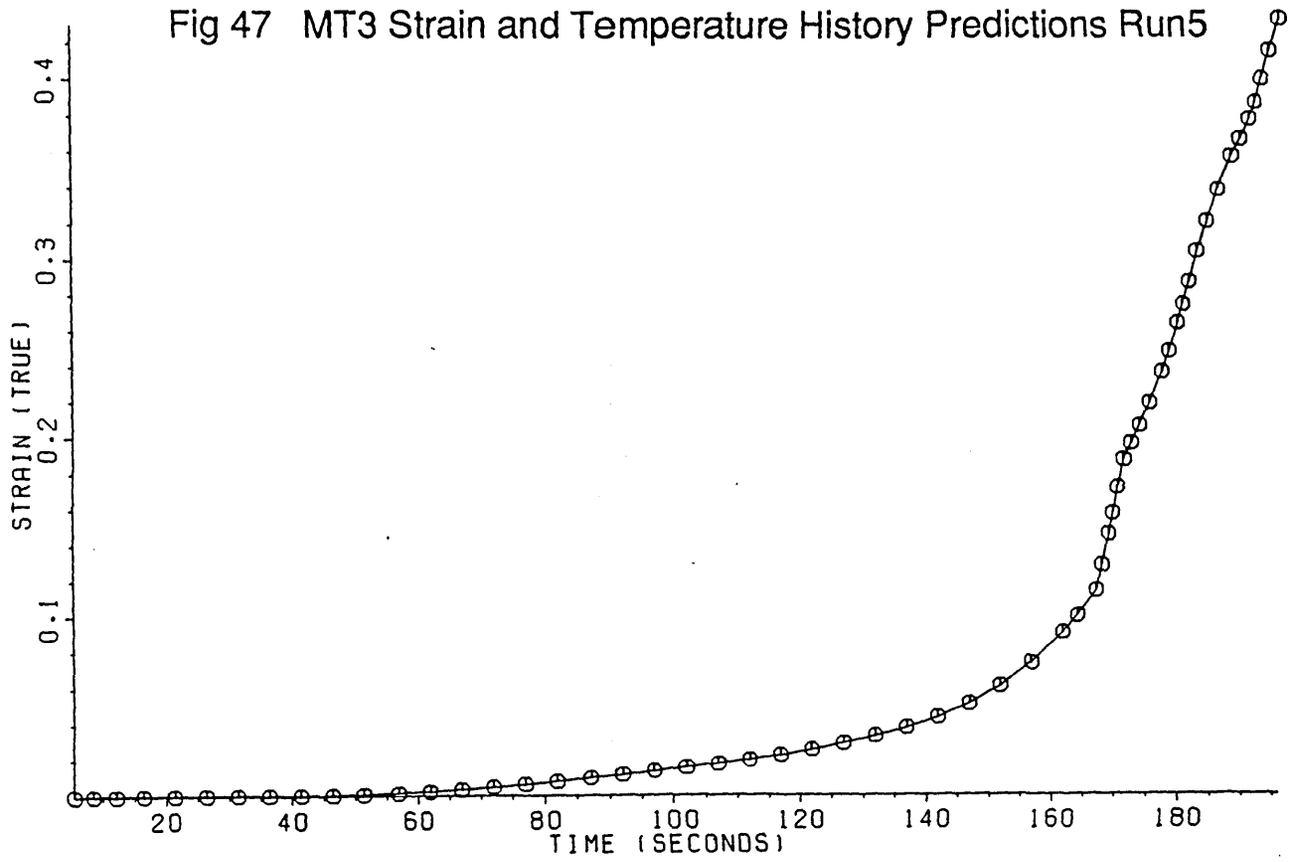

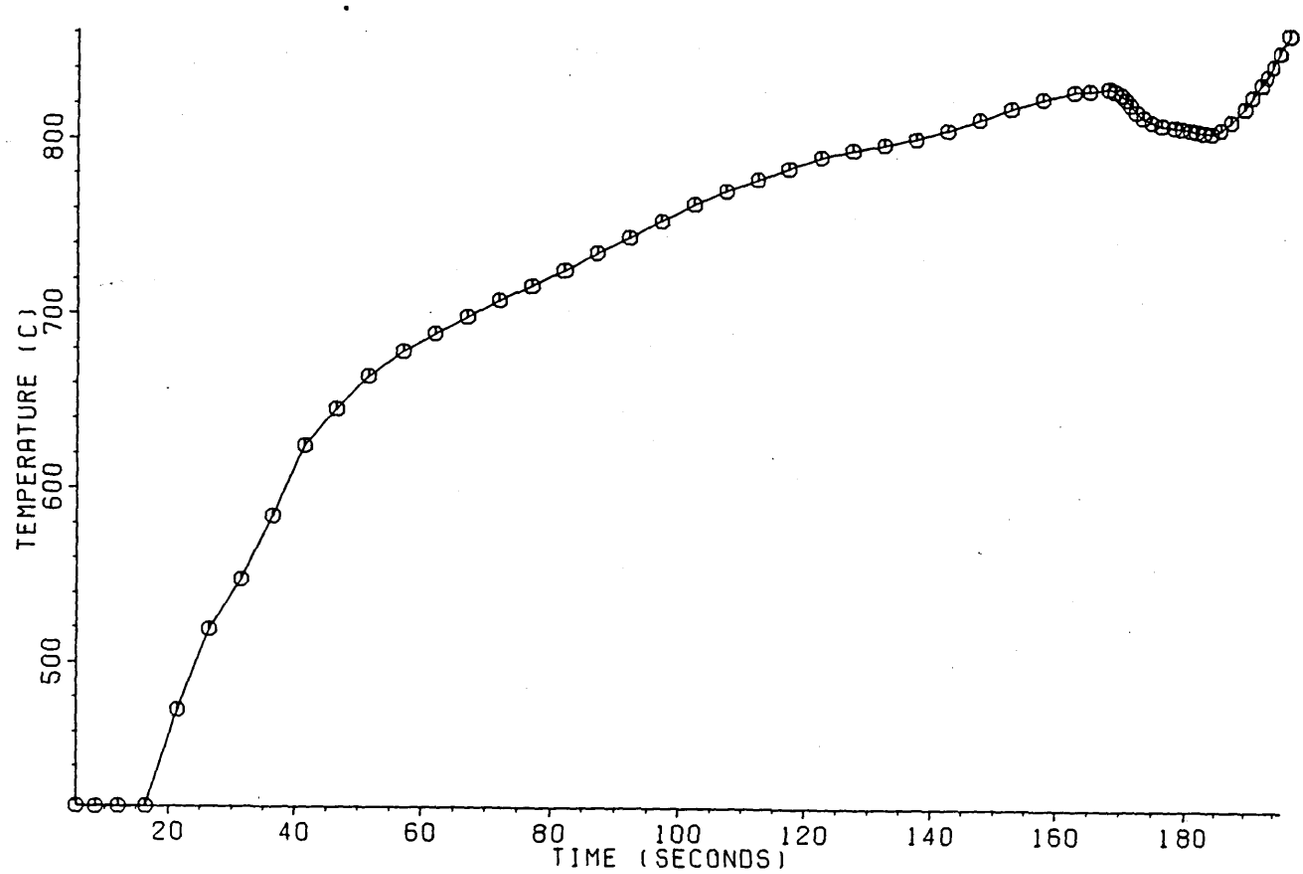

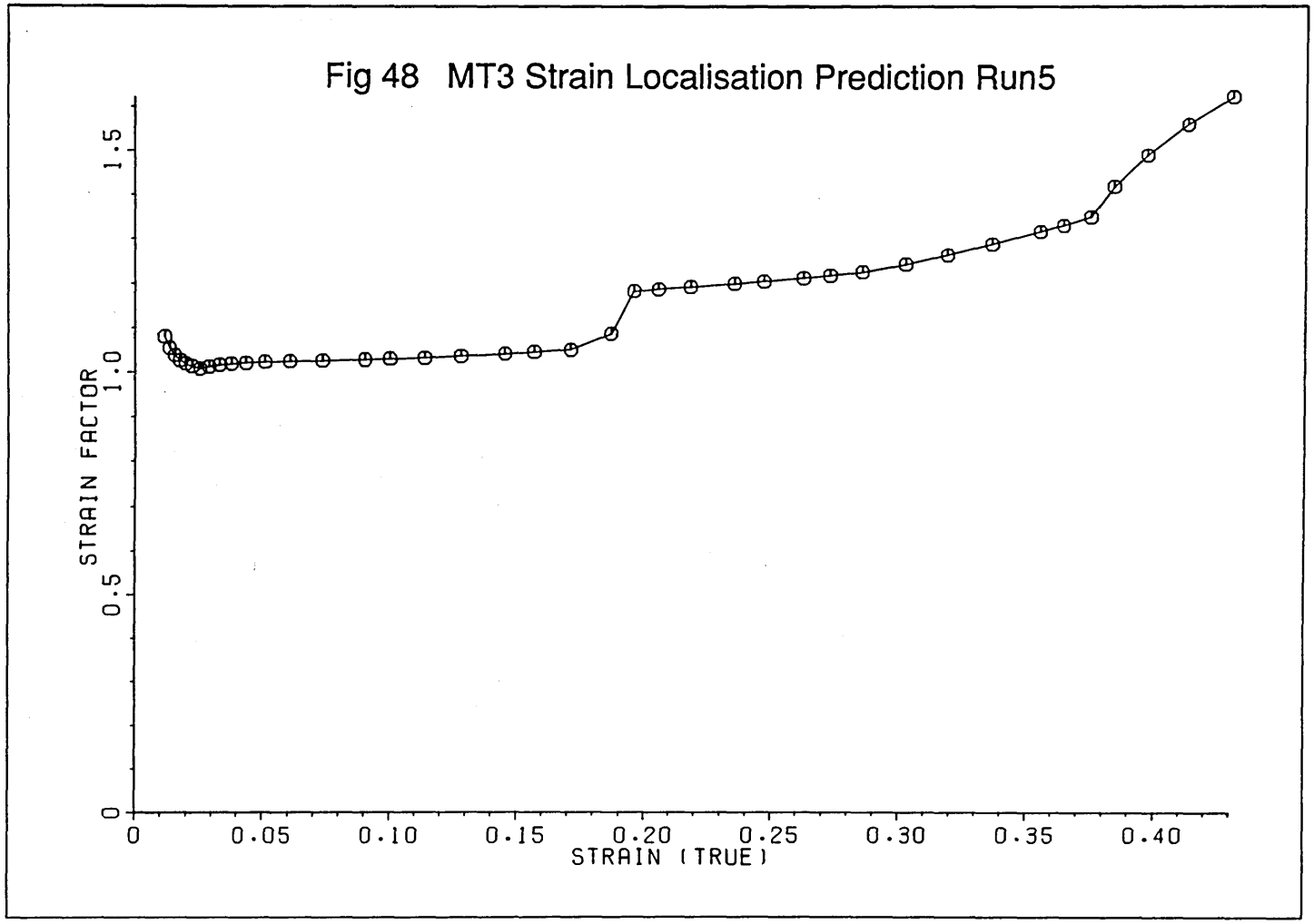
Fig 48 MT3 Strain Localisation Prediction Run5
STRAIN FACTOR
0
0.5
1.0
1.5
0
0.05
0.10
0.15
0.20
0.25
0.30
0.35
0.40
STRAIN (TRUE)

Fig 49 MT3 Cladding Temperature History Prediction Run 6

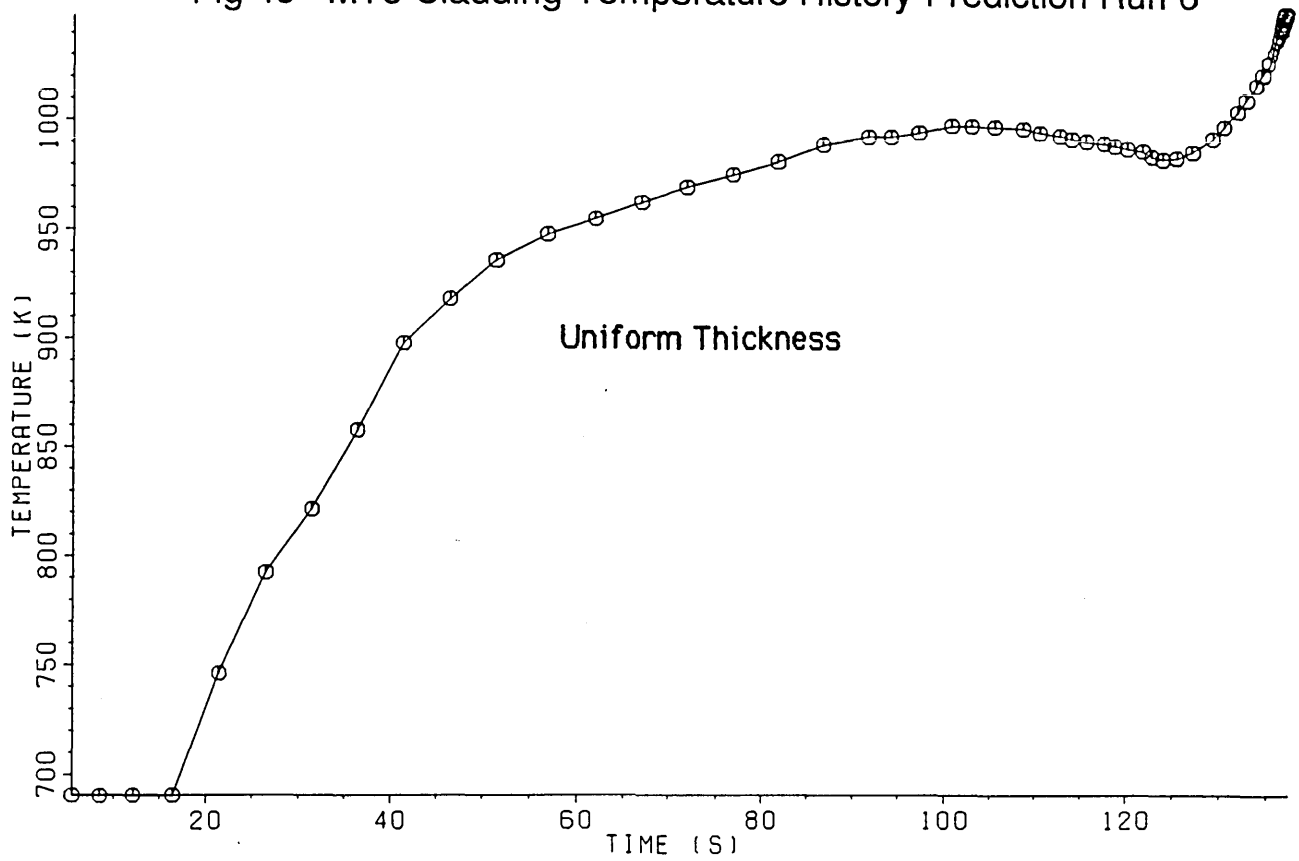

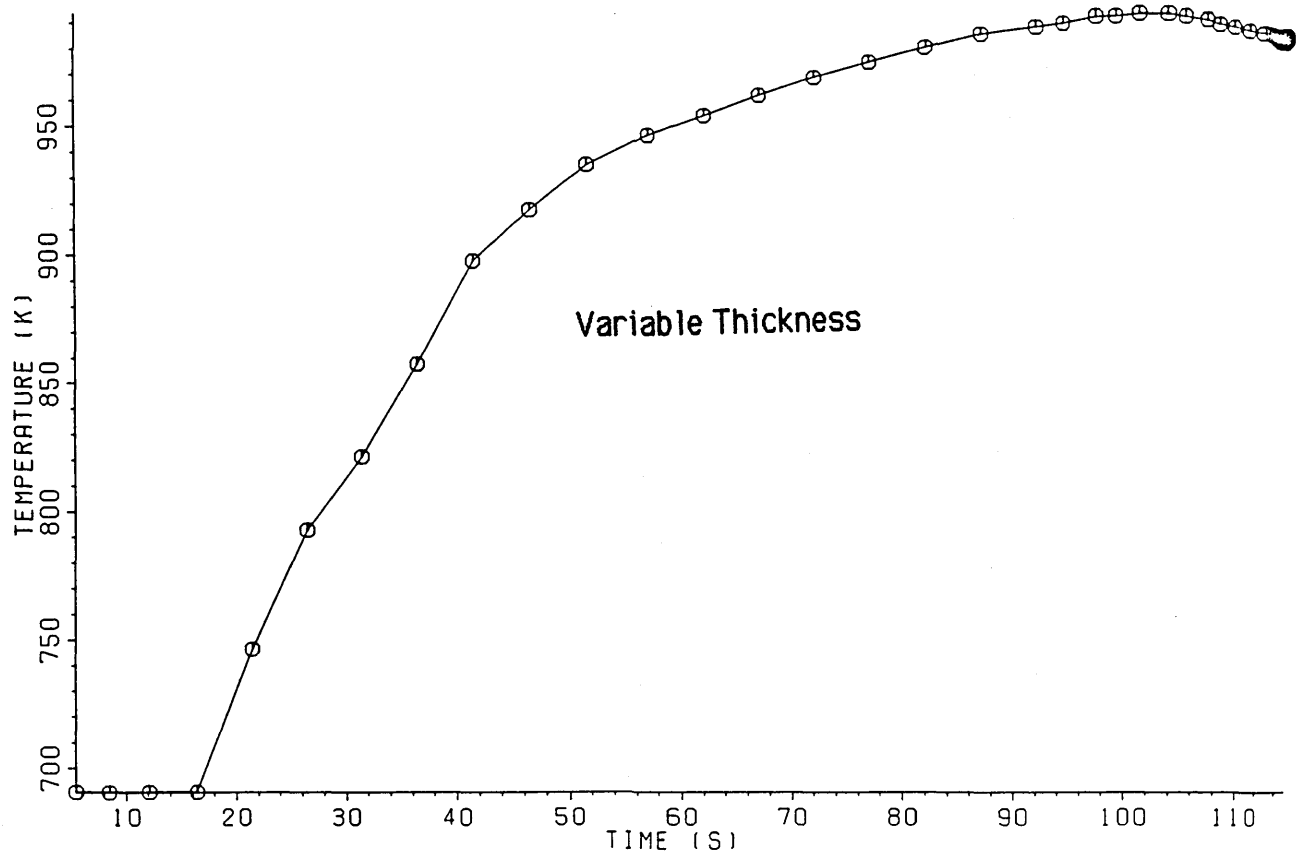

Fig 50 MT3 Strain History Prediction Run 6

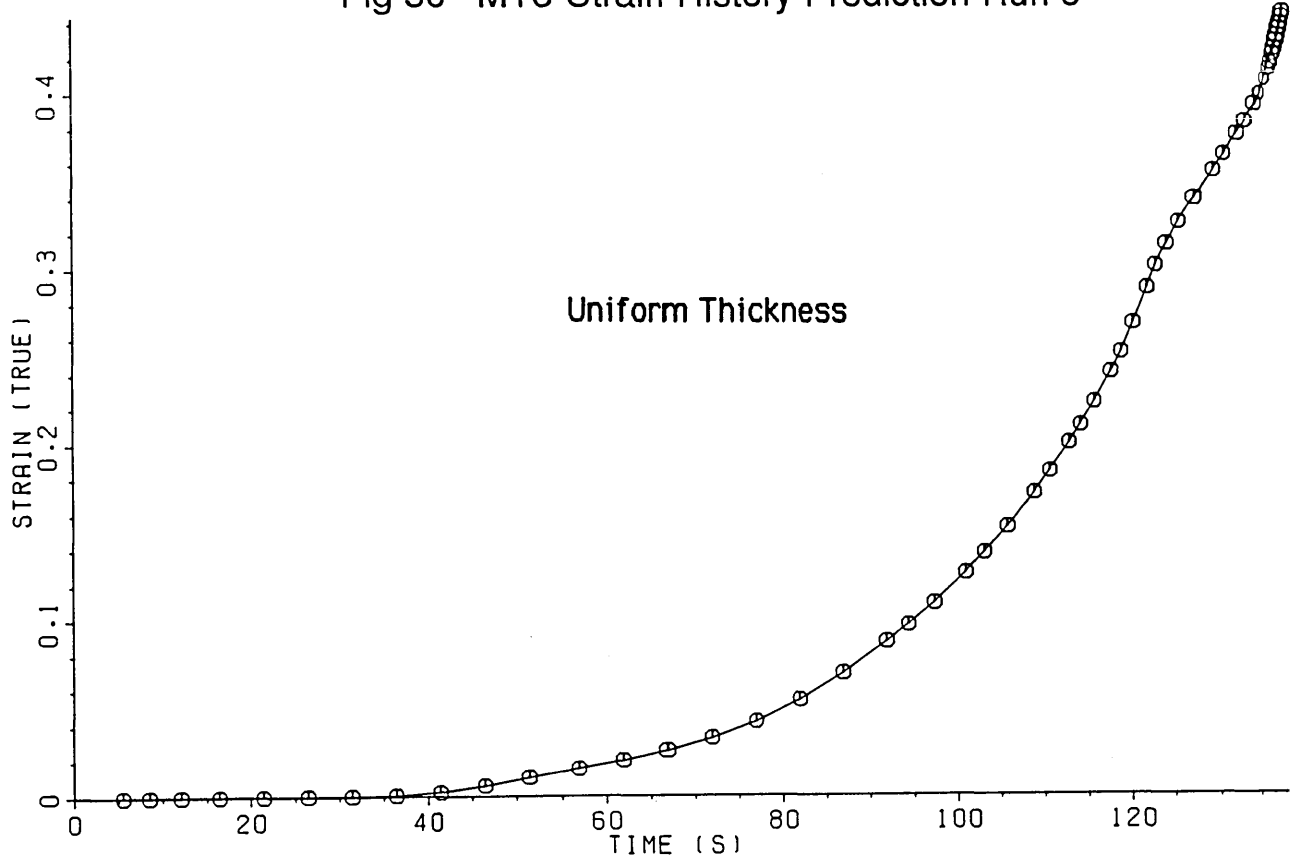

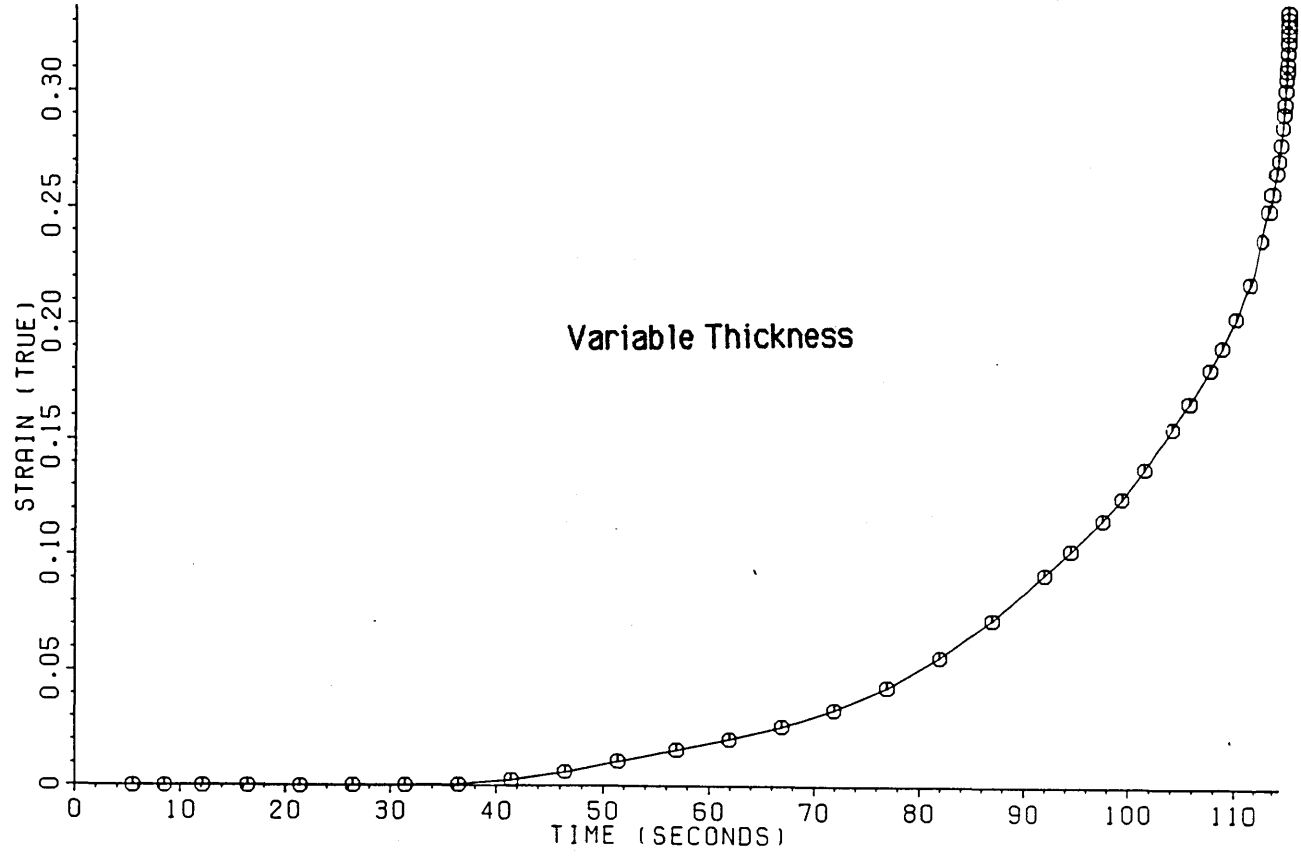

Fig 51 MT3 Pellet Offset Prediction Run 6

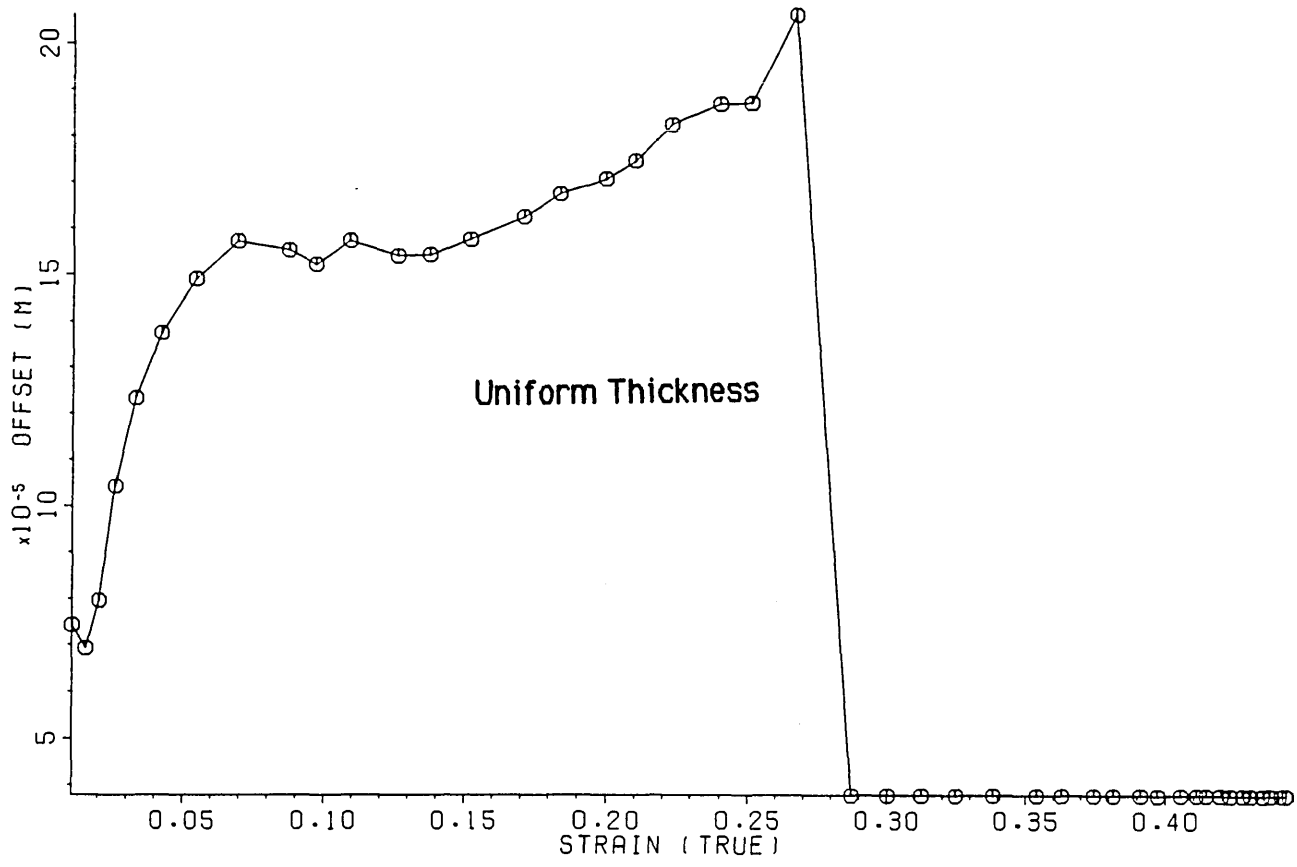

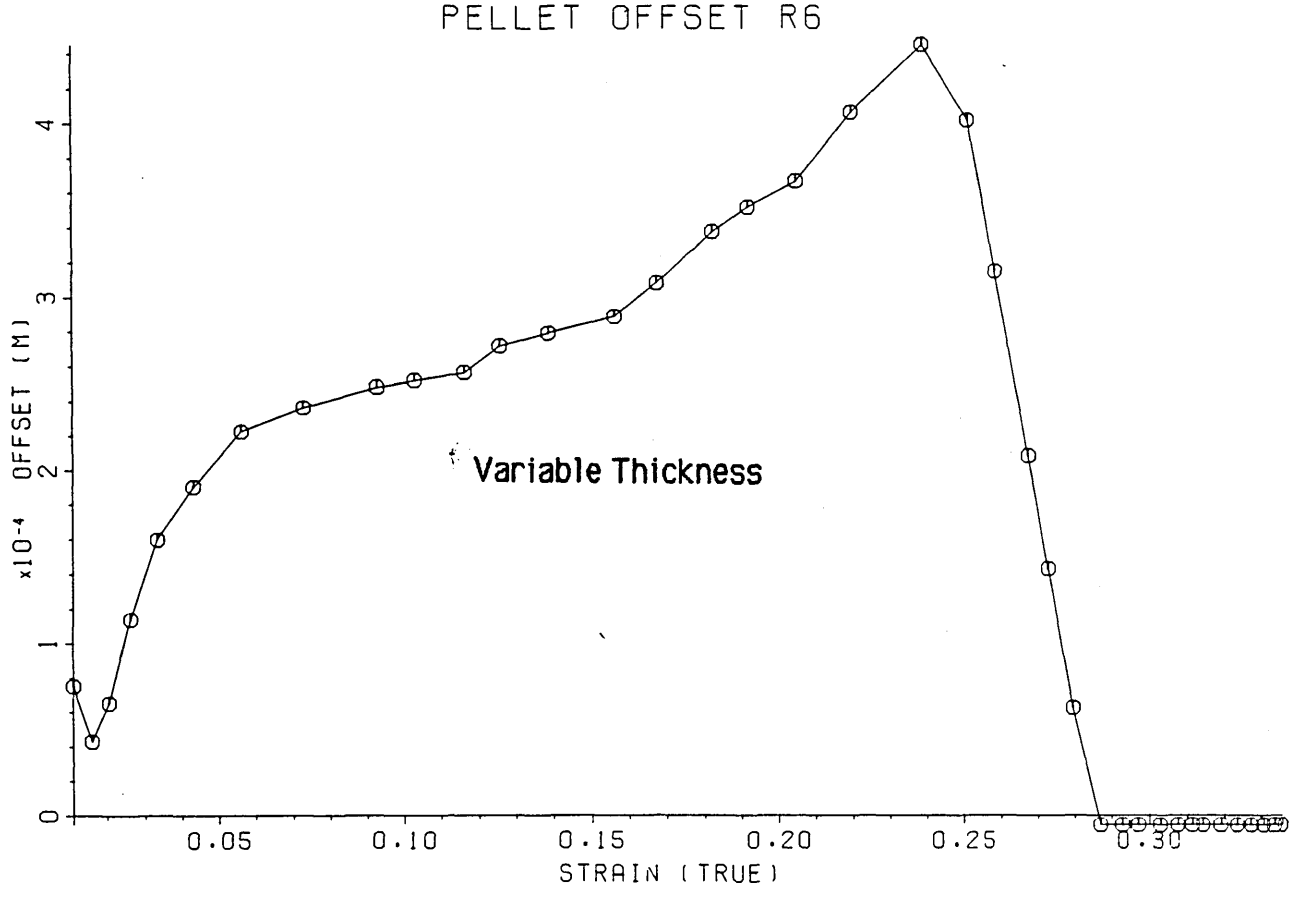

Fig 52 MT3 Cladding Temperature Difference Prediction Run 6

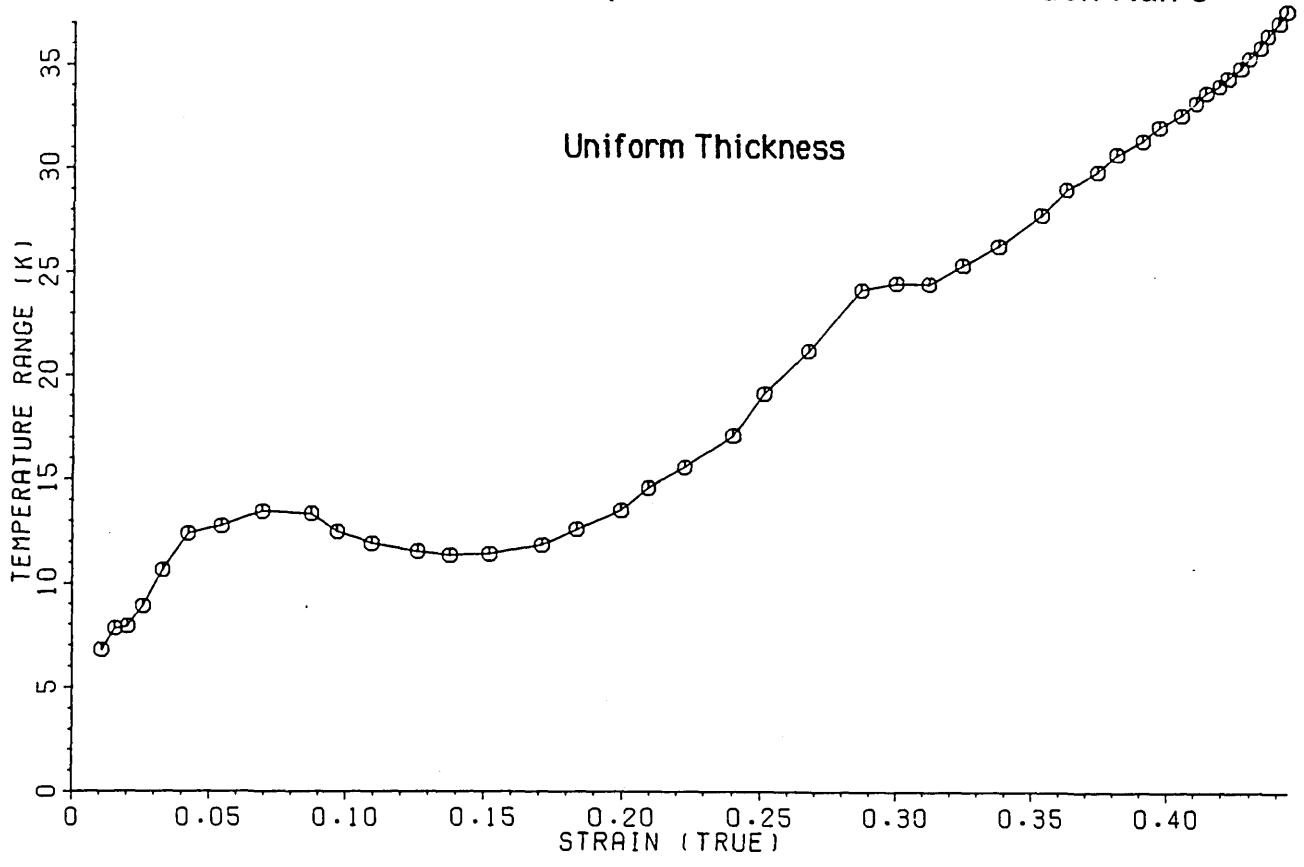

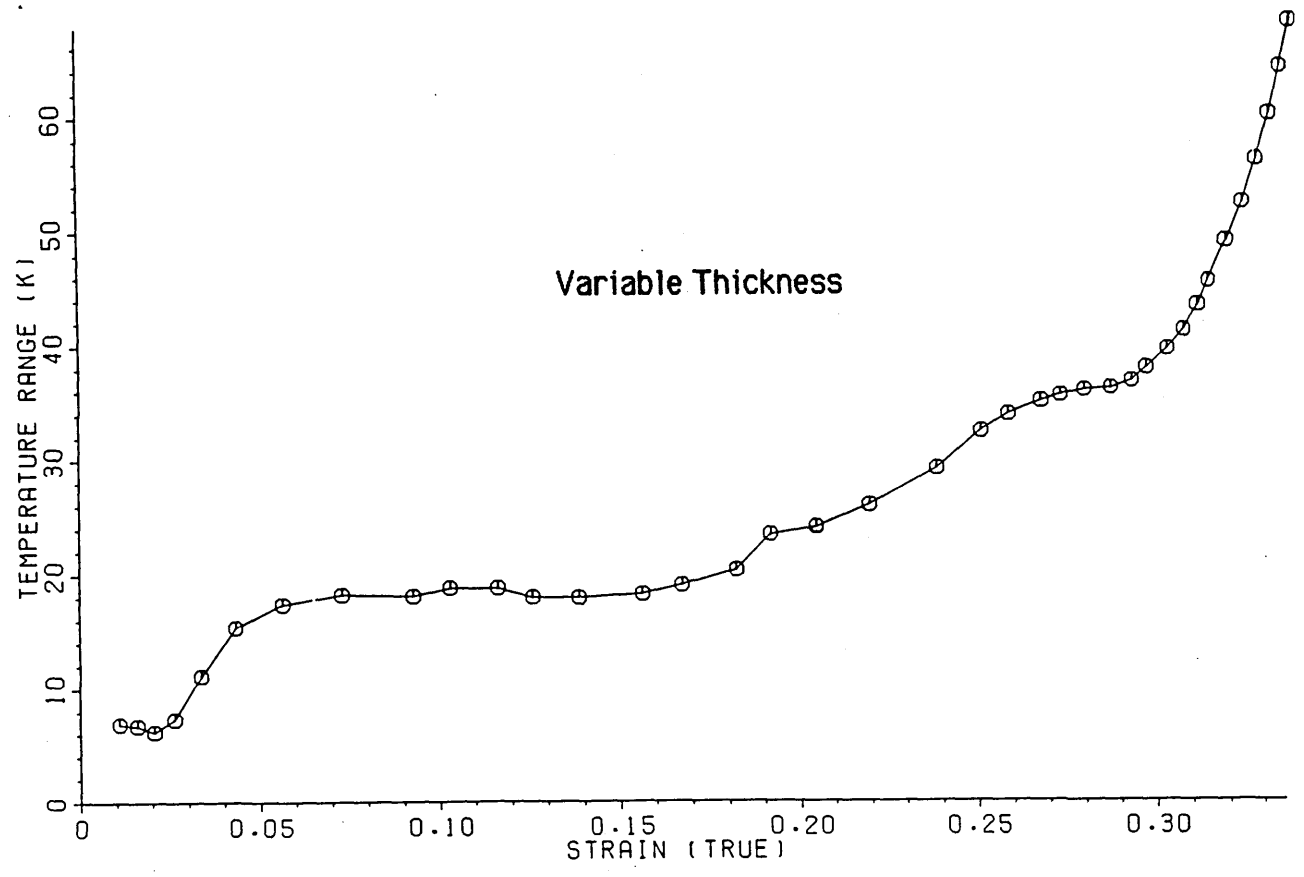

Fig 53 MT3 Strain Localisation Prediction Run 6

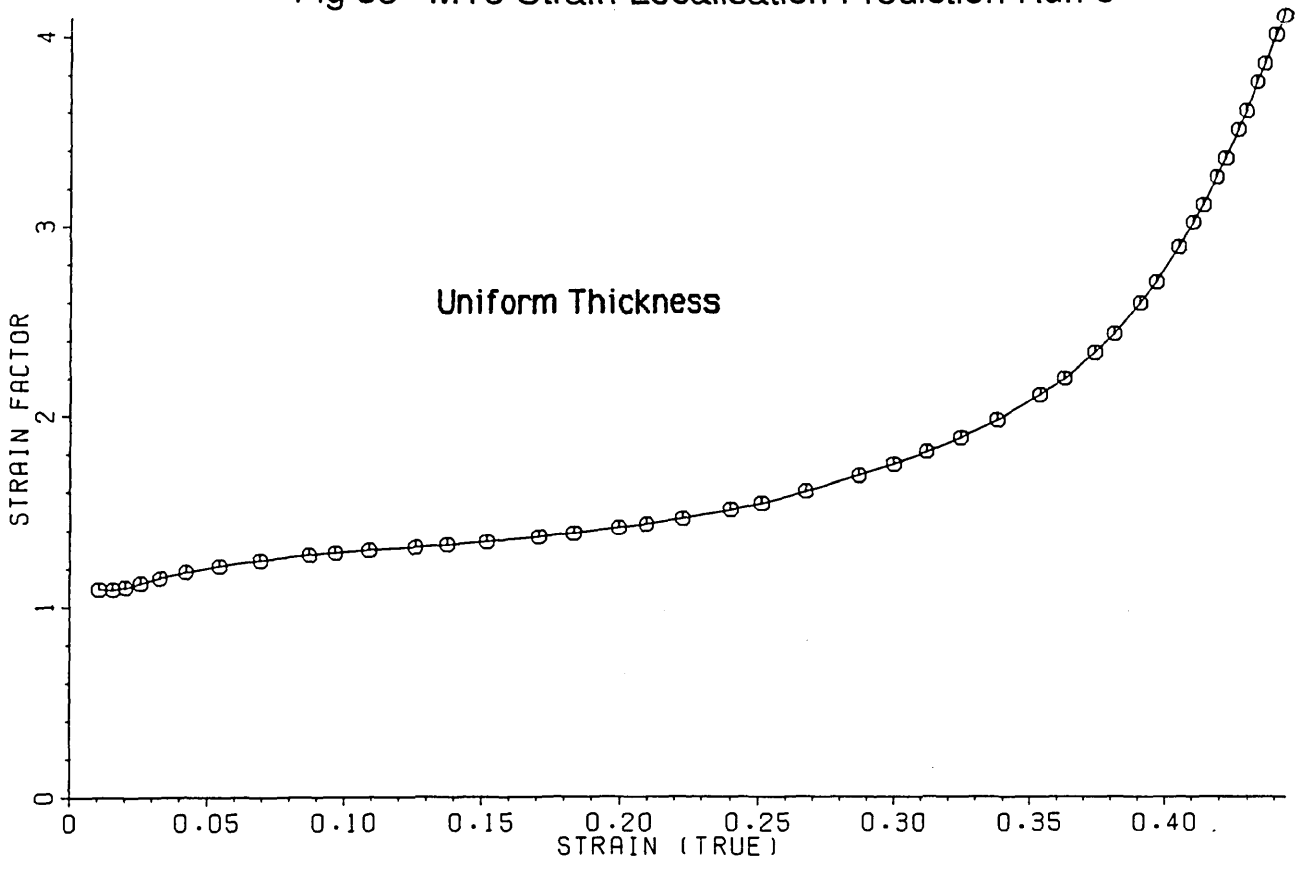

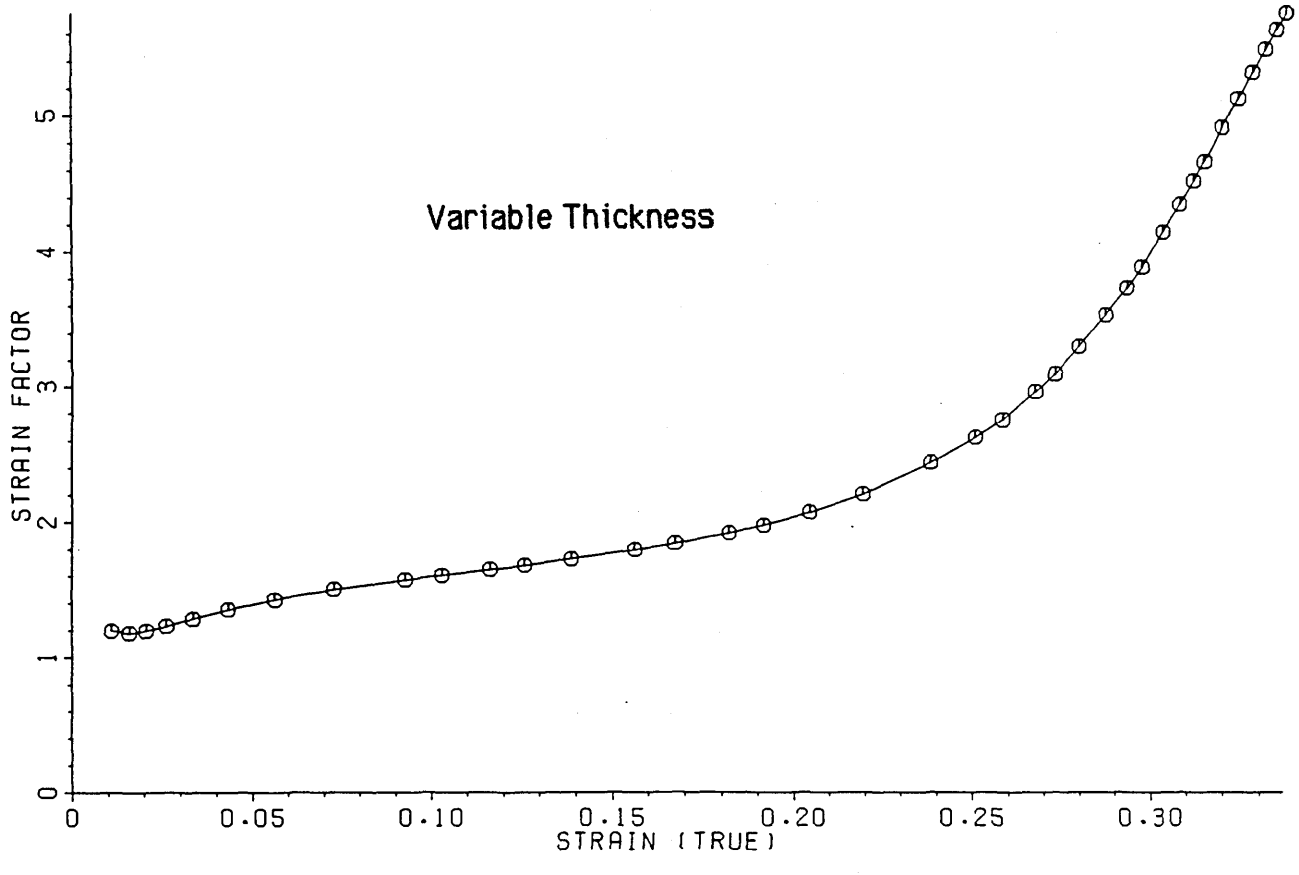

References

Baker L Just LC
"Studies of Metal-Water Reactions."
Argonne National Laboratory ANL-6548 (1962)

Barlow P
"PWR Clad Ballooning: The Effect of Circumferential Clad Temperature Variations on the Burst Strain/Burst Temperature Relationship."
Water Reactor Fuel Element Performance Computer Modelling, pp413-429
Applied Science Publishers (1983)

Borgwaldt H Gulden W
"SSYST, A Code - System for Analysing Transient LWR Fuel Rod Behaviour under Off-normal Conditions."
Water Reactor Fuel Element Performance Computer Modelling, pp663-687
Applied Science Publishers (1983)

Bowring RW Cooper CA Haste TJ
"MABEL-2: A Code to Analyse Deformation in a loss-of-Coolant Accident."
Part 1 : General Description, AEEW-R I5529 (1982)
Part 2: The Equations, AEEW-RI530 (1983)

Brittain I
"General Description of PWR Loss-of coolant Accident Analysis Methods Used in Studies at AEE Winfrith."
UKAEA Report, AEEW R1518 (1982)

Burman DL
"Role of Fuel-Clad Gap Heat Flux in Determining Clad Ballooning Strain in LOCA."
ANS Topical Meeting on Reactor Safety Aspects of Fuel Behaviour
Sun Valley Idaho, USA (1982)

Burton B Donaldson AT Reynolds GL and Barnes JP
"The Interaction of Oxidation and Creep in Zircaloy 2."
CEGB report RD\B\N4280 (1978)

Chapman RH Crowley JL Longst AW Hofmann G
"Zirconium Cladding Deformation in a Steam Environment with Transient Heating."
Zirconium in the Nuclear Industry
ASTM STP 681 (1982)

Chapman RH Crowley JL Longst AW
"Effect of Bundle Size on Cladding Deformation in LOCA Simulation".
Zirconium in the Nuclear Industry
ASTM STP 824 (1984)

Dearien JA et al.
"FRAP-T3: A Computer Code for the Transient Analysis of Oxide Fuel Rods."
TFPB-TR-194 (1974)

Donaldson AT. Horwood RAL. Healey T.
"Biaxial Creep Deformation of Zircaloy-4 in the High Alpha Phase Temperature Range."
Water Reactor Fuel Element Performance Computer Modelling, pp81-95
Applied Science Publishers (1983)

Douglass DL
"The Metallurgy of Zirconium."
International Atomic Energy Agency (1971)

Dressler G Matucha KH
"Yield & Fracture of Biaxially Stressed Zr4 Cladding Tubes at Room Temperature and 400^{o}c."
Zirconium in the Nuclear Industry, ASTM STP 633 (1977)

Ecob RC Donaldson AT Knowles G
"Deformation of Westinghouse PWR Fuel Cladding:
Creep Properties and Dislocation Structures of Alpha Phase Zircaloy-4 Observed in Constant Stress Tests".
Nuclear Fuel Performance, BINES (1985)

Eichorn et al.
"Measurements of Shear Stress in a Rod Bundle."
Nuclear Engineering and Design, vol 56, pp380-390 (1980)

Farbairn SA Piggot BDG
"Flow and Heat Transfer in PWR Rod Bundles in the Presence of Blockage Due to Clad Ballooning."
CEGB report Rx11/1019/84-EN, (1984)

Franklin D Franz WA
"Numerical Model for the Anisotropic Creep in Zirconium."
Zirconium in the Nuclear Industry, ASTM STP 633 (1977)

Garlick A Hindmarch P
"Cladding Deformation & Fuel Stack Mechanical Stability during Internal Pressurization Tests on Irradiated PWR Fuel."
UKAEA Report ND-R-628 (W) (1982)

Gulden W Meyder R Borgwaldt H
"SSYST-A Code System to Analyse LWR Fuel Rod Behaviour under Accident Conditions."
ANS Annual Meeting. (1982)

Gibson I H Coddington P Healey T Mann CA
"The UK MT-3 Ballooning Test in the Battelle NRU loop. "
AEE Winfrith Report, AEEW-R-1506 (1982)

Hagrman DL Reymann GA
"MATPRO VERSION 11 ; A Handbook of Materials Properites for use in the Analysis of Light Water Reactor Fuel Rod Behaviour."
Idaho National Engineering lab. (1979)

Haigh RE
"Modifications to BART to include Temperature and Strain Variation Around the Cladding."
NNC report, PWR/RX 802 (1984)

Haste TJ Gittus JH
"The Effects of Hot Spots upon Swelling of Zircaloy Cladding as Modelled by the Code CANSWEL-2."
Specialist Meeting on Safety Aspects of Fuel Behaviour in Off Normal Conditions Finland (1980)

Haste TJ
"Canswel-2: A Computer Model of the Creep Deformation of Zircaloy Cladding under Loss-of-Coolant Accident Conditions."
Part 1- Model Description
UKAEA Northern Division Report ND-R-814 (S) (1982)

Haste TJ
"A Study Using the MABEL-2C Code of the Effects of Pellet and Cladding Asymmetries on PWR fuel Deformation Under Conditions Relevant to the NRU MT-3 Ballooning Experiment"
UKAEA Northern Division Report ND-R-876 (S) (1983)

Haste TJ
"Modelling the Effect of Different Mechanical Restraints on PWR Fuel Rod Deformation under Conditions Relevant to the NRU MT-3 Experiment using the MABEL - 2D Code"
UKAEA Northern Division Report, ND-R-988 (S) (1984)

Healey T et al
"Ballooning Response of Nuclear and Electrically Heated PWR Fuel Rods Tested in the Halden Reactor and Under Laboratory Simulation Conditions."
International Conference on Nuclear Fuel Performance, BNES (1985)

Healey T Board S
"CEGB Proof of Evidence on Fuel Clad Ballooning."
Sizewel B PWR Public Enquiry, CEGB P37 (1982)

Hill R
"The Mathematical Theory of Plasticity."
Oxford Claredon Press (1950)

Hindle ED MANN CA
"Zircaloy PWR Fuel Cladding Deformation Tests under Mainly Convective Cooling Conditions."
UKAEA Northern Division Report, ND-R-364 (S) (1980)

Hindle ED Worswick D
"Variation in the Strain Anisotropy of Zircaloy with Temperature and Strain."
Sixth International Symposium on Zirconium in the Nuclear Industry,
ASTM STP 824 (1983)

Holt RA Sills HE Sagat S
"Model for the Kinetics of the Alpha to Beta Phase Transformation in Zircaloy 4."
Specialists Meeting on Fuel Element Performance Modelling, Blackpool (1980)

KARB EH et al
"Results of the FR2 in-pile test on LWR Fuel Rod Behaviour."
American & European Nuclear Societies Topical Meeting on Reactor Safety Aspects of Fuel Behaviour,
Sun Valley Idaho, USA (1981)

Mann CA Hindle ED PARSONS PD
"The Deformation of PWR fuel in a LOCA."
UKAEA Northern Division Report ND-R-701 (S) (1982)

Mc Adams WH
"Heat Transmition."
Mc Graw-Hill (1954)

Pawel RE et al
"Diffusion of Oxygen in Beta-Zircaloy and the High temperature Zircaloy - Steam Reaction."
zirconium in the Nuclear Industry,
ASTM STP 633 (1977)

Raff S
"Development of a Deformation and Failure Model for Zircaloy in the High Temperature Region for Application with Light Water Reactor Loss of Coolant Accident Studies."
University of Karlsruhe Dissertation, KfK 3184 (1982)

Rapley C W , Gosman A D
"The Prediction of Turbulent Flow and Heat Transfer in a Narrow Isosceles Triangular Duct."
International Journal of Heat and Mass Transfer ,vol 27 No2, pp253-262 (1984)

Rapley C W
"Fluid and Heat Flow in Tubes of Arbitrary Crossections"
PhD Thesis,
Imperial College Department of Mechanical Engineering (1980)

Routledge K
"The Sizewell B Fuel Clad Ballooning Safety Case."
NNC report PWR/RX662 (1982)

Sills HE Allan JD
"Fuel Deformation/Thermal Hydraulic Interaction During High Temperature Transients."
Water Reactor Fuel Element Performance Computer Modelling, pp621-631
Applied Science Publishers. (1983).

Sills HE Holt RA
"NIRVANA A High Temperature Creep Model for Zicaloy Fuel Sheathing."
Atomic Energy of Canada Ltd. Report, AECL-6412 (1979)

Uchida M Nakamura J
"Application of Transient Fuel Bundle Analysis Code FRETA-B to LOCA Simulation Experiments."
Water Reactor Fuel Element Performance Computer Modelling, pp631-649
Applied Science Publishers (1983)

Williams PW
"Numerical Computation"
Nelson (1979)

Yadigoroglu G Arrieta LA
"Analytical Modelling of Heat Transfer During the Reflooding Phase of the LOCA; The UC Flood Code."
Proceedings of the ANS/ASME/NRC International Topical Meeting on Nuclear Reactor Thermo-hydraulics pp1173-1196 (1980)

Appendix 1

Major Clad-ballooning Codes

The state of clad-ballooning codes is constantly changing, but brief descriptions of the major codes used in clad-ballooning studies follows:

BALLOON

Type; single pin R-θ-Z deformation.

Comments:

The BALLOON code is capable of modelling the deformation of anisotropic short balloons in some detail by using membrane equations, but some of the assumptions made lead to non-circular cladding. This prediction is not supported by a fuller treatment of the equations (Mathews 1980) and the experimental observation that the cladding is incapable of resisting bending moments.

BART (Haigh 1984)

Type: single pin R-Z flow and deformation

Comments:

BART is a Westinghouse proprietary code bought by the CEGB for use with the proposed Sizewell B reactor. Some details of the code are on restricted access. The code models the fluid flow during reflooding in some detail, but it assumes that the entrained droplettes always pass through a blockage. The flow is approximated to two regions, namely the subchannel immediately surrounding the rod and the rest of the reactor.

Recently BART has been extended to take account of azimuthal temperature variations at selected axial positions. The model uses an analytical solution of the heat-transfer equations which includes the following assumptions; uniform cladding thickness, quasi-steady conduction and a cosinusiodal temperature profile.

CANSWEL (Haste 1982)

Type; single pin R-θ-Z deformation.

Comments:

The CANSWEL code was developed by the UKAEA to predict the axial deformation and failure of cladding tube, given the cladding temperature history.

The axial temperature profile is input as a function of time and information is provided about the azimuthal temperature variation. The cladding is treated as a thin shell and remains circular until surrounding rods are contacted. After contact the behaviour depends upon input parameters.

FRAP-T (Dearien 1974)

Type; single pin R-z deformation and some flow.

Comments:

FRAP-T was developed for NRC and now contains a transient flow model capable of carrying out the analysis of an accident from the start of blow down to the end of reflooding. It does, however, not allow for cross flow in

the rod bundle, so the flow conditions are less accurately modelled at high strains. The code BALLOON can be run with FRAP-T to predict the azimuthal temperature distribution at selected locations and hence determine the failure strain.

MABEL (Bowring 1982)

Type; mainly single pin quasi-three dimensional deformation and flow.

Comments:

The MABEL code was developed by the UKAEA and incorporates the CANSWEL deformation model. MABEL carries out R-θ solution of the temperature and strain field, in a single pin, at all axial nodes. Some account is taken of the behaviour of surrounding rods by the use of input parameters. These parameters determine the extent to which the behaviour of the other rods reflect that of the rod studied in detail.

The thermo-hydraulic part of the code is capable of modelling the flow in four subchannels surrounding the pin of interest. Account is taken of flow diversion due to ballooning or bowing. The model currently assumes quasi-steady, homogenous, two phase flow, so it is normally used only to perturb input thermo-hydraulic conditions obtained from two phase flow codes such as RELAP or TRAC. The pellet stack is assumed to remain intact and the eccentricity of the pellets and the cladding is prescribed by the user.

SSYST (Gulden 1982)

Type: single pin R-Z input flow conditions

Comments:

Developed at KFK, the code is modular with considerable choice of routines. Rigorous treatment of azimuthal temperature gradients is to be added, but some allowance is made for this by running the AZI model. Treatment of the interaction of cladding deformation and coolant conditions exists, but the main thermo-hydralic model used is RELAP and this is not run iteratively.

TAPSWEL (Holmes 1984)

Type: single pin R-θ heat conduction and deformation

Comments

TAPSWEL is also a Westinghouse proprietary code bought by the CEGB. The code uses a uniform finite difference grid spacing. Localisation of strain is modelled by redistribution of material between control volumes at the end of each time step. Movement of the pellet stack and cladding is specified by prescribing a relative offset based upon experience. This remains constant during the calculations.

Appendix 2

Program Structure

The code contains the following routines:

Routine	Called by	Purpose
CAPAST	SOLVE1D	Material heat capacity calculations
CKMN	CTSTRT	Failure stress
CTSTRT	PHASCH	Failure strain
CREEP	DEFORM	Local deformation rate
DAMP	DEFORM	Iteration control
DEFORM	MAIN	Deformation profile
EPROP	DEFORM	Clad elastic properties
FAZECH	PHASCH	Phase change dynamics
HEAT	MAIN	Heat-transfer coefficient
HEATGEN	MAIN	Thermal neutron flux
HTCAL	SOLVE	Surface heat transfer term
ISTORY	MAIN	Controls History plotting
KEFF	SOLVE1D	Material thermal conductivity
MAIN	_____	Control routine
PELGOM	MAIN	Geometry calculations
PHASCH	MAIN	Clad properties

PLOT	ISTORY, PLOTT	Line-printer graphics
READIN	MAIN	Data input
SOLVE	MAIN	2D temperature field
SOLVE1D	MAIN	1D temperature field
TDMA	SOLVE,SOLVE1D	Tridiagonal-matrix algorithm
TDMA2	HEATGEN	Tridiagonal-matrix algorithm
TOUCH	DEFORM	Constrains pellet offset
UPDATE	MAIN	Updates time-dependent variables

Program Structure Chart

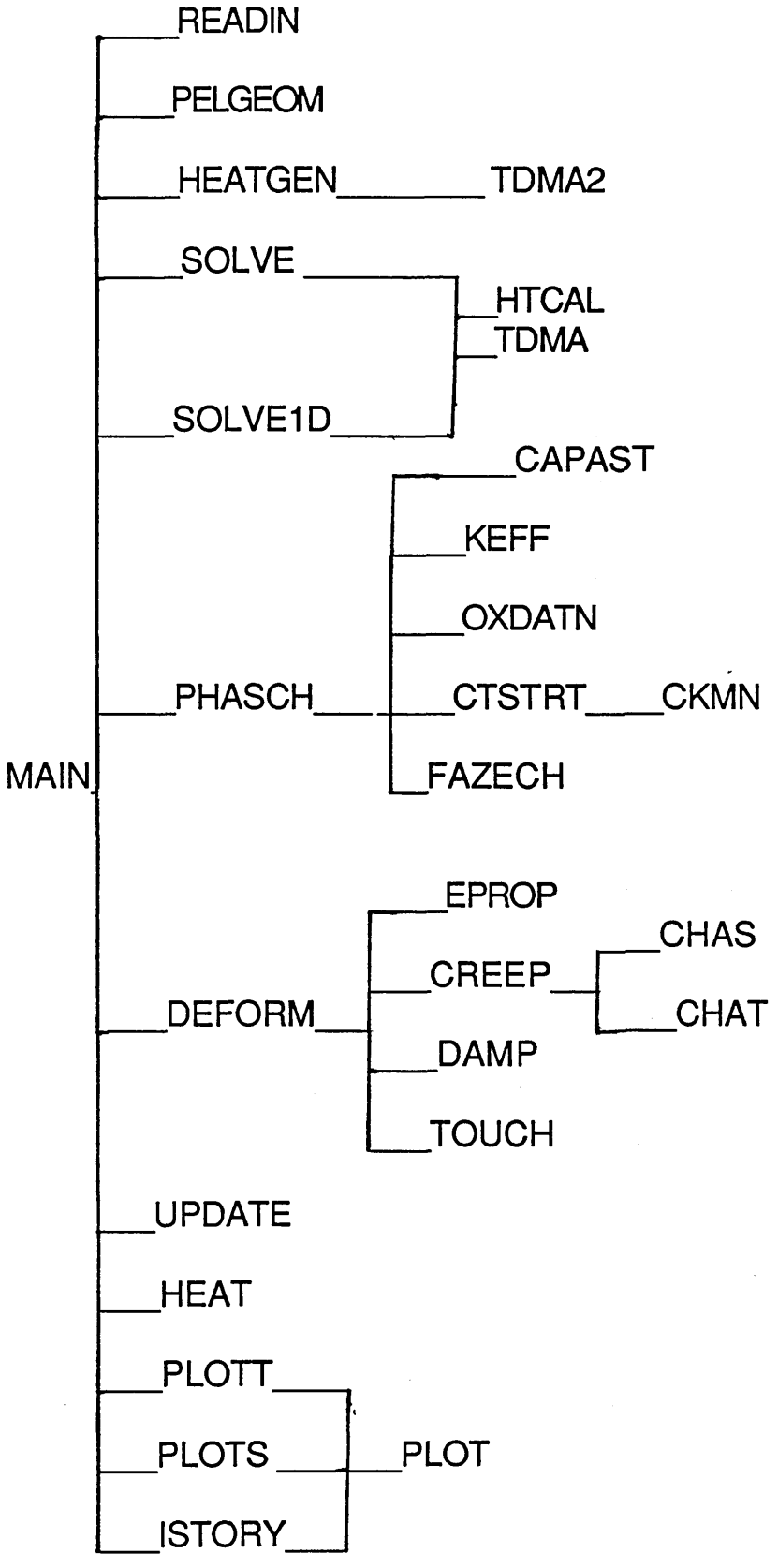

Appendix 3

Iteration using the trapezium Method

The trapezium method of iteration takes two function values from previous iterations and uses them to calculate the gradient of the function. It then proceeds in the same way as Newton's technique (Williams 1979). Like Newton's technique it is fast, but sometimes diverges rapidly and causes calculations to fail. Furthermore, two function values are used to obtain the derivative, so the calculation can be applied only after the first iteration. These difficulties are overcome by expressing the problem as though it is to be solved by successive over relaxation and then using previous residual values to set the over-relaxation factor.

The magnitude of the relaxation factor is the reciprocal of the gradient of the curve and can be calculated as follows;

$$f_1 = f_0(R_0 /(R_0 - R_1))$$

where R_0 and R_1 are the old and new values of the residual respectively.

Convergence problems can be dealt with simply by constraining the over-relaxation factor to remain between set values (say 0.1 and 1.95).

The first iteration can also be dealt with more efficiently using this method. The slope of the curve will probably not change much between time-steps, so the factor used to obtain the solution in the previous time-step is retained by setting the initial residual R_0 to a large value.

Appendix 4

Finite-difference Heat Transfer Solution

The code solves the time-dependent heat-conduction equation with non-uniform thermal properties and distributed heat sources. The solution is discretised on a two-dimensional, polar mesh. The material is divided into three regions; the fuel pellet, the pellet-clad gap and the cladding. The cladding is represented by a single finite difference node in the radial direction, but the noding in the other two regions can be set by the user.

The discretisation is carried out by the use of control-volume analysis and nodes are placed at the centre of the control volumes. Thermal properties are assumed uniform throughout the control volumes, but vary stepwise between volumes. Account is taken of the discontinuity of temperature gradient which occurs at the control-volume boundary. This is particularly important where the control-volume boundary coincides with the physical boundary between two materials.

Boundary Conditions

The solution field is surrounded by four zero heat-flux boundary conditions. The heat transfer to the coolant is modelled as a separate term. This can be described either in terms of the coolant temperature and mean heat-transfer coefficient or the average clad temperature. In both cases the local heat-transfer coefficients are calculated using a correlation involving the pitch-to-diameter ratio.

The Source Terms

Three different source terms are modelled. They are:

1 Nuclear Heating

Heat generated by fission, or the decay of fission products, is assumed to occur only in the fuel pellet. The heat generation profile is determined by the diffusion of thermal neutrons. The user is required to supply a single macroscopic absorption cross section and the diffusion coefficient. This approximation only applies to fuel at the start of its life. Other conditions can be approximated by the selection of suitable parameters.

2 Deformation Work

The heat generation, resulting from the product of stress and strain, is included. This increases the localization of deformation once rapid failure starts, and hence reduces the predicted diametral failure strain by about one or two percent. It makes negligible difference to the failure time prediction.

3 Exothermic Cladding Oxidation

At high temperatures the zircaloy-steam reaction can generate significant heat and can influence clad temperatures. Local calculation of cladding oxidation is made and the resulting heat generation is used in the heat-transfer solution routine.

The Solution Method

The temperature field is solved using the Tri-diagonal Matrix Algorithum in a process of line iteration and block adjustment. A one-dimensional solution is obtained in the radial direction, assuming that the current temperature values for adjacent segments of the rod are correct. The temperature values obtained are used to update previous temperatures for that segment of the rod, by the application of a relaxation factor. This line iteration process is repeated for all segments. Then the block adjustment process is used. The equations for energy conservation at all the nodes in a segment are added togeather, and a one dimensional solution is obtained in the azimuthal direction for block adjustments. These adjustments are added to all temperature values in a segment, then the line iteration process recommences. The direction of the sweep, used in the solution technique, is alternated so that the solution method does not introduce temperature gradients.

Appendix 5

Testing Elements of the Code

The code was constructed in modular form and each module was used to perform calculations before it was inserted into the code. The thermal conductivity and specific heat capacity routines were initially coded using simple expressions obtained from text books. Then, when these expressions were replaced by more accurate routines, a comparison of calculation results was made. The resulting change in calculated fuel centre temperature was found to be less than $5^{o}C$. This gives confidence in the accuracy of the routines.

The temperature field solution routine was tested by setting thermal properties and boundary conditions to constant, uniform values, then comparing the result of calculations with the corresponding analytical solution.

Testing was also carried out on the completed code by changing the type of coolant boundary conditions used in the thermal calculations. initially, heat transfer coefficient boundary conditions were used to calculate fuel pellet and cladding temperatures. Then the resulting cladding temperatures were used as boundary conditions instead of the heat-transfer coefficients. Agreement was found between the calculated fuel temperature fields.

Finite Difference Mesh Refinement

Mesh refinement studies were carried out to demonstrate that mesh-independent solutions could be obtained and to select the correct nodalization for subsequent calculations. Two types of calculation were performed; steady state heat conduction and transient deformation.

Steady state heat conduction calculations were carried out assuming decay heat power levels and a pellet excentricity value of one. Provided that the radial nodalization exceeded 8 nodes and the azimuthal nodalisation exceeded l6 nodes per half rod, the solution was found to be independent of nodalisation to within the prescribed tolerance of $0.1^{o}C$.

Transient deformation calculations were carried out with meshes of 20, 24 and 28 circumferential nodes per half rod. These calculations proved to be more sensitive to mesh refinement than simple thermal calculations. Although no significant difference occurred in the average strain histories, the extent of strain localization differed.

The strain localization factor is calculated by dividing the peak strain by the average strain and is used to give an indication of the stability of the deformation.

The strain localization factor is plotted against strain for different mesh sizes in figure 29. Results of calculations using 24 and 28 nodes per half sector are close enough to justify the use of 24 nodes in further calculations.

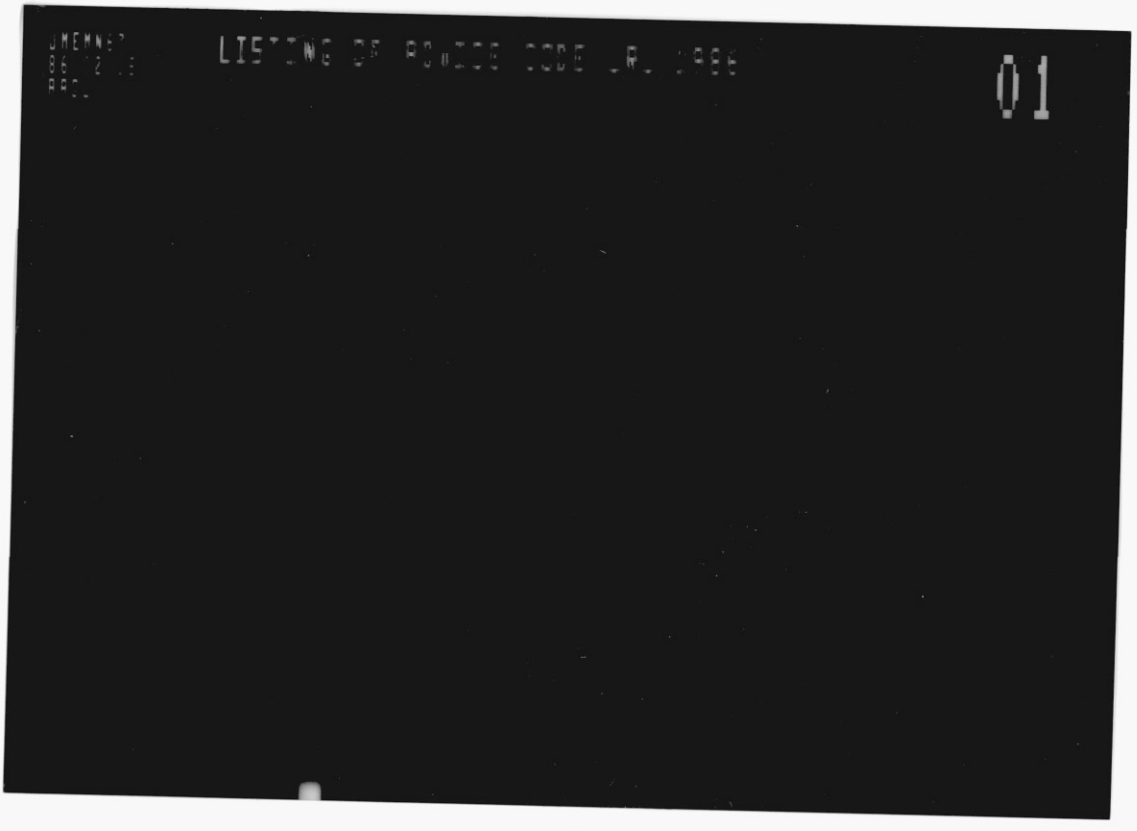
01